TURUN YLIOPISTO

Geochemical characteristics of felsic and intermediate plutonic rocks in Pasalanmäki, Leppävirta on Archean-Proterozoic boundary

Aino Savakko

Geology (bedrock)

Master's thesis

Laajuus: 30 op

Supervisors:

Esa Heilimo

Perttu Mikkola

29.11.2023

Turku

Pro gradu -tutkielma

Pääaine: Geologia
Tekijä: Aino savakko
Otsikko: Felsiset ja intermediääriset syväkivet Pasalanmäellä Leppävirralla Arkeeinen-Proterotsooinen rajalla
Ohjaajat: Esa Heilimo, Perttu Mikkola
Sivumäärä: 60 sivua + liitteet 42 sivua
Päivämäärä: 29.11.2023

Pasalanmäen aluetta Leppävirralla on tutkittu aikaisemmin malmipotentiaalin näkökulmasta, keskittyen erityisesti alueen mafisiin intruusioihin. Kuitenkin alueen tarkempi kivilajien kuvaus ja luokittelu, näiden alkuperän tunnistaminen ja tutkiminen on jäänyt osittain tekemättä. Tämän tutkimuksen tavoitteena on saavuttaa tarkka ymmärrys Pasalanmäen alueen kallioperän intermediääristen ja felsisten plutonisten tonaliittien, gneissien, granodioriittien ja juonien petrologiasta ja synty-ympäristöstä. Tämä toteutetaan kivinäytteiden mineraalien tutkimisella ja kivien luokittelulla, kivilajin ja esiintymistyypin mukaan. Pääalkuaineiden, hivenalkuaineiden ja harvinaisten maametallien pitoisuuksien perusteella selvitetään kivien alkuperäistä synty-ympäristöä. Matemaattisella mallinnuksella laskettiin mahdollisen fraktioituneen kiteytymisen vaikutusta kivien koostumukseen.

Pasalanmäeltä kerätyt felsiset ja intermediaariset kivinäytteet olivat pääosin biotiitti-sarvivälketonaliitteja tai plutonisia gneissejä, joilla on vastaava mineralogia. Myös koostumukseltaan felsisempiä granodioriitteja ja alueen nuorempia juonia kerättiin näytteiksi. SiO_2 vaihteli näytteiden ja näyteryhmien välillä ollen alimmillaan 53 pp. %. Eu/Eu* oli kaikissa näytteissä 0,30 ja 5,82 välillä ja $(La/Yb)_n$ suhde vaihteli 2,0 ja 74,0 välillä, lukuun ottamatta kahta juoni näytettä.

Tutkittujen näytteiden Eu/Eu* ja $(La/Yb)_n$ suhteet ovat tyypillisiä adakiiteille ja osa tutkituista näytteistä on La/Yb vs. Yb ja Sr/Y vs. Y suhteiden perusteella adakiitteja. Tässä tutkimuksessa löydetyt adakiittisia geokemiallisia piirteitä omaavat näytteet ovat plagioklaasi kumulaatteja. Tutkimuksessa esitetyn mallin mukaan useat mineraalit ovat kivien muodostumisen aikana kiteytyneet kumulaatteina alkuperäisestä magmasta. Pasalanmäen kallioperän felsiset ja intermediääriset plutoniset kivet ovat geokemian perusteella muodostuneet saarikaari ympäristössä ja kuuluvat varhaisempaan tai myöhäisempään Svekofenniseen magmatismiin, joka tapahtui Raahe-Laatokka vyöhykkeellä.

Avainsanat: Arkeeinen-proterotsooinen raja, Raahe-Laatokka hiertovyöhyke, Svekofennia, Pasalanmäki, Leppävirta, Svekofenninen magmatismi, intermediääriset syväkivet, felsiset syväkivet, juonet, saarikaari magmatismi, adakiitit

Master's thesis

Subject: Geology
Author: Aino Savakko
Title: Geochemical characteristics of felsic and intermediate plutonic rocks in Pasalanmäki, Leppävirta on Archean-Proterozoic boundary
Supervisors: Esa Heilimo, Perttu Mikkola
Number of pages: 60 pages + attachments 42 pages
Date: 29.11.2023

The area of Pasalanmäki in Leppävirra has previously been studied from the point of ore potential, focusing especially on the mafic intrusions that can be found in the area. However, a more detailed description and classification of the rock species of the area, identification and study of their origin has been partially left undone. The aim of this study is to achieve a proper understanding of the petrology and the environment of origin of the intermediate and felsic plutonic tonalites, gneisses, granodiorites and dikes in the Pasalanmäki area. This is done by studying the petrography of different rock types and classifying the rocks, according to the rock type and it's relation to the bedrock. Based on the concentrations of major elements, trace elements and rare earth metals, the original rock forming environment is determined. Mathematical modeling was used to calculate the effect of possible fractional crystallization on the composition of the rocks.

The felsic and intermediate rock samples collected from Pasalanmäki were mainly biotite hornblende tonalites or plutonic gneisses with similar mineralogy. Granodiorites with a more felsic composition and dikes representing the youngest rocks of the area were also collected as samples. SiO_2 varied between samples and sample groups, being at least 53 wt%. Eu/Eu* varied between 0.30 and 5.82 and $(La/Yb)_n$ varied between 2.0 and 74.0 in all samples, except for two dike samples.

The seen Eu/Eu* and $(La/Yb)_n$ ratios are typical for adakites, for example, some of the examined samples are adakites based on La/Yb vs. Yb and Sr/Y vs. Y concentrations. The samples with adakitic geochemical characteristics found in this study are also presumably plagioclase cumulates, and according to the model presented in the study, several minerals may have crystallized as cumulates from the original magma during the formation of the bedrock. The felsic and intermediate plutonic bedrock of Pasalanmäki was, based on geochemistry, formed in an island arc environment and may belong to the earlier or later Svecofennian magmatism, which occurred at the Raahe-Ladoga zone.

Key words: Archean-Proterozoic boundary, Raahe-Ladoga shear zone, Svecofennia, Pasalanmäki, Leppävirta, Svecofennian magmatism, intermediate plutonic rocks, felsic plutonic rock, dikes, island arc magmatism, adakites

Content

1. Introduction 7

2. Geological background 9

2.1 Regional geology 9

2.2 Evolution of Fennoscandian shield from Archean to early Paleoproterozoic 10

2.3 End of divergent plate tectonics and Svecofennian magmatism 11

2.4 Lithostratipraghy of Raahe-Ladoga shear zone and the study area 12

3. Materials and methods 16

3.1 Field Observations 16

3.2 Thin sections 16

3.3 Whole rock geochemistry 17

4. Results 18

4.1 Field descriptions and collected samples 18
4.1.1 Plutonic rocks 18
4.1.2 Gneissic rocks in field descriptions 18
4.1.3 Dikes in field descriptions 20

4.2 Petrography 21
4.2.1 Plutonic rocks: tonalite 21
4.2.2 Plutonic rocks: granodiorite 23
4.2.3 Plutonic rocks: granite 24
4.2.4 Plutonic rocks: diorite 25
4.2.5 Gneisses 26
4.2.6 Dikes 27

4.3 Results from the geochemistry 29
4.3.1 Geochemistry of tonalites and gneisses 30
4.3.2 Geochemistry of diorite 32
4.3.3 Geochemistry of granodiorites 33
4.3.4 Geochemistry of granite 34
4.3.5 Geochemistry of dikes 34

5. Discussion 39

5.1 Comparison, tectonic setting and source of Pasalanmäki tonalites and gneisses 39
5.1.1 Island arcs; subduction related origin of the Pasalanmäki bedrock 39
5.1.2 Chemical similarities to preorogenic and syntectonic rock geochemistry 41
5.1.3 Adakite like chemical features: amphibole fractionation and garnet control 43

5.2 Fractional crystallization of tonalites and gneisses in Pasalanmäki 46
5.2.1 Plagioclase fractionation and development of Eu/Eu* compared to Sr 47
5.2.2 Potassium feldspar fractionation in the gneisses and tonalites 50
5.2.3 The missing MREE in granodiorites and amphibole fractionation 51

5.3 Magmatic evolution of the Pasalanmäki plutonic rocks 53

6. Conclusions 55

Acknowledgements 56

References 57

Attachments 61

Attachment A. Sample code, x- and y-coordinates in ETRS-TM35FIN, field rock name and rock type 61
Attachment B. SEM-report of some studied minerals 63
Attachment C. Petrography of the studied samples 86
Attachment D. Geochemical analyses of the samples 91

1. Introduction

Archean-Proterozoic boundary (AP boundary) in Finland is located in between Svecofennia province and Karelia province. The AP boundary is locally challenging to separate in the bedrock due to metamorphism caused by Svecofennian magmatism and shearing in the Raahe-Ladoga shear zone. Bedrock near AP boundary can be dated using different methods. With geochemical studies, the origin of the bedrock can be connected to a particular tectonic environment, which can used to correlate the studied rocks with specific crust forming episodes.

Pasalanmäki in Leppävirta, is located within the AP boundary. From 1968 to 1972 the geology in Pasalanmäki and surrounding areas in Leppävirta was studied by Outokumpu mining Ltd (Parkkinen 1974). At the time, ore potential studies and mapping focused on the mafic intrusions and rock types, in hopes of revealing nickel ores. During these studies it was concluded that the bedrock in Pasalanmäki represented mostly metamorphosed volcanic sediments that would have been deposited originally on top of Archean basement and would represent Karelian schists (Parkkinen 1974). Fagerström (1990) estimated that bedrock northwest from the study was partly hornblende gneisses, similar to Pasalanmäki gneisses and tonalites, which originated from island arc magmatism. More recently Tuppurainen et al. (2022) estimated that based on single grain U-Pb data from zircons, the bedrock in Pasalanmäki would be 1.93-1.89 Ga old, where gneisses and tonalites represent the older Svecofennian magmatism. Archean bedrock wasn't found in the area, with exception of some dikes that were estimated to be the youngest lithology in the study area that had inherited Archean zircons in them (Tuppurainen et al. 2022). Still to this day the petrology and petrogenesis of the bedrock in Pasalanmäki and rocks in Pasalanmäki remain poorly understood.

This study is a part of the joint project of Geological Survey of Finland, university of Turku, university of Oulu and university of Helsinki, where the bedrock of Pasalanmäki is being restudied for in-depth understanding of the areas rock types, petrogenesis, age and ore potential. This study's aim was to create a proper understanding of the petrology and origin of intermediate and felsic rocks in Pasalanmäki. For achieving this, the following points are studied: What types of intermediate and felsic rocks can be found on the study area, and can they be classified based on mineralogy? Are the rocks in Pasalanmäki derived from one parental

magma or does the area have rocks from multiple magmatic sources? What type of magmatism created the plutonic rocks and what types of processes affected the magmatism?

For this study, rocks were collected as hand samples from Pasalanmäki, which represent either gneisses, plutonic rocks or dikes according to the field classification. Thin sections and geochemical analyzes were prepared from the samples. Firstly the samples were divided based on the thin sections and field observations. Based on geochemistry, some of the groups were further subdivided due to the differences in Eu-anomaly.

2. Geological background

2.1 Regional geology

Fennoscandia is one of the crustal segments in East-European craton along with Volgo-Uralia and Sarmatia (Figure 1; Gorbatschev and Bogdanova 1993). East-European craton is composed of two shield areas, Fennoscandian shield in Fennoscandia and Ukrainian shield area in Sarmatia crustal segment (Nironen 2017). East European craton is characterized by Precambrian bedrock, and it's separated from the younger bedrock in the south by Trans European suture zone (Nironen 2017; Gorbatschev and Bogdanova 1993). In the north East-European craton is limited to Timian fold belt (Nironen 2017). Different segments of this craton are separated by aulacogens (Gorbatschev and Bogdanova 1993).

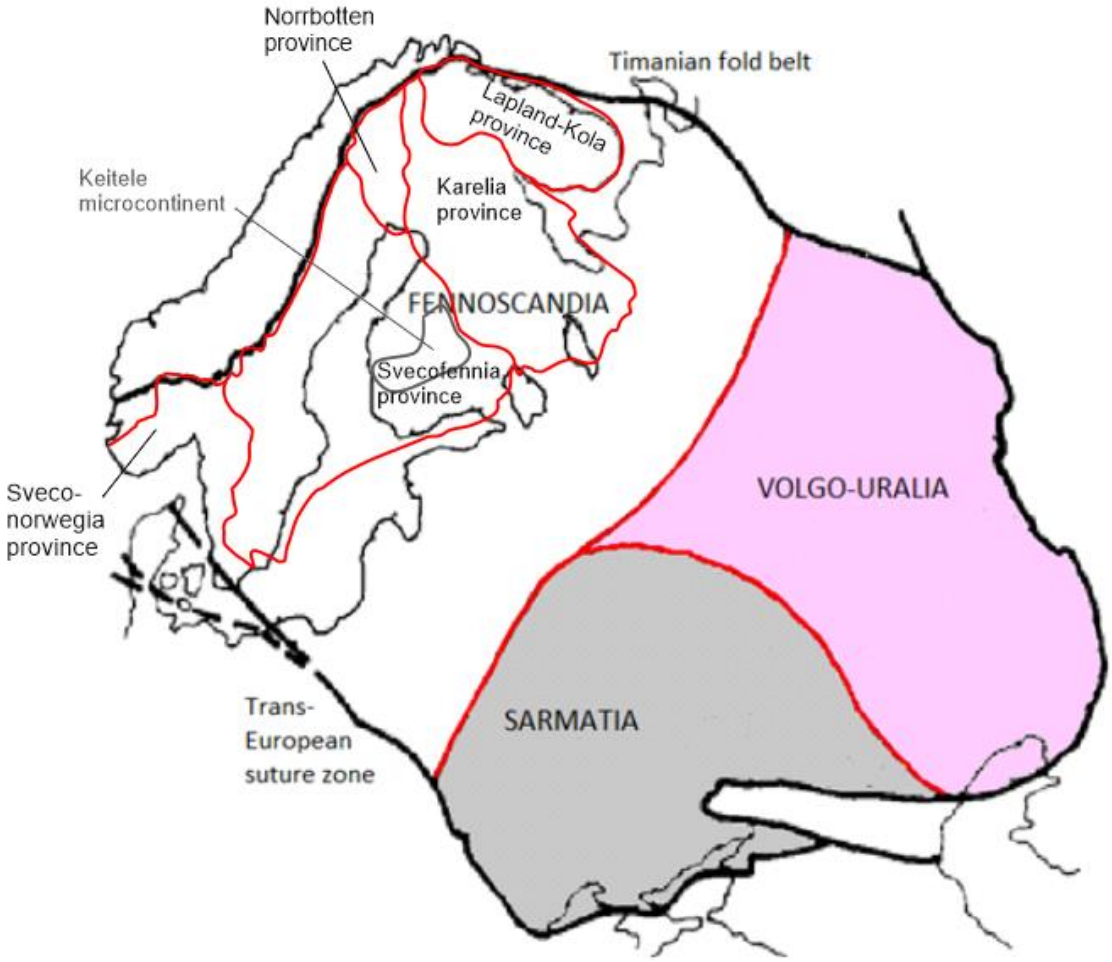

Figure 1. East-Europian craton and its crustal segments, Fennoscandia, Volgo-Uralia and Sarmatia. Modified after Nironen 2017; Lahtinen et al. 2005; Gorbatschev and Bogdanova 1993.

Shield part of Fennoscandia crustal segment has been divided into several provinces, which from north to south are, Lapland-Kola province, Karelia province, Norrbotten province, Svecofennia province and Sveconorwegian province (Figure 1; Nironen 2017, Gorbatschev and Bogdanova 1993). In Lapland-Kola, Karelia and Norrbotten provinces, bedrock was formed partially during Archean era. Svecofennia and Sveconorwegian provinces were formed during Proterozoic era (Nironen 2017).

2.2 Evolution of Fennoscandian shield from Archean to early Paleoproterozoic

First pieces of bedrock in Fennoscandian shield, currently in Karelia province, were already existing during the Mesoarchean era (Nironen 2017; Gorbatschev and Bogdanova 1993). Karelia province (at the time Karelia continental nucleus) formed stable continent to against which Belamorian belt, Lapland-Kola province and Svecofennian province were accreatiated later (Gorbatschev and Bogdanova 1993). The bedrock terrains formed during Neoarchean era are related to the formation of Supercontinent Superia (also known as Kenorland), where Archean Karelia and Lapland-Kola provinces collided creating the Belomorian orogeny belt in between them (Nironen 2017; Gorbatschev and Bogdanova 1993).

The breakup of Archean craton is related to the breakup of Supercontinent Superia around 2.5 Ga ago (Nironen 2017). According to Nironen (2017) the extension and formation of rifting basins in Fennoscandia started already in the end of Neoarchean era and main breakup of the craton occurred 2.1 Ga ago. First signs of extension in in Karelian province date back to 2.44 Ga ago, where mafic layered intrusions were formed. After 2.2 Ga, the increased number of metasedimentary rocks, covering Archean bedrock, implies a change to open sea sedimentary systems in Archean craton (Nironen 2017). Mantle plume activity was present in the break-up of Karelian craton (Lahtinen et al. 2015). E-W and ESE-WNW trending dikes, aged 2.1 Ga old (Vuollo and Huhma 2005) and volcanics that have OIB (ocean island basalt) characteristics, are remnants of 2.1 Ga old plume activity in the area (Lahtinen et al. 2015). At 2.1 Ga failed rift was formed in northern part of current Finland, Karelia and Archean Lapland-Kola province rifted apart (Nironen 2017) and 1.98 Ga ago Lapland-Kola orogeny started on the north side of Karelia craton, possibly causing more extension in the southwest edge of Karelia province (Lahtinen et al. 2015). 1.95 Ga ago a rift basin and more ocean-ward ridge tectonic settings were formed along the southern edge of Karelia province.

2.3 End of divergent plate tectonics and Svecofennian magmatism

1.92 Ga ago the divergent tectonics in southern edge of the Karelia craton ended and continent-continent/arc collision in the area started the Svecofennian orogeny (Nironen 2017). The Svecofennian orogeny from 1.9 Ga to 1.8 Ga ago is related to the formation of Baltica paleocontinent, Laurentia paleocontinent and supercontinent Columbia.

According to Nironen (2017) around 1.92 ago active continental margin was closed on the north-western side of Archean craton by Norrbotten and Karelia provinces colliding with each other creating orogeny. While the orogenic belt developed, accretion of Keitele microcontinent and volcanic arc to Karelia continent margin from south-west took place (Nironen 2017; Figure 1). In this setting it is estimated that the subduction was towards southwest due to lack of subduction related magmatism in the Karelia province. Archean component hasn't been found in the island arc rocks of this area (Lahtinen et al. 2005).

According to Nironen (2017) the accretion of Keitele microcontinent caused slab break-off at the subduction zone, whereas Lahtinen et al. (2015) considered that slab breakoff occurred during the initial continent-continent collision. This event caused a metamorphic peak that culminated at high amphibolite or granulite facies, at 1.91 Ga ago (Nironen 2017; Korsman et al 1984). At this time a fold and thrust belt was formed and Jormua and Outokumpu ophiolites were thrust onto the continental margin of the Karelia province (Nironen 2017; Lahtinen et al. 2015; Ekdahl. 1993). The continent-continent collision that happened between Keitele microcontinent and Karelia province caused shearing and thrusting in the Archean-Proterozoic boundary (Lahtinen et al. 2005). It is estimated that ductile deformation along the shear zones (Raahe-Ladoga shear zone) in the AP boundary continued up to 1.87 Ga ago. The Raahe-Ladoga shear zone in AP boundary is currently considered to separate the Archean crust from the Svecofennian province (Ekdahl 1993).

Development of the rest of the Svecofennian province can be explained with two varying theories. In the first it is considered that after the collision subduction ended in the AP boundary and new continent arc (forearc; Lahtinen et al. 2005) was formed south from the AP boundary in the Tampere schist belt. The late- to post collisional magmas started to intrude previously formed bedrock in the AP boundary at around 1.89 – 1.88 in a back-arc setting (Lahtinen et al. 2015). From 1.89 to 1.88 Ga ago two microcontinents, Bothnia and Bergslagen collided to still

forming continental margin from the south (Nironen 2017). Peak of the Svecofennian magmatism, metamorphism and deformation is thought to be 1.88 to 1.87 Ga ago, at the time when microcontinent Bergslagen collided to Keitele microcontinent (Nironen 2017; Lahtinen et al. 2005). The second theory is based on a north-west dipping continuous subduction in the south-west edge of Karelia province from 1.91 to 1.86 Ga ago (Hermansson et al. 2008). This subduction zone would have slowly hinged back from its original setting during this period and minor changes in continental margin development directions would have create temporary extensional phases in the subduction area. Hinge and extension caused by it created the back arc type magmatism during the subduction (Hermansson et al. 2008).

2.4 Lithostratipraghy of Raahe-Ladoga shear zone and the study area

Savo schist belt (referred in the following text as Savo supersuite on Raahe-Ladoga shear zone) is a 300-350 km long geological formation between Karelia and Svecofennia provinces that extends to southeast and northwest from the study area (Figure 2). Savo supersuite mostly represents high grade metamorphosed marine sediments (Lahtinen et al. 2005) and oldest Svecofennian magmatism in the Raahe-Ladoga zone is 1.93 to 1.92 Ga old (Luukas et al. 2017). These metavolcanic Vihanto and Pyhäsalmi suites are part of Northern Ostrobothnia supergroup (Figure 2; Mäki et al. 2015). Plutonic equivalents of the Northern Ostrobothnia supergroup rocks are included in the Venetpalo and Kokkoneva suites that formed scattered intrusions along Raahe-Ladoga shear zone (Ekdahl 1993; Figure 2). These rocks are thought to be formed in arc-magmatism before the Keitele microcontinent accreated to Archean Karelia province (Kousa et al. 2018). The 1.93-1.92 Ga old rocks in Northern Ostrobothnia supergroup have partly coeval ages with Kalevian group in Viinijärvi suite (Figure 2) paragneisses in Karelian schisht belt (Ekdahl 1993). Viinijärvi paragneisses were deposited on the rifted margin of the Archean craton, before and during early Svecofennian orogeny (Mikkola et al. 2022; Lukkarinen 2008).

Parkkinen (1974) estimated that the Leppävirta area would have been Karelian schist on top of Archean basement gneiss. In the study made by Fagerström (1990), it was estimated that the bedrock in Karttula northwest from the study area is predominately paragneisses and hornblende gneisses that were formed in island arc environment based on geochemical features. Fagerström (1990) estimated that the Karttula area (Figure 2) and Parkkinen (1974) estimated that the Leppävirta area has been metamorphosed on upper amphibolite facies, partly migmatising already existing bedrock. The extent of early Svecofennian magmatism is still

studied, and in the study made by Kousa et al. (2018) the area of early Svecofennian magmatism was extended from Rautalampi to Jäppilä-Virtasalmi block in Viholanniemi, southeast from the study area (Figure 2).

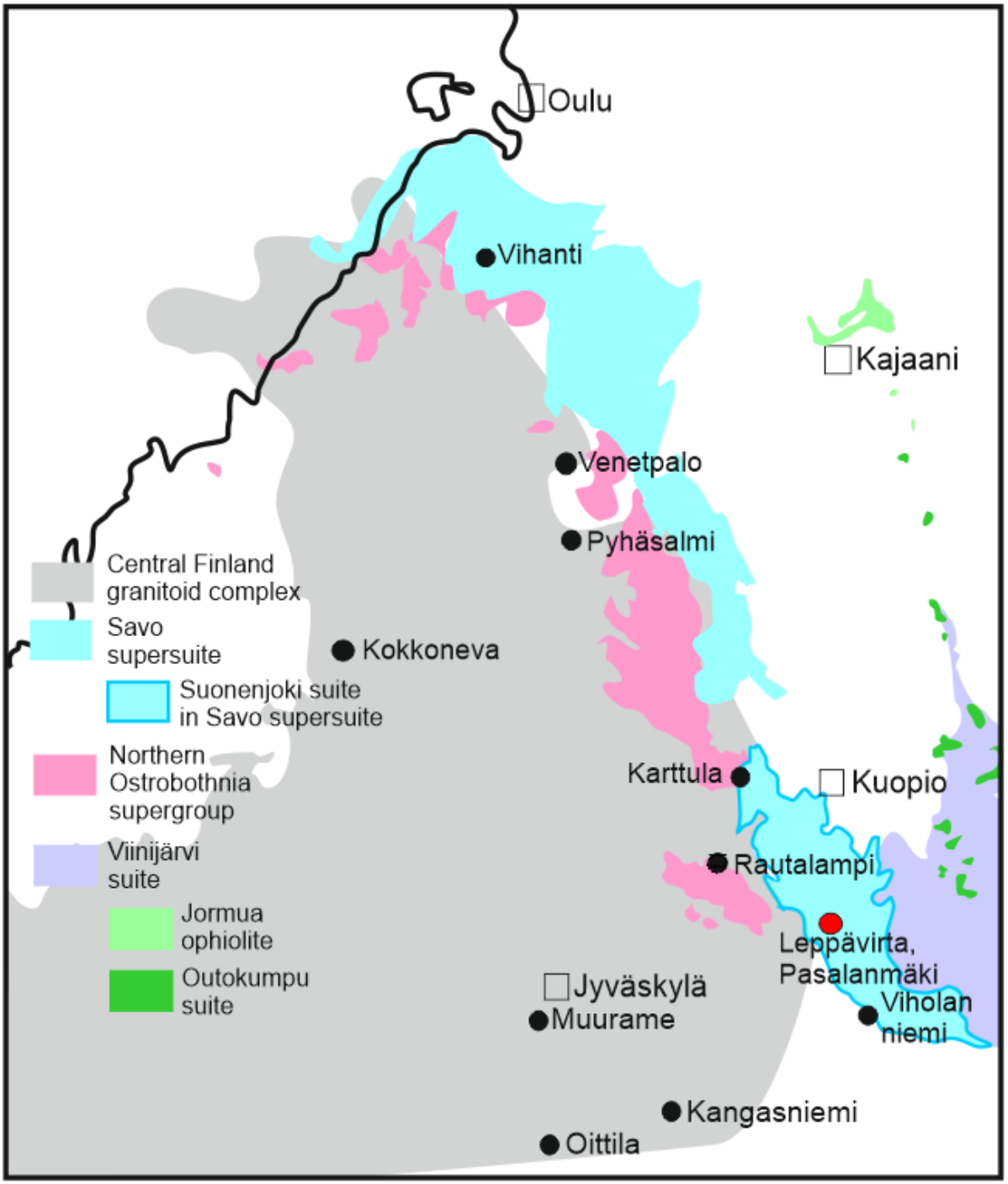

Figure 2. Map from the area surrounding Pasalanmäki and major tectonic units in it. Modified after DigiKP and Maanmittauslaitos karttapaikka.

The study area in Pasalanmäki, Leppävirta is currently thought to represent older Svecofennian magmatism from 1.93 Ga to 1.91 Ga ago (Tuppurainen et al. 2022; DigiKP). It is located in the boundary zone of Karelia and Svecofennia province, in the Raahe-Ladoga shear zone (Figure 2). According to the DigiKP, the area is included in the Suonenjoki suite which is part of the savo supersuite. Suonenjoki suite consists mainly of paragneisses that have been migmatised. Most of the migmatite neosomes are tonalitic in composition and are locally hard to separate from plutonic rocks due to extensive melting (Mikkola et al. 2016). In current bedrock map the Suonenjoki suite paragneisses and Northern Ostrobothnia supergroup paragneisses (figure 2) are separated by Iisvesi mylonite zone (Mikkola et al. 2016). Bedrock in the Pasalanmäki area was considered to be hornblende biotite gneisses, surrounded by paragneisses (DigiKP). In the most resent bedrock map from the area (Figure 3) the study area has been divided into granodiorite, granite, hornblende biotite gneiss and paragneiss.

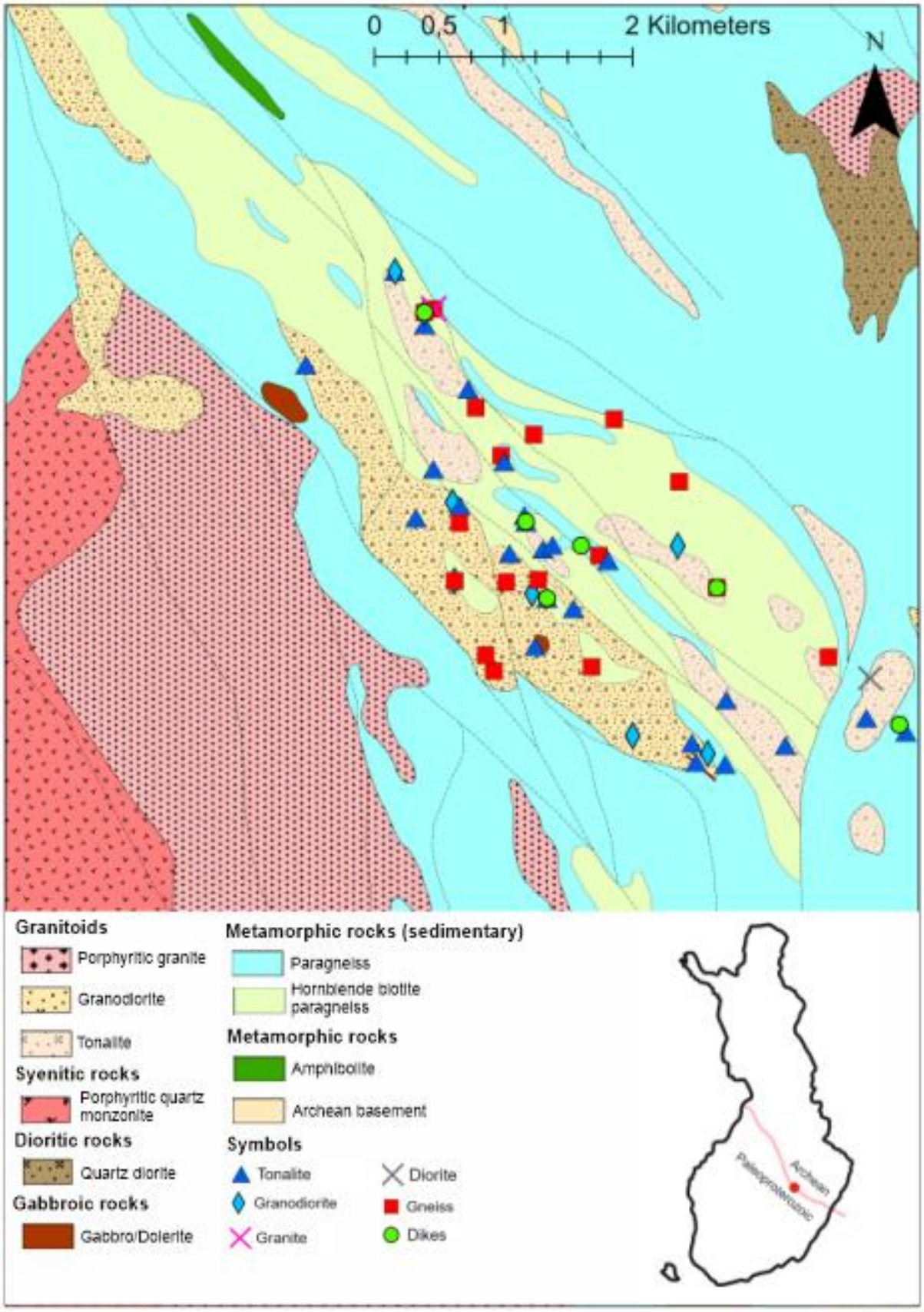

Figure 3. Unpublished project map from the study area. Index map modified after Lahtinen et al. (2012)

3. Materials and methods

3.1 Field Observations

During the summer of 2021, 65 samples that represented felsic or intermediate rocks were collected from the study area (Figure 3; attachment A) by trainees working for Geological Survey of Finland. Multiple samples were taken from some of the outcrops in means of sampling different lithostratigraphic units identified in the field and brief descriptions of the studied outcrops were written as well. Samples were collected with geological hammer or mini drill. Additional field visit was executed for 3 days by the author of this thesis, during summer 2022 to revise and in-depth understand the bedrock of Pasalanmäki. Based on the field work the samples were divided to; plutonic rocks, gneisses, and dikes. Field division of the lithological units was based on grain size and degree of deformation.

3.2 Thin sections

Most of the studied thin sections were prepared in the University of Turku and six thin sections were prepared by Geological survey of Finland. Collected samples were send to University of Turku in where they were sawed to pieces, suitable for thin section preparation, and thin sections were made in Geohouse laboratory. Phenom desktop scanning electron microscope (SEM) was used in Geohouse for some of the thin sections for establishing the chemical composition of unidentified accessory mineral that was estimated to be allanite (attachment B).

Plutonic rocks were classified and named using the guidelines of Le Maitre (1989) estimating the modal amount of major minerals (attachment C). In plutonic rocks, if rocks represented a mela-variety of the rock type in question, mafic minerals found in the thin sections are listed as part of the rock name. If studied sample represent leuco-variety of the rock type, it's described as rock type + leucocratic in composition. Dikes were named using same classification methods, but in the sample name they are named as rock type + dike. Gneissic rocks were classified using guidelines from Fettes and Desmons (2007), where minerals that were present in the thin section quantities above 5 % are mentioned in the rocks name. As all the studied gneissic samples had quartz and plagioclase in them, they are not mentioned in the sample name.

3.3 Whole rock geochemistry

Whole rock geochemistry analyses were made from all the 65 samples in ALS Global laboratories. X-ray fluorescence (XRF) was used for analysing major elements in samples and inductively coupled mass spectrometry (ICP-MS) was used for other elements. Samples were preparated in borate fusion for the analyses. Analysed oxides were Al_2O_3, BaO, CaO, Cr_2O_3, Fe_2O_3, K_2O, MgO, MnO, Na_2O, P_2O_5, SO_3, SiO_2, SrO, and TiO_2 (attachment D). Other analysed elements were Ba, Ce, Cr, Cs, Dy, Er, Eu, Ga, Gd, Hf, Ho, La, Lu, Nb, Nd, Pr, Rb, Sm, Sn, Sr, Ta, Tb, Th, Tm, U, V, W, Y, Yb and Zr. Ba, Cr and Sr were analysed with the ICP-MS.

4. Results

4.1 Field descriptions and collected samples

All samples were divided into plutonic rocks, gneisses, or dikes. Based on grain size samples that were fine-grained (Ø < 1 mm) and had more migmatised appearance were classified as gneisses and samples that had larger grain size were classified as plutonic rocks. Based on field work 38 of the 65 samples were plutonic rocks, 19 samples were gneisses and eight samples represented younger cross cutting dikes. In some cases, it was rather difficult to separate plutonic rocks from gneisses and in some sample points gneissic tonalite and tonalite type gneisses were described from the field as well. Potassium-metasomatism has likely altered some of the studied samples in plutonic and gneissic rock groups. Locations of the collected rock samples are given in attachment 1.

4.1.1 Plutonic rocks

Plutonic rocks collected from the study area were mostly tonalites. Some of the granite and granodiorite outcrops could be potassium metasomatized tonalites. Grain sizes varied from medium grained (2 mm to 4 mm; Figure 4A-D) to fine (1 – 2 mm; Figure 4E-H) and phaneritic texture varied from more gneissic (Figure 4A-E) to sheared (Figure 4F-4H). Mafic enclaves were common in plutonic rocks in the study area (Figure 4A, 4D, 4E, 4G). In some outcrops epidote was abundant in the field (Figure 4C). Felsic dikes, common in all the studied outcrops, were cross cutting tonalites and granodiorites (Figures 4G-H). In some areas the dikes were deformed (Figure 4G) and some have remained undeformed postdating the local deformation in the area (Figure 4H).

4.1.2 Gneissic rocks in field descriptions

Gneisses are typically hornblende-biotite gneisses or biotite-hornblende gneisses. Some granodioritic gneisses were observed from the study area as well. Gneisses have fine grain size (< 1 mm), phaneritic to aphanitic texture (Figure 5A-B and 5F) and are more deformed than rocks classified as plutonic rocks. Some gneisses were metamorphosed to a point where they had been partly migmatised (Figure 5A-B and 5D). Gneissic rocks had commonly signs of banding (Figure 5A-B) and ptygmatic (Figure 5A) folding (Figure 5C). Mafic inclusions (Figure 5D) and cross cutting dikes (Figures 5D-F) were present in some of the gneissic outcrops.

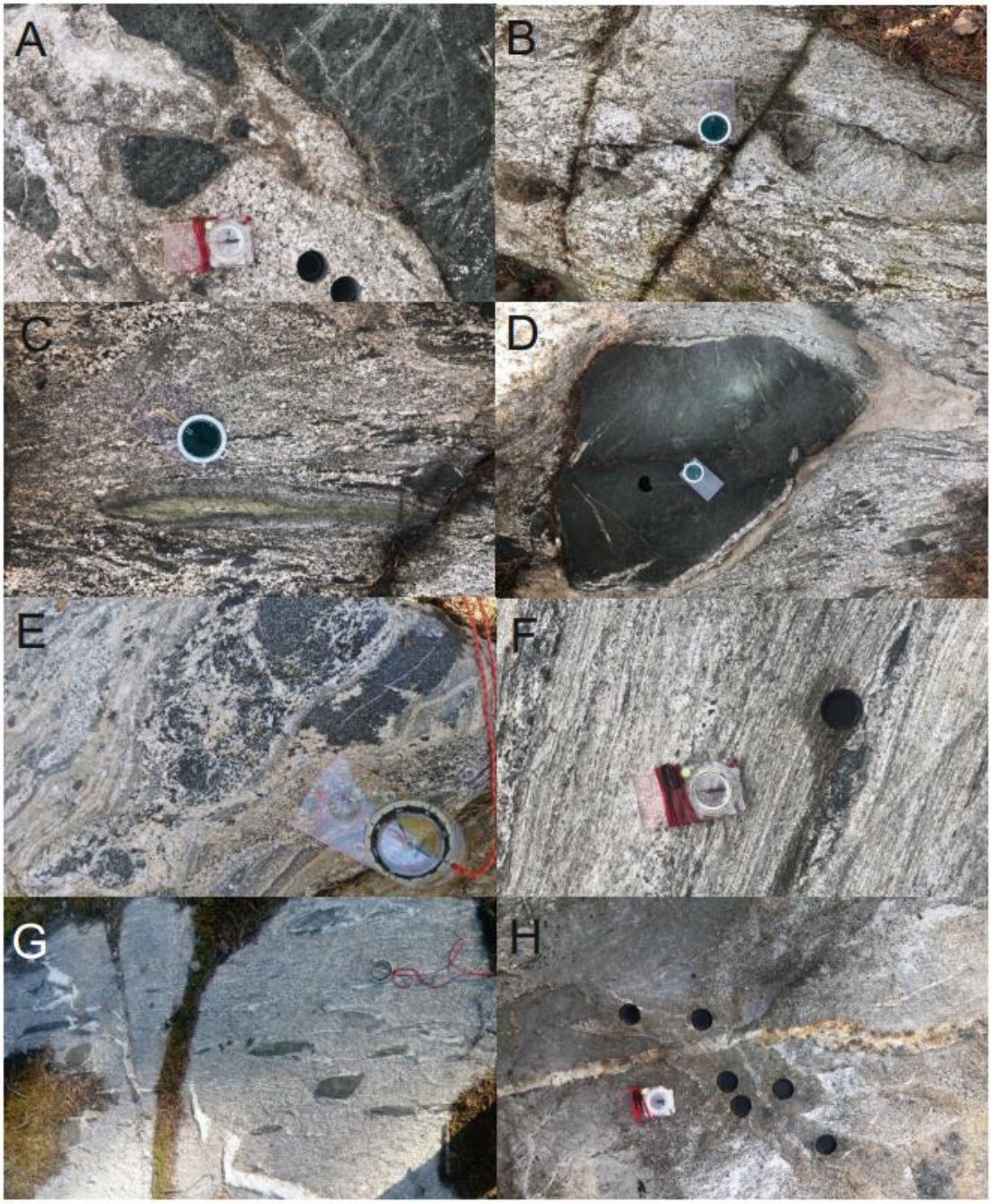

Figure 4. Different tonalite outcrops from the field. A) Medium grained tonalite with gneissic texture from outcrop VSVE-2021-17. B) Medium grained tonalite with gneissic and locally sheared texture from outcrop VSVE-2021-9. C) Medium-grained tonalite with gneissic appearance from outcrop KK8$-2020-203. In this picture, left from the compass, is an epidote enclave. D) From the outcrop KK8$-2020-203 as well, with mafic enclave on the bedrock. E) Fine-grained granodiorite and mafic enclave in it from outcrop VSVE-2021-6. F) Very sheared and small-grained tonalite from outcrop KK8$-2020-406. G.) Sheared fine-grained tonalite that has mafic enclaves and deformed trondhjemite dike, from outcrop KK8$-2020-801. H.) From the outcrop KK8$-2020-801, in this picture the trondhjemite dike is less deformed. Size of the compass is 11 cm.

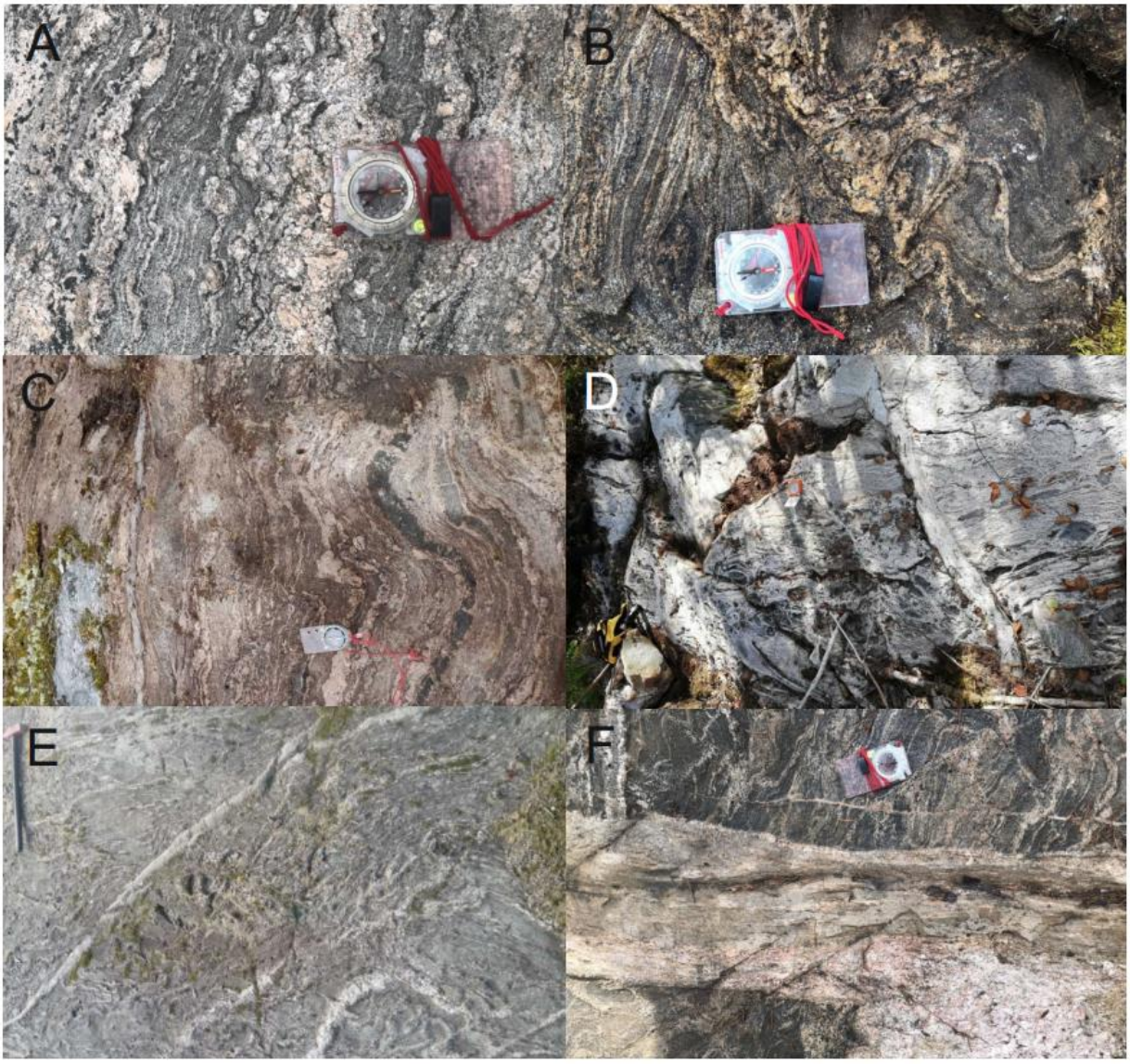

Figure 5. Different hornblende-biotite and biotite-hornblende gneisses found on the study area. A) Hornblende-biotite gneiss and ptygmatic vein from outcrop VSVE-2021-11. B) Banded and folded migmatite gneiss from outcrop KK8$-2020-706. C) Picture of the outcrop KK8$-2020-706 in larger scale. Biotite-hornblende gneiss in this picture shows overall folding. D) Migmatised hornblende gneiss from outcrop KK8$-2020-1111, in the front of the picture, felsic dike is cross cutting the gneiss. E) Fine grained hornblende-biotite gneiss and felsic dike from outcrop KK8$-2020-810 that seemed to have overall more felsic minerals in it when compared to other gneissic outcrops. F) In picture, a large granite dike is cross cutting the gneissic rock, in outcrop KK8$-2020-702. Size of the compass is 11 cm.

4.1.3 Dikes in field descriptions

During field work, dikes were determined to be youngest unit of lithostratigraphy, and generally the most felsic rocks found in the area. Some of the dikes have gone through deformation either by being sheared after intruding the existing bedrock or by brittle deformation (Figure 4G). It was estimated that dikes were either granitic or throndhjemitic in composition. All felsic dikes

were cross cutting the gneissic or plutonic rocks texture (Figure 4H and 5D-F). During field work it was estimated that larger intrusions of the granitic/granodioritic dike magma could be in the study area as well.

4.2 Petrography

Thin sections were used for determining the modal composition of the samples in more detail. Based on the estimated modal composition plutonic rocks were divided into tonalites (n=26), granodiorites (n=10), granite (n=1) and diorite (n=1). Rocks classified as gneisses during fieldwork, were kept as a separated group (n=19) and dikes created the sixth group based on field notes and modal composition (n=8).

4.2.1 Plutonic rocks: tonalite

Main minerals in tonalite samples are plagioclase, quartz, hornblende, and biotite. Common accessory minerals were titanite, chlorite, zircon, and allanite (Figure 6). Some samples represent mela-varieties of tonalite (n=7), and in those cases, the mafic minerals found in the rock are mentioned on the sample name as prefix (hornblende tonalite or biotite hornblende tonalite). Grain size in tonalite samples varies from 1 to 2 mm in diameter and common textures are anhedral granular (Figure 7) or subhedral granular. One sample in the tonalite group is protomylonite that has grain size of > 4 mm (Figure 6). Corona-textures of hornblende, and undetermined white amphibole (Figure 7) are found in two tonalite samples. Hornblende with poikilitic texture is common in some thin sections. Usual mineral alterations are plagioclase sericitization to muscovite (Figure 7) and clinopyroxenes complete uralitization into hornblende, based on the mineral texture. Hornblende grains in some samples had started to turn into biotite and furthermore occasionally biotite grains had turned into chlorite (Figure 7).

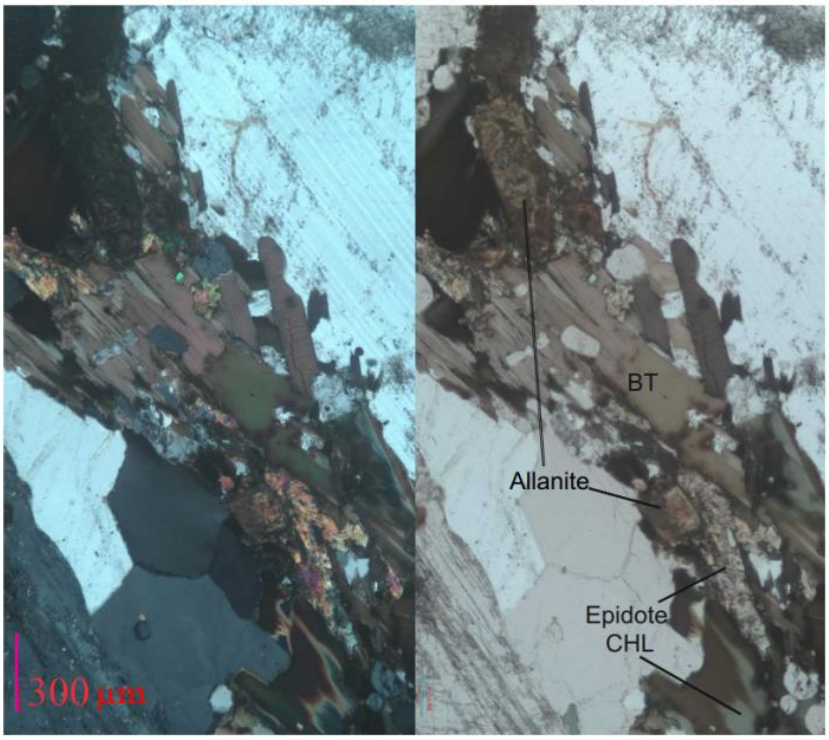

Figure 6. Thin section of the sample VSVE-2021-17.2, picture of the protomylonite tonalite. Biotite forms continuous ribbons between the larger plagioclase grains and quartz grains. Allanite and epidote are found in these ribbons. Biotite (BT) has partly started to turn into chlorite (CHL). On the left picture with XPL, and on the right with PPL.

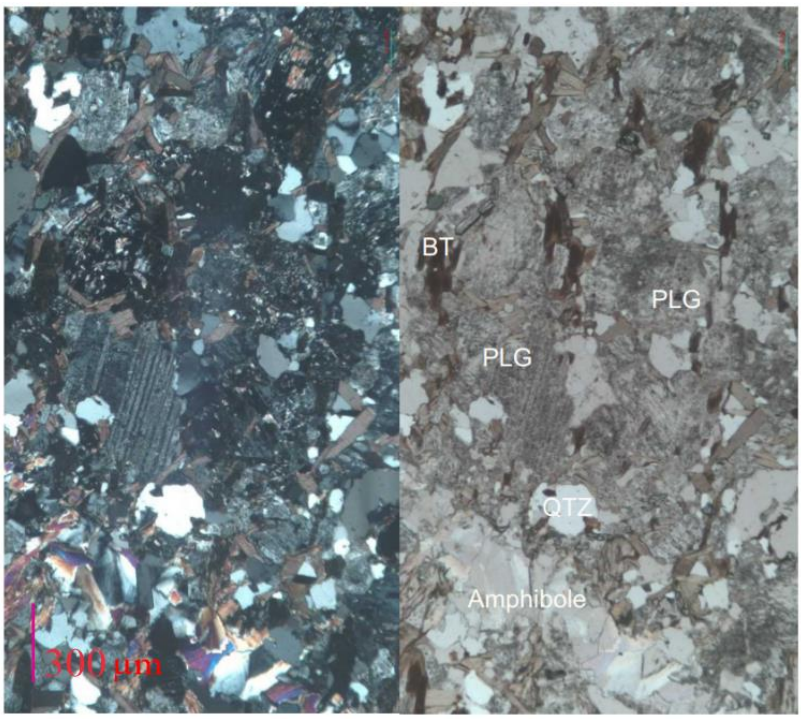

Figure 7. Thin section from sample KK8$-2020-102. Plagioclase (PLG) displays typical sericitization to small-grained muscovite. Other main minerals are biotite (BT) and quartz (QTZ). In bottom of the picture small vein consisting of white amphibole can be seen. Picture on the left is taken with XPL and picture on the right with PPL.

4.2.2 Plutonic rocks: granodiorite

Granodiorites have same main minerals as tonalite group samples, quartz, plagioclase, biotite and hornblende, with presence of potassium feldspar (microcline) as main mineral. Accessory minerals in granodiorites are titanite, chlorite, zircon, and allanite as well. Three leucogranodiorites contain less than 5 % of biotite and no hornblende. Mela granodiorites weren't found from these samples. Granodiorites commonly have anhedral granular texture. Grain size in granodiorites varies between 1-2 mm in diameter and in some samples potassium feldspar and plagioclase form larger grains up to 4 mm in size.

Hornblende with poikilitic texture is present in some of the thin sections. Common alterations are plagioclase sericitization to muscovite and clinopyroxenes complete uralitization into hornblende, based on pyroxene cleavage. Potassium feldspar is found in the samples as larger grains when compared to other minerals in the thin section (Figure 8), or as anhedral grains that are surrounded by smaller quartz grains and in some cases myrmekite grains.

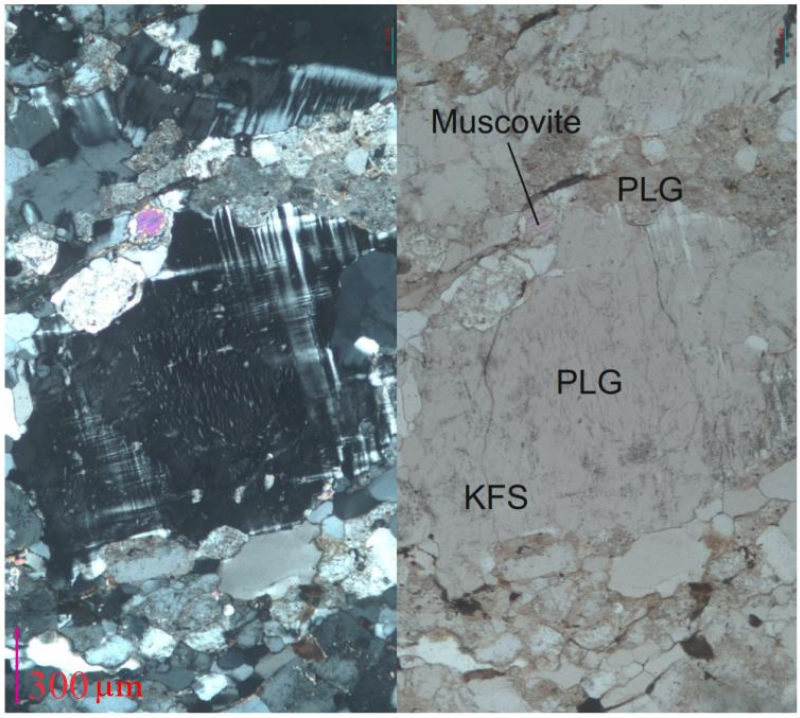

Figure 8. Picture is from the sample KK8$-2020-202. In the picture a large potassium feldspar grain (KFS) that has plagioclase grain (PLG) in it. On the left, picture in XPL and on the right in PPL.

4.2.3 Plutonic rocks: granite

Sample VSVE-2021-10.1 is based on modal examination a granite with leucocratic composition. Main minerals of this sample are quartz, microcline potassium feldspar, and plagioclase (Figure 9). Garnet, biotite and titanite are found in small amounts of less than 5%. Accessory minerals allanite, chlorite, opaque minerals and plagioclase alteration to sericite are compatible with other plutonic rocks. Granite is protomylonite in texture, plagioclase and microcline K-feldspar forming large grains in it. Size of these grains varies from 3 to 4 mm in diameter. In this sample, microcline K-feldspar seems to be an alteration product of plagioclase. Myrmekites are found from this sample as well (Figure 10).

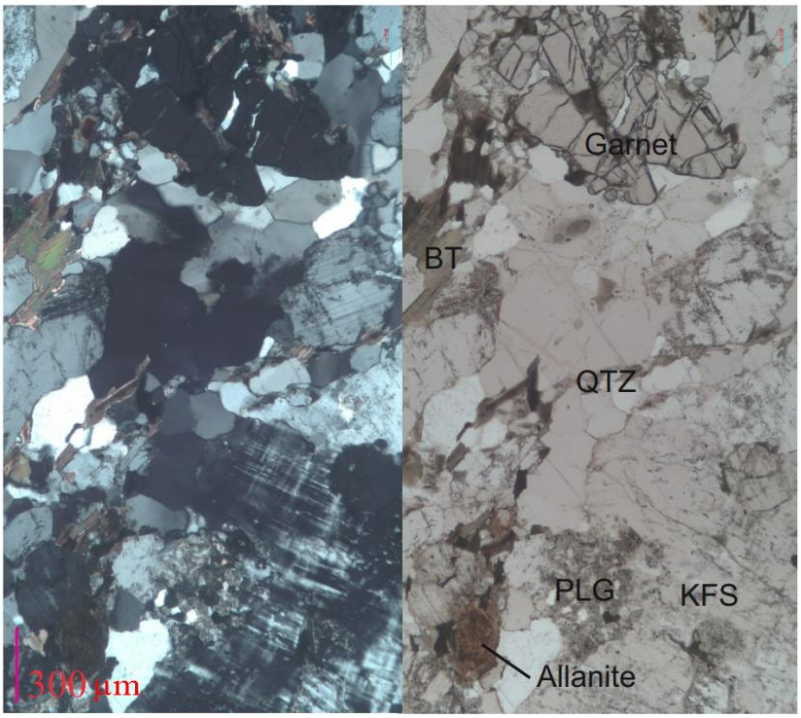

Figure 9. Sample VSVE-2021-10, Main minerals in this thin section are plagioclase (PLG) and potassium feldspar (KFS). Biotite (BT), garnet and allanite are found as accessory minerals. On the left in XPL and on the right on PPL.

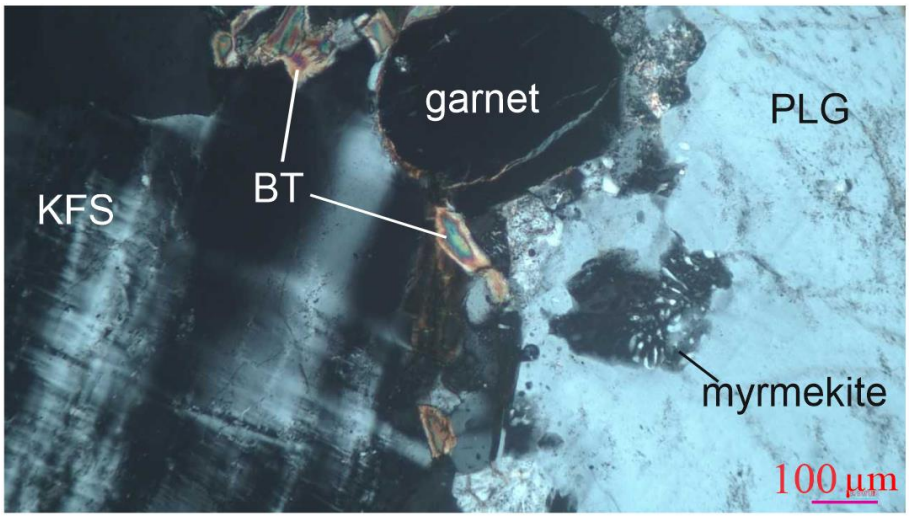

Figure 10. This picture is from the sample VSVE-2021-10. Small myrmekite grain inclusion is found inside of plagioclase (PLG). Other minerals in this thin section were potassium feldspar (KFS) and biotite (BT). Picture taken in XPL.

4.2.4 Plutonic rocks: diorite

Sample MOTU-2021-9.1 is based on modal composition a diorite. Main minerals found in this sample are plagioclase (labradorite), biotite, clinopyroxene (Figure 11) and hornblende. Accessory minerals are quartz, chlorite and titanaugite (Figure 11). This sample has subhedral granular texture and grain size varies between 1 and 3 mm in diameter.

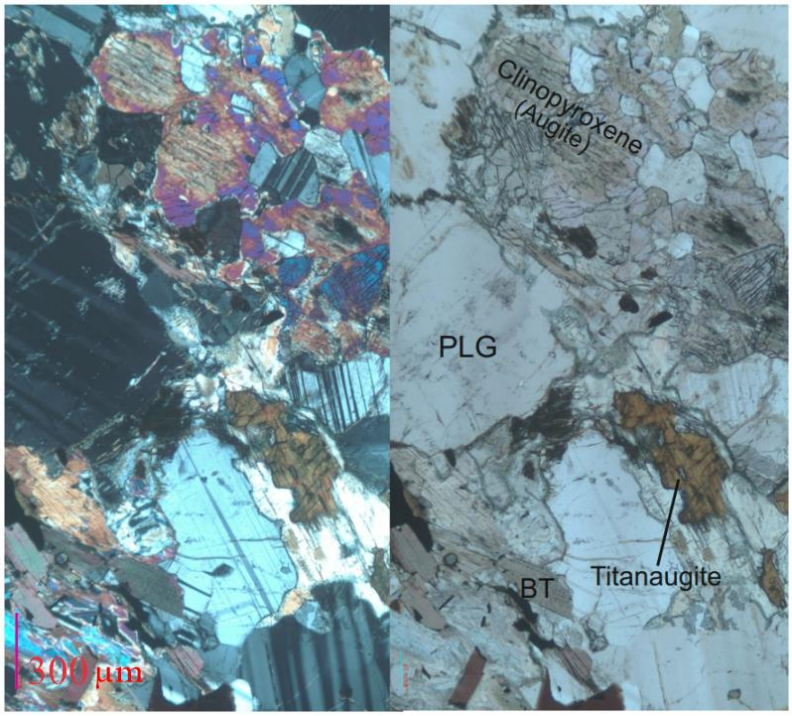

Figure 11. Pictures from the sample MOTU-2021-9.1. In this sample titanaugite can be seen inside clinopyroxene (augite) grains. Other minerals seen in this picture are plagioclase (PLG) and biotite (BT). On the left in XPL and on the right in PPL.

4.2.5 Gneisses

Gneisses form a group of samples that have similar modal composition to tonalite, granodiorites, and granites. Gneisses with equal modal compositions to tonalite were named hornblende-biotite gneisses and biotite-hornblende gneisses. Biotite-potassium-feldspar gneisses have modal composition of granites and granodiorites. Accessory minerals in gneissic rocks are compatible to plutonic rocks, titanite, chlorite, zirconium and allanite are commonly found. Gneisses have smaller grain size than plutonic rocks (≤1 mm). Anhedral granular texture is common in gneissic samples, with exception of one protomylonite. Gneissic banding and shearing (Figure 12) are visible in some thin sections. Poikilitic hornblende is common (Figure 13), and two samples have corona texture of hornblende and white clinoamphibole.

Mineral alterations are similar to plutonic rocks. Plagioclase grains are partly sericitized. Clinopyroxene has completely uralitized to hornblende. Potassium-feldspar in gneisses, can be seen in larger grains, or in grains surrounded by quartz and myrmekites, like in granodiorites and granites.

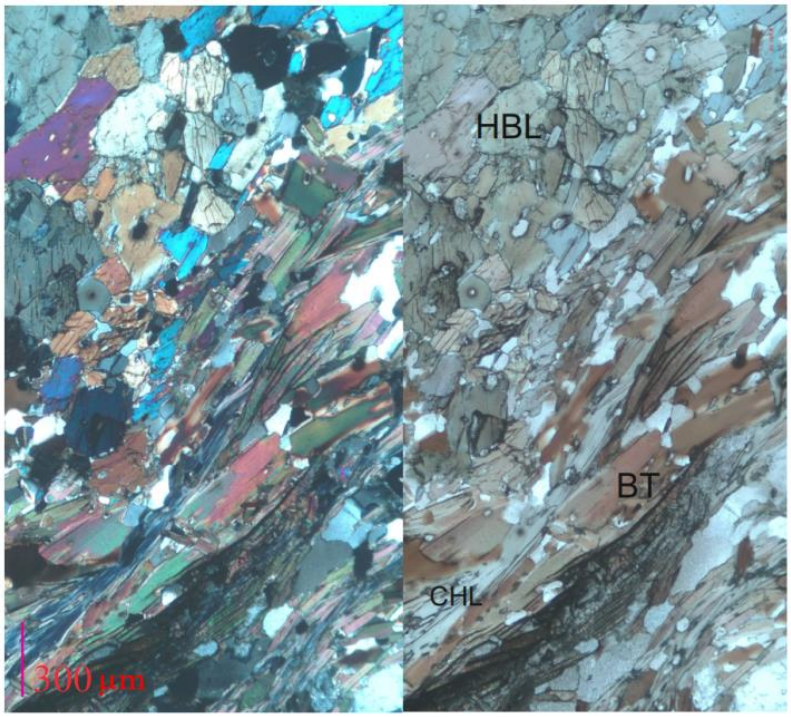

Figure 12. Picture is from the sample KK8$-2020-603.5, chlorite-biotite-hornblende gneiss. In this sample biotite (BT) and its alteration product chlorite (CHL) form continuous banding along the thin section. Other minerals seen in this picture are hornblende (HBL). On the left is picture in XPL and on the right with PPL.

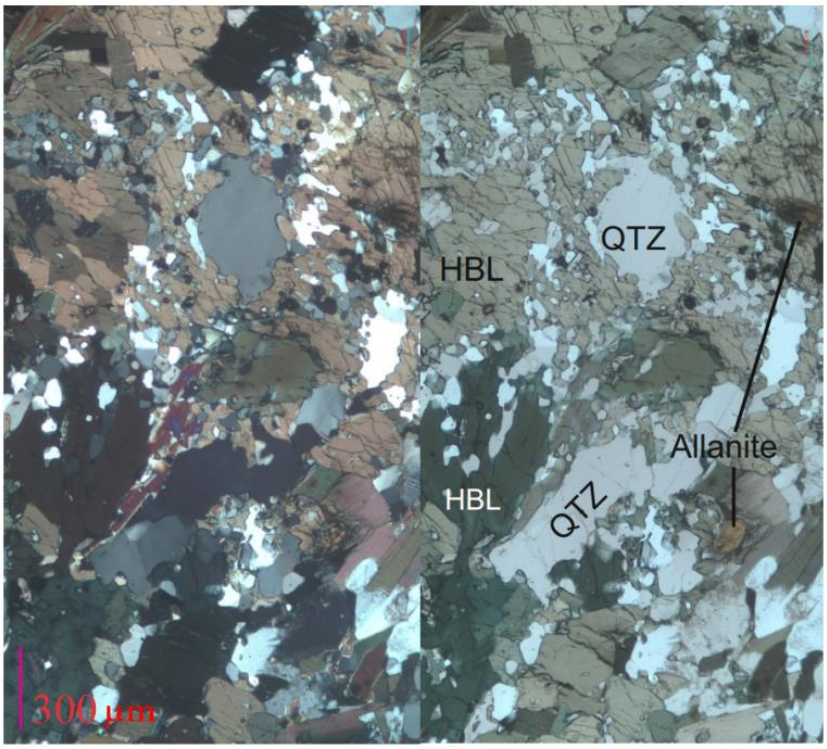

Figure 13. Picture from the sample KK8$-2020-706.3, which was hornblende k-feldspar biotite gneiss. Hornblende (HBL) has poikilitic texture in this sample. Other minerals seen on this picture are allanite and quartz (QTZ). On the left in XPL and on the right in PPL.

4.2.6 Dikes

Based on their modal composition the dikes are tonalites, granodiorites and granites. Half of the dikes are leucocratic and overall, the dikes are the most felsic rocks from Pasalanmäki. Main minerals in all the dikes are quartz and plagioclase, K-feldspar is found in granitic and granodioritic samples. Common accessory minerals are allanite, muscovite, titanite and zircon. Two samples contain euhedral garnet as accessory mineral (Figure 13). Common mineral alteration in dikes are plagioclase sericitization to muscovite (Figure 14). Most of the dikes have anhedral granular texture and two samples were sheared. Grain size varies from 1-2 mm in diameter to 4 mm in sheared/protomylonite rocks.

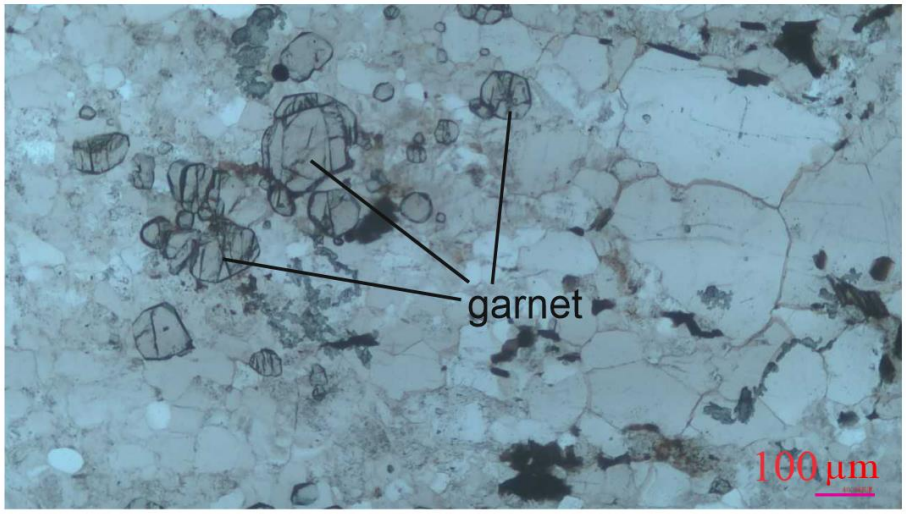

Figure 13. Picture of the sample KK8$-2020-611 in PPL showing small garnet grains in the sample.

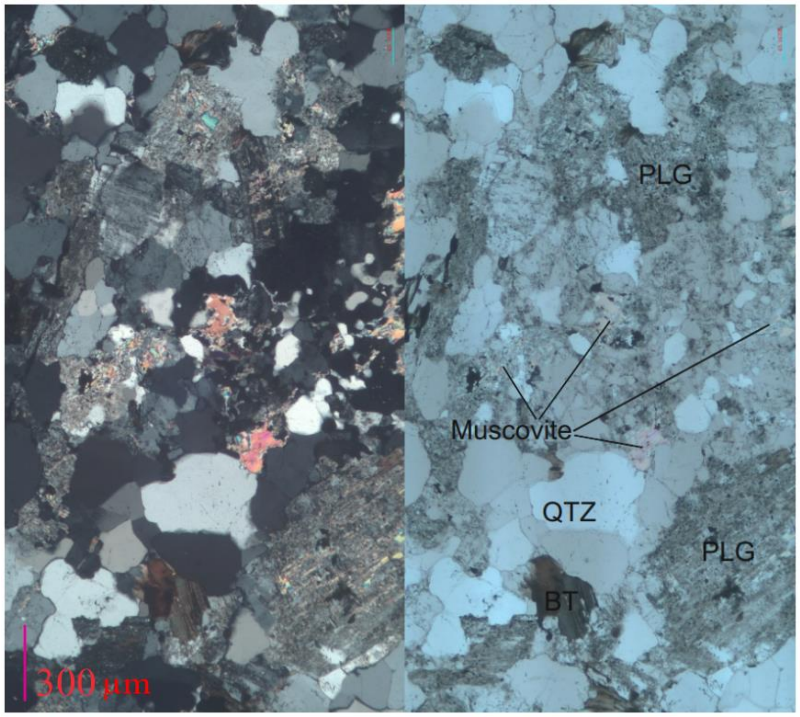

Figure 14. Pictures from the sample KK8$-2020-104, in this sample the plagioclase (PLG) sericitization to muscovite had affected all plagioclase grains. Other mineral seen in this thin section are quartz (QTZ) and biotite (BT). On the left picture in XPL and on the right in PPL.

4.3 Results from the geochemistry

Tonalite and gneiss group samples have similar geochemistry in main and trace elements and therefore are considered to be geochemically one group. As a group the granodiorites are distinctively more felsic than the tonalites and gneisses. Granite and diorite have varying geochemical properties. Dikes created the sixth group based on field notes and modal composition. All samples, but four, plot into calc-alkaline series field in AFM diagram (Figure 15).

In figures 16-20, the analyses are compared to syntectonic plutonic rocks (1.90 – 1.88 Ga old) from the south-eastern margin of Central Finland Granitoid Complex (Heilimo et al. 2018) and to 1.93-1.91 Ga older Svecofennian (referred also as preorogenic) tonalites and associated supracrustal rocks from the Rautalampi area (Lahtinen 1994). Comparison fields in figures 16-19 are drawn with 95 % accuracy.

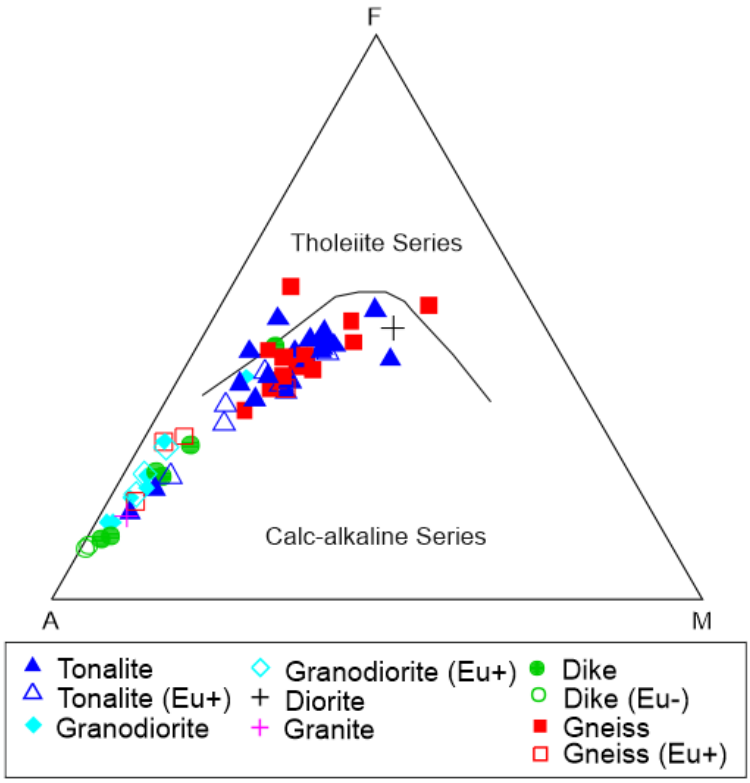

Figure 15. AFM diagram for distinguishing tholeiite series rocks and calc-alkaline series rocks from each other. AFM diagram after Irvine and Baragar (1974).

4.3.1 Geochemistry of tonalites and gneisses

On total alkali versus silica (TAS) diagram tonalite and gneiss analyses plot mostly to the diorite, monzonite and granodiorite fields (Figure 16). Most felsic samples in tonalite and gneiss groups have according to TAS a granitic composition. On Al_2O_3/Na_2O+K_2O versus $Al_2O_3/CaO+Na_2O+K_2O$ (A/NK versus A/CNK) diagram, most of the samples in tonalite and gneiss analyses are metaluminous, where some of the analyses from both groups, represent peraluminious compositions (Figure 17).

Silica (SiO_2) content varies in tonalite and gneiss samples from 53 to 76 wt. %, majority being compositionally intermediate rocks (Figure 18). The concentration of Al_2O_3 varies between 12 and 19 wt. % and displays larger scatter in the intermediate samples than in the felsic samples (Figure 18 A). MgO, FeOt and CaO have negative correlation with SiO_2. In tonalites and gneisses, MgO content varies between 1 and 5 wt. % (Figure 18 B). Mafic gneisses and tonalites have concentrations of FeOt > 10 wt. % and more felsic samples 1 wt. % > FeOt (Figure 18 C). Mafic tonalites and gneisses (SiO_2 < 60 wt. %) have generally CaO < 6 wt. %, and most felsic samples have less than 1 wt. % of CaO in them with exception of felsic gneisses, where SiO_2 is more than 65 wt. %, that have CaO < 2 wt. % (Figure 18 D).

Alkalis (K_2O and Na_2O) do not correlate with SiO_2. Tonalites and gneisses have generally low K_2O content, less than 3 wt. % and only three gneisses and three tonalites, that have more felsic composition, have K_2O higher than 4 wt. % (Figure 18 E). The amount of Na_2O in all the tonalite samples is more than 3 wt. %, and only one gneissic sample has less than 3 wt. % of Na_2O in it (Figure 18 F). Tonalites that have positive Eu-anomaly are generally depleted in K_2O and gneiss analyses that have positive Eu-anomaly are generally enriched in K_2O when compared to other analyses.

From large ion lithophile elements (LILE), rubidium (Rb), barium (Ba) and strontium (Sr), do not have a clear correlation with SiO_2 (Figure 19). All tonalite and gneiss analyses have less than 2000 ppm of Ba in them (Figure 19 A). Rb content varies from 50 ppm to 150 ppm (Figure 19 B). In all the samples, except from one gneiss analyse, the Sr content is 200-900 ppm (Figure 19 C).

From high field strength (HFS) elements, cerium is commonly low (<100 ppm) in tonalites and gneisses when compared to granodiorites and dykes with exception of one tonalite sample that has over 250 ppm of Ce (Figure 19 D). In intermediate rocks the concentration of yttrium varies between 10 and 40 ppm and in most felsic analyses Y concentrations can be less than 10 ppm (Figure 19 E). Zircon content varies from 50 ppm to 200 ppm, excluding four outliers with Zr > 300 ppm (Figure 19 F).

Tonalites and gneisses display similar rare earth element (REE) patterns (Figure 20 A, B). Analyses in both groups, tonalites and gneisses, have variable Eu-anomalies, ranging from strongly positive to slightly negative, Eu/Eu*= 0.67-5.82, with exception of two tonalites that have Eu/Eu* < 0.5. All samples display LREE/HREE fractionation with $(La/Yb)_n$ varying between 2.5 and 72.9. Samples with positive Eu-anomalies have lower total REE concentrations then the samples with negative Eu-anomalies (Figure 20 A, B).

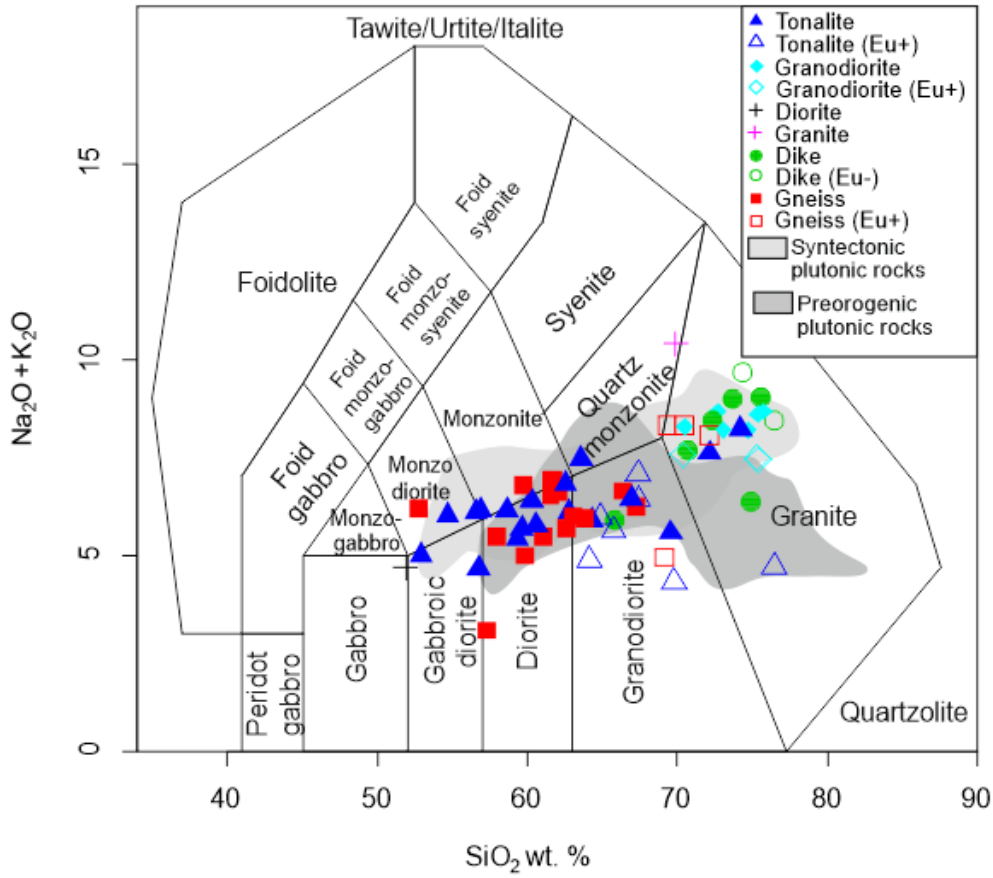

Figure 16. Total alkali versus silica (TAS) diagram (Middlemost 1994) with studied samples. Analyses are compared to Syntectonic (1.90–1.88 Ga; Heilimo et al. 2018) analyses and preorogenic analyses (older Svecofennian magmatism; 1.93–1.91 Ga; Lahtinen 1994).

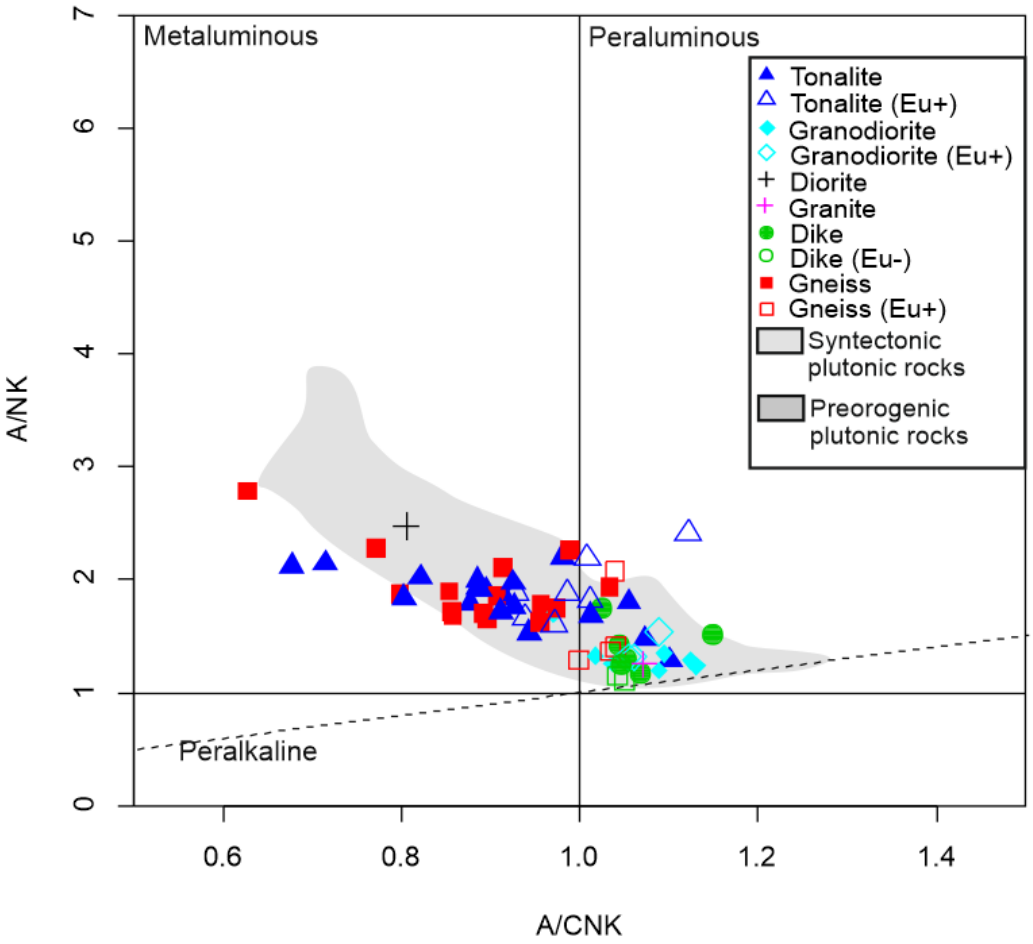

Figure 17. A/NK (Al_2O_3/Na_2O+K_2O) versus A/CNK ($Al_2O_3/CaO+Na_2O+K_2O$) diagram for discriminating metaluminous and peraluminous rocks from each other, with studied samples and syntectonic comparison data. A/NK versus A/CNK from Shand (1943).

4.3.2 Geochemistry of diorite

The sample classified mineralogically as diorite plots on the boundary between gabbro and gabbroic diorite on the TAS diagram (Figure 16). On the A/NK vs. A/CNK plot the diorite has metaluminous composition (Figure 17). Diorite analyse has relatively high Al_2O_3 (17 wt. %) when compared to rest of the samples (Figure 18 A). It has almost 6 wt. % of MgO, almost 10 wt. % of FeOt and 8 wt. % of CaO in it, similarly to most mafic tonalite and gneiss analyses (Figure 18 B-D). K_2O and Na_2O contents are comparable to tonalite and gneiss groups more mafic samples, K_2O being less than 2 wt. % and Na_2O being slightly over 3 wt. % (Figure 18 E, F).

In LILEs, the diorite sample has similar chemical properties as the most mafic tonalites and gneisses (Figure 19). Barium concentration is less than 1000 ppm and Rb concentration less

than 50 ppm (Figure 19 A, B). Concentration of Sr is moderate when compared to other samples in this study, slightly over 600 ppm (Figure 19 C). In HFS-cations, the sample has 50 ppm of Ce, 25 ppm of Y, and 100 ppm of Zr, similarly the most mafic tonalite and gneiss analyses (Figure 19 D – F). Diorite analysis is relatively enriched in LREEs and relatively poor in HREEs (Figure 20 B), where $(La/Yb)_n$ value is 7.1. This sample has very weak negative Eu-anomaly, Eu/Eu*= 0.91, similarly to some tonalite and gneiss analyses.

4.3.3 Geochemistry of granodiorites

Granodiorites form a group that on the TAS plot into the granite and granodiorite fields (Figure 16). On A/NK vs. A/CNK all analyses except from one, are peraluminous in composition (Figure 17). SiO_2 content of the analyses varies between 63 wt. % and 76 wt. %, most of the samples in this group having > 67 wt. % of SiO_2 (Figure 18). Granodiorite samples have Al_2O_3 content of 16-12 wt. % (Figure 18 A). All analyses in this group have less than 1 wt. % of MgO, with exception of one intermediate composition sample (Figure 18 B). FeOt and CaO content of the granodiorite analyses is less than 5 wt. % similarly to dikes and felsic tonalites and gneisses (Figure 18 C and D). Most of the granodiorite analyses have more than 3 wt. % of K_2O in them and all analyses have less than 4 wt. %, some even < 3 wt. %, of Na_2O, which sets this group aside from the tonalite and gneiss groups (Figure 18 E, F).

From LILE concentration, all granodiorites have less than 2000 ppm of Ba, over 50 ppm of Rb varying to the one sample that has over 200 ppm of it (Figure 19 A, B). Sr content is less than 400 ppm in eight out of ten samples (Figure 19 C). From HFS-elements, Ce content of the samples varies between 50 ppm to over 200 ppm in one of the analyses (Figure 19 D).
Concentration of Y in granodiorites is commonly ~ 10 ppm with exception of one sample that has over 30 ppm of Y. (Figure 19 E). The amount of Zr varies in the analyses from 100 ppm to 400 ppm (Figure 19 F).

In granodiorites, similar REE patterns are observed as in tonalites and gneisses (Figure 20 A-C). Samples are relatively enriched in LREE elements, have $(La/Yb)_n$ of 9,1-74,0 and have variable Eu-anomalies, with Eu/Eu* ranging from 0.30 to 2.60 (Figure 20 C). As an exception from the tonalites and gneisses, some granodiorites with positive Eu-anomalies have slight relative enrichment in thulium, ytterbium and lutetium HREEs in them.

4.3.4 Geochemistry of granite

Sample that based on modal composition is granite, falls into quartz monzonite field on the TAS diagram (Figure 16). Based on the A/NK vs. A/CNK diagram the granite sample is peraluminous in composition (Figure 17). Granite sample has 69 wt. % of SiO_2 and 15 wt. % of Al_2O_3 in it (Figure 18 A). The analyse has less than 1 wt. % of MgO in it (Figure 18 B). FeOt and CaO concentrations in the granite sample are less than 2 wt. % (Figure 18 C, D). The granite sample differs from all the other samples in the potassium oxide and sodium oxide concentrations (Figure 18 E, F). Granite sample has over 8 wt. % of K_2O in it, and less than 2 wt. % of Na_2O.

From LILEs, this analyse is enriched in Ba, having concentration of over 5000 ppm in it (Figure 19 A) Concentrations of Rb is 150 ppm and Sr is 500 ppm. (Figure 19 B, C). In HFS-elements, this sample has low concentrations of Ce and Zr, both being less than 50 ppm and 20 ppm on Y (Figure 19 D-F). Granite has a differing REE-patterns when compared to other samples in this study (Figure 20). Granite analyse is relatively weakly enriched in LREE and displays only weak LREE/HREE fractionation ($(La/Yb)_n$=2.0) and weakly negative Eu-anomaly (Eu/Eu* = 0.79).

4.3.5 Geochemistry of dikes

All dikes have SiO_2 concentration of more than 65 wt. %, but seven samples out of eight have SiO_2 content of > 70 wt. % (Figure 16), making the dikes the most felsic group of rocks in Pasalanmäki. On TAS the dike group samples plot into granite and granodiorite field and in A/NK vs. A/CNK all samples are peraluminous (Figures 16 and 17).

The amount of Al_2O_3, MgO, FeOt and CaO have negative correlation with the concentrations of SiO_2. Al_2O_3 content of the samples is quite similar, varying between 13 wt. % and 15 wt. % (Figure 18 A). All dike samples have less than 1 wt. % of MgO, excluding the SiO_2 poorest sample which has 2 wt. % of MgO (Figure 18 B). FeOt. varies in these samples from 6 wt. % to < 1 wt. % (Figure 18 C). All samples have less than 4 wt. % of CaO in them (Figure 18 D). The dike samples have high content of K_2O in them, six out eight samples have potassium oxide content above 4 wt. % (Figure 18 E). Amount of Na_2O varies in this group, some of the samples having more than 4 wt. % of Na_2O and some samples having just 2 wt. % in them (Figure 18 F).

From LILEs, the dikes have similar amounts of Ba (< 2000 ppm) compared to other groups of this study (Figure 19 A). Two of the dike samples seem to be enriched in Rb (> 250 ppm), when compared to other dike analyses that have less than 150 ppm of Rb (Figure 19 B). Dike analyses have all less than 400 ppm of Sr in them (Figure 19 C). The concentration of Ce in these samples ranges from low (< 50 ppm), when compared to other studied samples, to over 100 ppm. The amount of Y varies between 10 ppm and 70 ppm. Zr concentration ranges between 50 ppm and 400 ppm, where 50 ppm are some of the lowest Zr concentrations found in studied samples and 400 ppm being one of the highest concentrations found in the samples used for this study (Figure 19 D-F).

In the dike group there are two distinctively different REE-patterns (Figure 20 D). Six samples out of eight have been relatively enriched in LREEs, where $(La/Yb)_n$ varies between 8.5 and 35.4, as most of the other samples in this study. They have negative Eu-anomalies (Eu/Eu* = 0.47 – 0.68) and have relatively low amounts of HREEs. The two other dike analyses display enrichment in HREE relative to LREE with $(La/Yb)_n$ values 0.54 and 0.66 together with strongly negative Eu-anomalies (Eu/Eu* = 0.09-0.1).

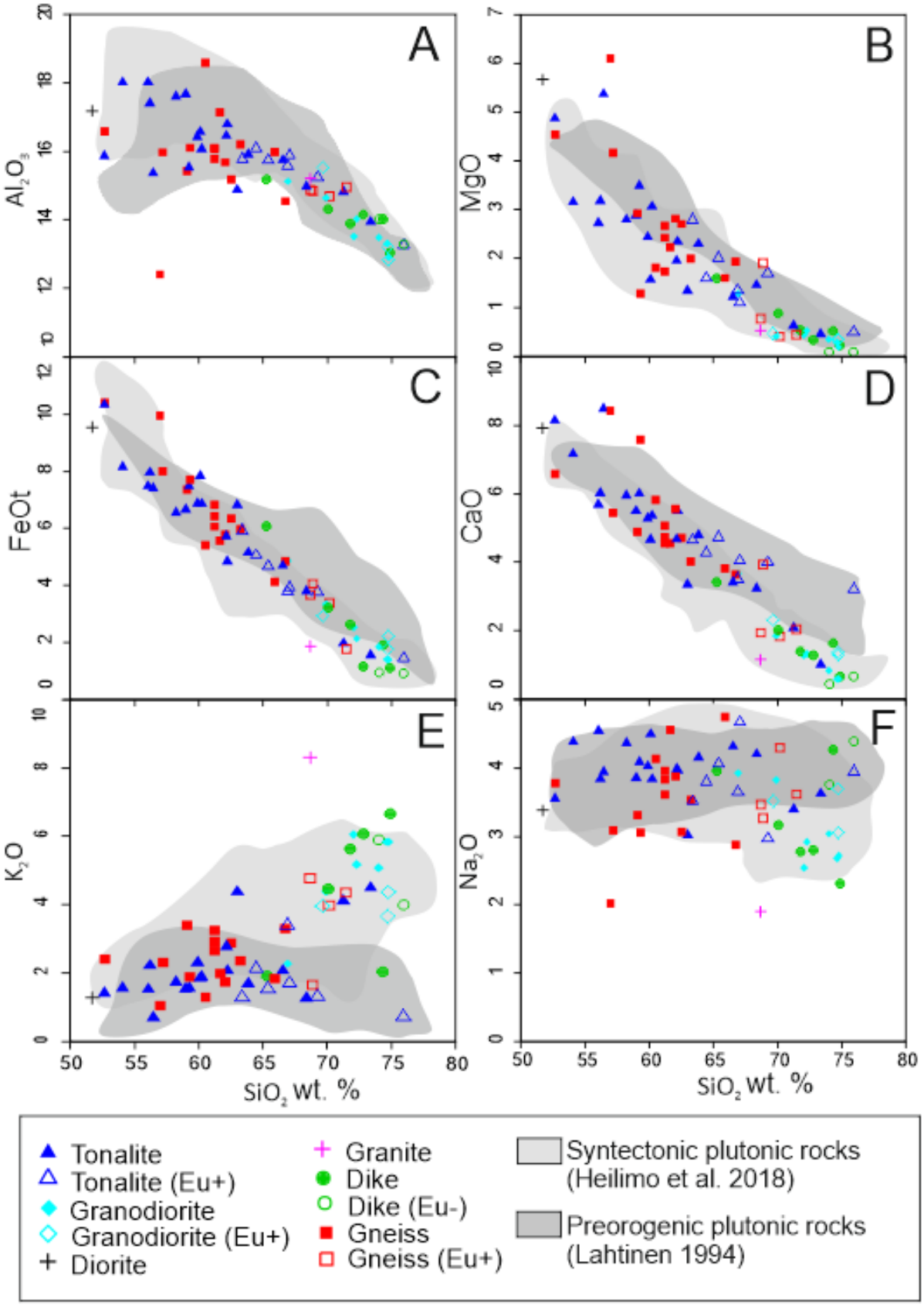

Figure 18. Harker diagrams for major elements of the studied samples, with syntectonic and preorogenic plutonic rocks. A) Al_2O_3, B) MgO, C) FeOt, D) Cao, E) K_2O, and F) Na_2O.

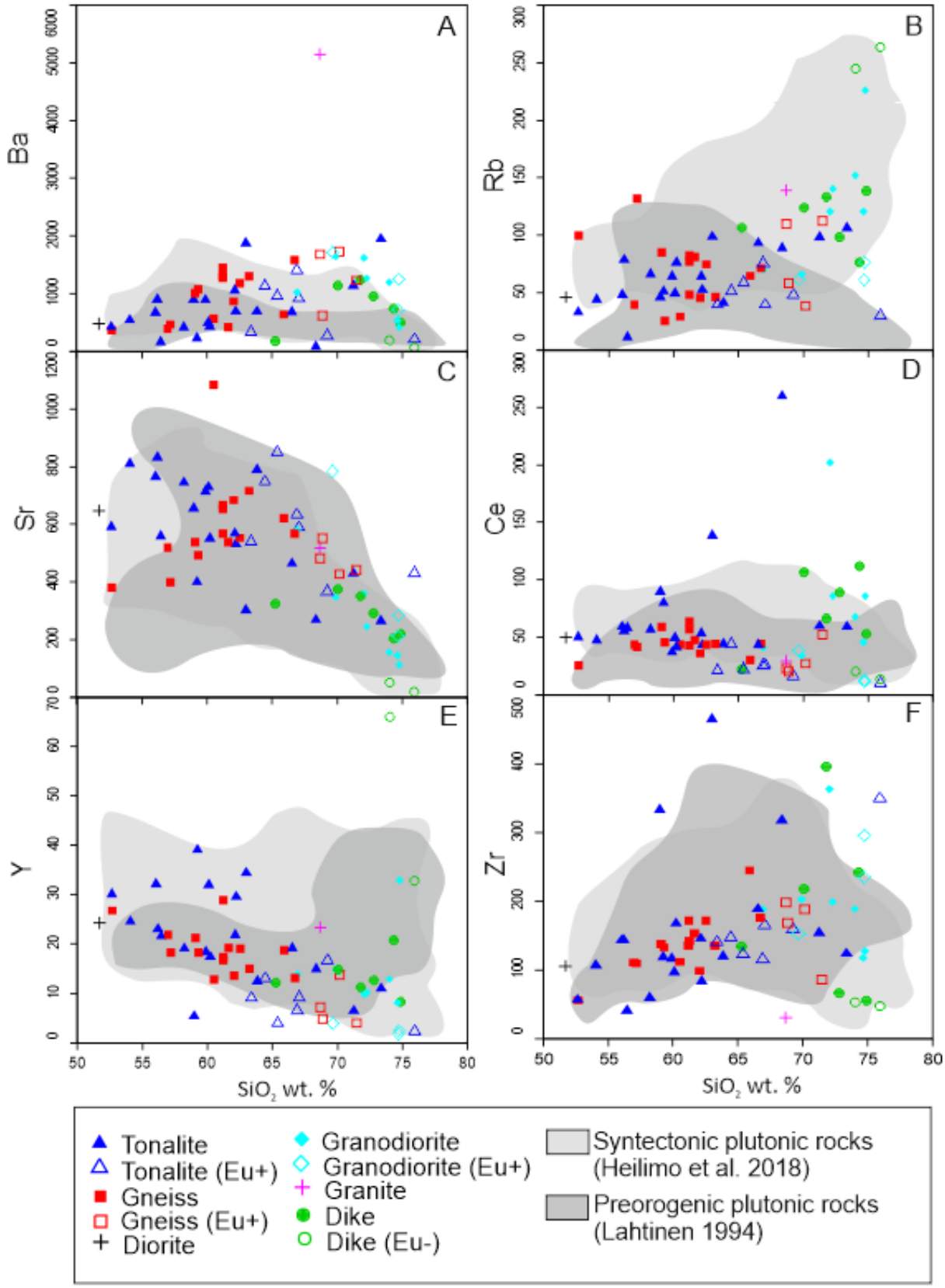

Figure 19. Harker diagrams for trace elements with syntectonic plutonic rocks and preorogenic plutonic rocks. A) Ba in ppm, B) Rb in ppm, C) Sr in ppm, D) Ce in ppm, E) Y in ppm, and F) Zr in ppm.

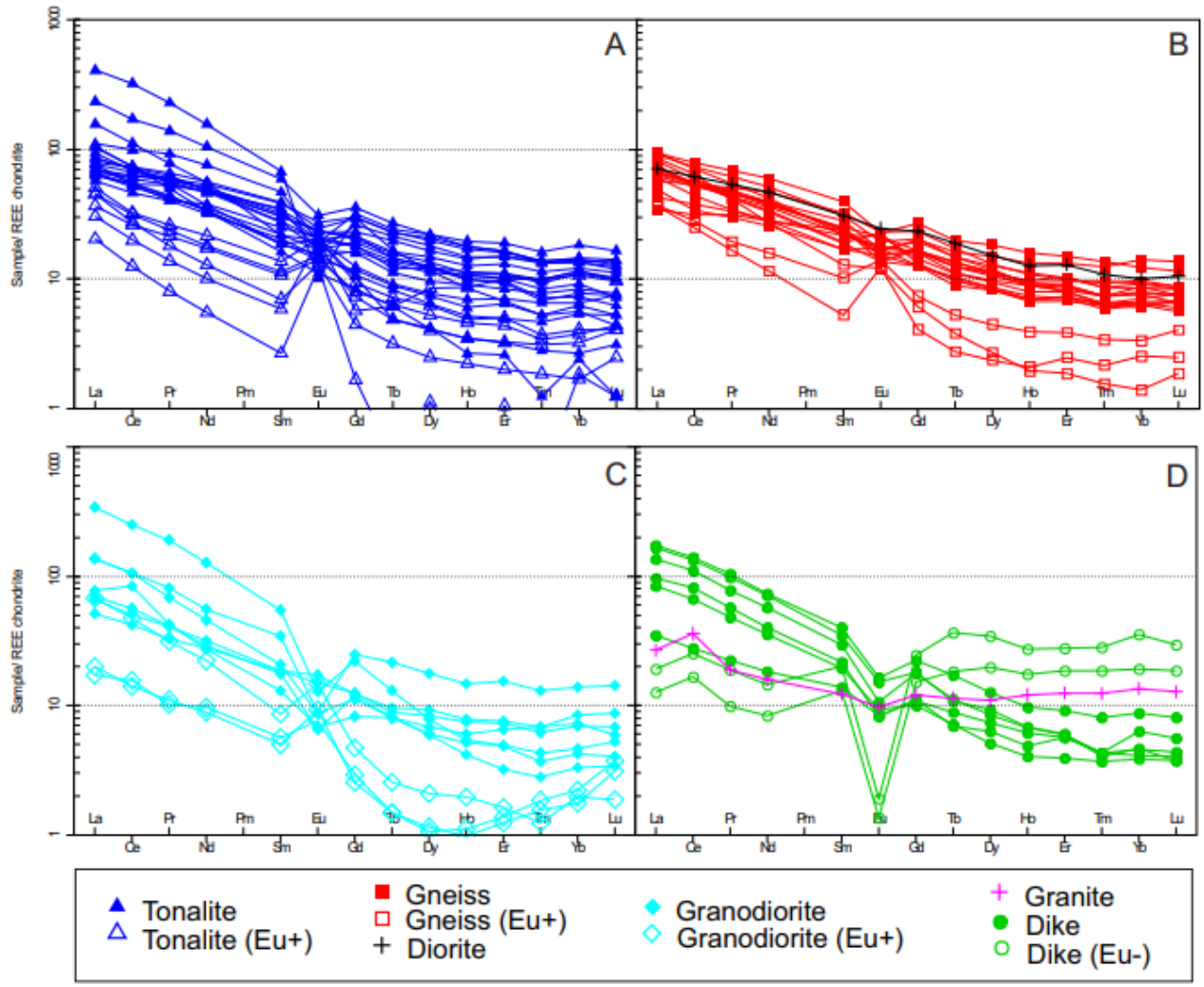

Figure 20. REE plots for the studied samples. REE chondrite values after Boynton (1984). A) Tonalite groups samples, B) gneisses and diorite samples. C) Granodiorite samples. D) Dikes and granite samples. Analyses that have distinctively different Eu-anomaly when compared to other analyses in the same group are marked with different symbol.

5. Discussion

5.1 Comparison, tectonic setting and source of Pasalanmäki tonalites and gneisses

Tonalites and gneisses predominantly have same parental magma based on the similar geochemical characteristics (Figures 15-20). Based on the syntectonic comparison data (Heilimo et al. 2018) and preorogenic (older Svecofennian magmatism; Lahtinen 1994) it seems that the tonalite and gneiss groups have similar geochemical characteristics to both preorogenic and syntectonic rocks. The more felsic group created by granodiorites and dikes has similarities only with the syntectonic comparison data. The studied samples have many similarities with island arc magmatism related rocks, indicating that these samples could originate from island arc magmatism as well. Some of the studied samples have adakitic features in them and indicators of fractionating crystallization in the stability fields of amphibole and garnet.

5.1.1 Island arcs; subduction related origin of the Pasalanmäki bedrock

Studied samples from the Pasalanmäki area have similar geochemical features to Svecofennian syntectonic plutonic rocks and to preorogenic/ early Svecofennian magmatism plutonic rocks, which were both arc magmas (Heilimo et al. 2018; Lahtinen 1994), indicating that these samples could have island arc or continental arc magma type origin. This idea is supported by the overall tectonic development of the Leppävirta-Rautalampi-Karttula area, where island arc(s) and arc magmatism were at least according to Lahtinen (1994), Lahtinen et al. (2005) and Nironen (2017) present during early stages of Svecofennian orogeny.

Another common rock type from this area from the early stages of Svecofennian orogeny were paragneisses and other metamorphosed sedimentary rocks, but metaluminous nature of the studied samples, overall, the amount of Al_2O_3 in the studied samples (Figure 18 A), mineralogy and petrography of the studied samples implies that these rocks aren't paragneisses or S-type plutonic rocks derived from them. Lack of Archean zircons from the rocks in the study area (Tuppurainen et al. 2022) implies that the Archean basement was also an unlikely source for these rocks.

Island arcs are formed in a subduction environment where oceanic plate is subducting under another oceanic plate (eg. Gill 1981). The structure of the island arc formation is complex and

often several units related to the island arc are formed. These are fore arc, a type of sedimentary basin, which forms in between subduction zone and the island arc. Behind the island arc, a back arc basin is formed, where volcanism is often MORB-type. Occasionally, after the development of island arc belt, a secondary arc is formed later behind the main arc (eg. Gill 1981).

It is hard to distinguish primitive arc magmas because characteristics of the arc magma can be altered in many ways, the melting source can have varying composition, depth and the degree of the source melting varies (Pearce 1984). Also fractional crystallization and magma mixing can take place in arc environment and alter the compositions as well. More felsic rocks formed in island arc setting are usually tonalites, granodiorites and quartz diorites, having hornblende and biotite as the most common mafic minerals (Pearce 1984), similarly to majority of the samples in this study. Gneisses and tonalites in this study are mostly metaluminous in nature, grading into peraluminous (Figure 17), which is characteristic to island arc granites. Majority of the subduction related magmas, including arc magmas, are calc-alkaline in nature and only most primitive island arc granites can be tholeiitic in nature. Most of the studied samples in this study create a continuous line in AFM diagram on the calc-alkaline series (Figure 15). The content of Y is commonly less than 30 ppm in volcanic arc granites (SiO_2 varies between 56 and 80 wt. %) and content of Rb less than 100 ppm (Pearce 1984). Based on figures 19 B and E, tonalite and gneiss samples in this study have similar amounts of Y and Rb as volcanic arc granites.

Island arc magmas can be divided into high-K, medium-K and low-K groups based on potassium content (Gill 1981). In high-K and medium-K island arc magmas the REE-content has similar features as in REE-patterns of the studied samples, where the rocks are enriched in LREE when compared to HREE. Enrichment of LREE and overall fractionated REE-patterns in general is typical for island arc magmas (Tatsumi et al. 1986). This type of REE-patterns are seen on these samples (Figure 20), which could support the island arc origin of this bedrock. Negative niobium and titanium anomalies on primitive mantle normalized spider diagrams can be considered to be an evidence of arc magmatism as well (Tatsumi et al. 1986), such anomalies are shown by most of the tonalite, diorite and gneiss analyses (Figure 21).

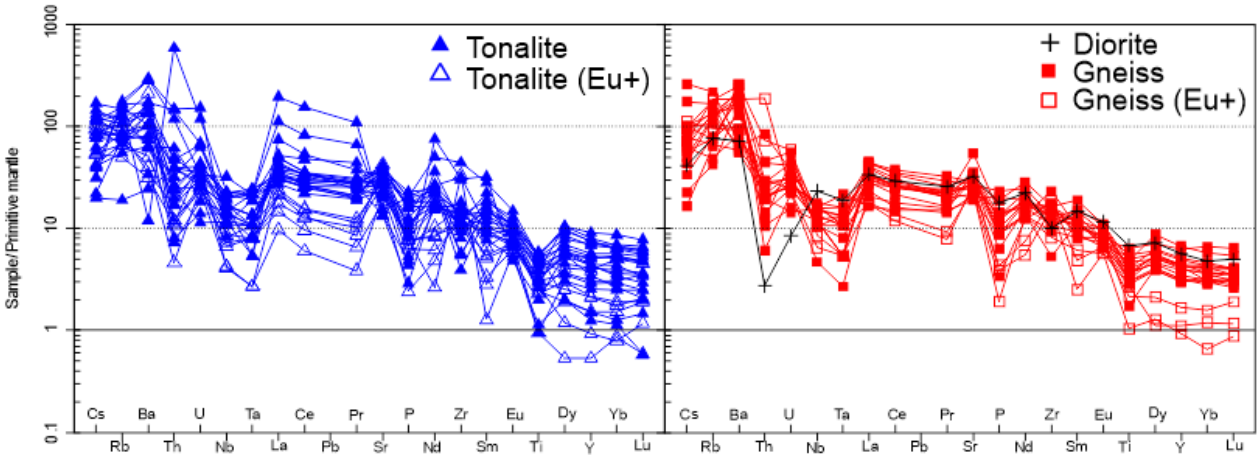

Figure 21. Studied samples normalized to primitive mantle after McDonough and Sun (1995) values.

5.1.2 Chemical similarities to preorogenic and syntectonic rock geochemistry

Studied tonalites and gneisses have based on major element data, trace element data and REE-distribution similarities with syntectonic (Svecofennian orogeny) 1.88-1.87 rocks. The preorogenic age (older Svecofennian magmatism; 1.93 to 1.91 Ga old bedrock) of the studied bedrock is supported by a study made by (Tuppurainen 2022).

From Heilimo et al. (2018) study, these rocks were compared to samples from Kangasniemi granodiorites (in Pirkanmaa intrusive suite), Jyväskylä suite (including Muurame lithodeme and Vaajakoski lithodeme) and Oittila suite, all which had SiO_2 of more than 50 wt %. Kangasniemi granodiorites are ca. 1895 Ma old intermediate to felsic variably deformed granodiorites and tonalites. In chondrite normalised REE patterns, they have weakly negative Eu-anomalies and are enriched in LREE, when compared to HREE, which is a similar chraracteristic to samples from this study (Figure 20). Rocks in this lithodeme are formed in arc environment. Jyväskylä suite (Muurame lithodeme and Vaajakoski lithodeme) are 1885-1880 Ma old intermediate to felsic granitoids and quartz diorites. From these two lithodemes the Muurame lithodeme has distinctive negative Eu-anomaly whereas Vaajakoski lithodeme doesn't have a visible Eu-anomaly on chondrite normalised REE-diagrams. The enrichment of the LREE elements when compared to HREE elements in Vaajakoski lithodeme is similar to studied gneiss and tonalite samples (and occasionally granodiorites and dikes) as seen in this study. Both of these lithodemes were formed in arc environment as well.

The Oittila suite is the youngest (1875 Ma) and most felsic suite of the used syntectonic comparison data. Rocks in this suite form mostly granodioritic and granitic dikes. Most of the samples in Oittila suite show distinctive negative Eu-anomalies similarly to seen in the dikes in this study. Relative enrichment of HREE in two studied dike samples (20 D) is similar to enrichment of HREE in some samples in Oitttila suite.

From the study made by Lahtinen (1994) the samples in this study were compared to all studied non s-type gneisses and tonalites/amphiboles samples from the Rautalampi area including Rastipää, Tyyrinmäki and Pukkiharju area, and the reference data from closely surrounding areas (Kangasjärvi, Leväniemi, Pielavesi, Venetpalo), that had SiO_2 content of more than 50 wt. %.

From the two groups in the study made by Lahtinen (1994), divided based on yttrium content, none of the samples in this study seem to be compatible with the high-Y group. Majority of the analyses in this study have when compared to SiO_2 negative correlation with Y (19 E), which is incompatible with the comparison data high-Y group where Y and SiO_2 correlate positively. High-Y group samples have higher CaO and FeO values in Harker diagrams than the low-Y group, and from the samples in this study, none of the samples seem to be compatible with those features either (18 C, D). Samples in the low-Y group (including most of the reference samples from the surrounding area) had varying Eu-anomalies and enrichment of LREE when compared to HREE, which is a similar geochemical characteristic to the samples used in this study (Figure 20). The studied rocks in the study from Lahtinen (1994) represent a primitive island arc setting changing to a more evolved arc environment and some of the samples had indications of depleted mantle and a subducting component as a source for magmatism. The high-Y group was formed from residue melts of tholeiitic island arc basalt melts.

As the preorogenic analyses and syntectonic analyses have compatible major and trace element concentrations, it is hard to distinguish the studied analyses to be either preorogenic or syntectonic based on geochemistry. Overall, tonalites and gneisses have partly similarities with the preorogenic reference data, but granodiorites and especially younger dykes do not have consistent geochemical similarities with preorogenic plutonic felsic rocks (Figures 18, 19 & 20 C, D).

5.1.3 Adakite like chemical features: amphibole fractionation and garnet control

Adakites are group of rocks that have distinctive geochemical features, and they most likely originate from a certain geotectonical setting (Moyen 2009). Defant and Drummond (1990) defined adakites to be rocks that have more than 56 % wt. of SiO_2, at least 15 wt. % of Al2O3, at least 3.5 wt. % of Na_2O and usually less than 3 wt. % of MgO in them. To this Martin et al. 2005 added that adakites should have K_2O/Na_2O ratios around 0.4 and #mg should be around 50. The studied samples from Pasalanmäki have chemical features in major and trace elements and in REE-chemistry that indicate that some of the rocks in this study are adakites. Adakites are thought to be arc rocks that were formed in a subduction environment from basaltic slab melts (Defant and Drummond 1990; Martin 1999; Martin et al. 2005; Moyen 2009). This theory was further developed by Martin et al. (2005) who estimated that adakites originate from slab melts that have been chemically modified by mantle wedge and mantle peridotite. Macpherson et al. (2006) and Castillo (2012) interpreted that the adakites are produced in arcs, in subduction environments, only from basaltic magmas derived from mantle wedge, without slab melts.

Especially from the gneiss and tonalite groups majority of the samples have more than 56 wt. % of SiO_2 and more than 15 wt. % of Al_2O_3, at least 3.5 wt. % of Na_2O and less than 3 wt. % of MgO (Figure 18 A, B, F) as well as majority of the reference data. Most of the studied samples and comparison data don't have #mg of 50 or more and only few samples seem to have K_2O/Na_2O ratios of 0.4 (Figure 22 A & B). #Mg values of 40 would represent more ordinary island arc magmas (Moyen 2009). In figure 21 the positive Sr anomaly can be considered to be an adakitic feature as well, whereas negative Ti-anomaly is not common in adakties (Moyen 1999).

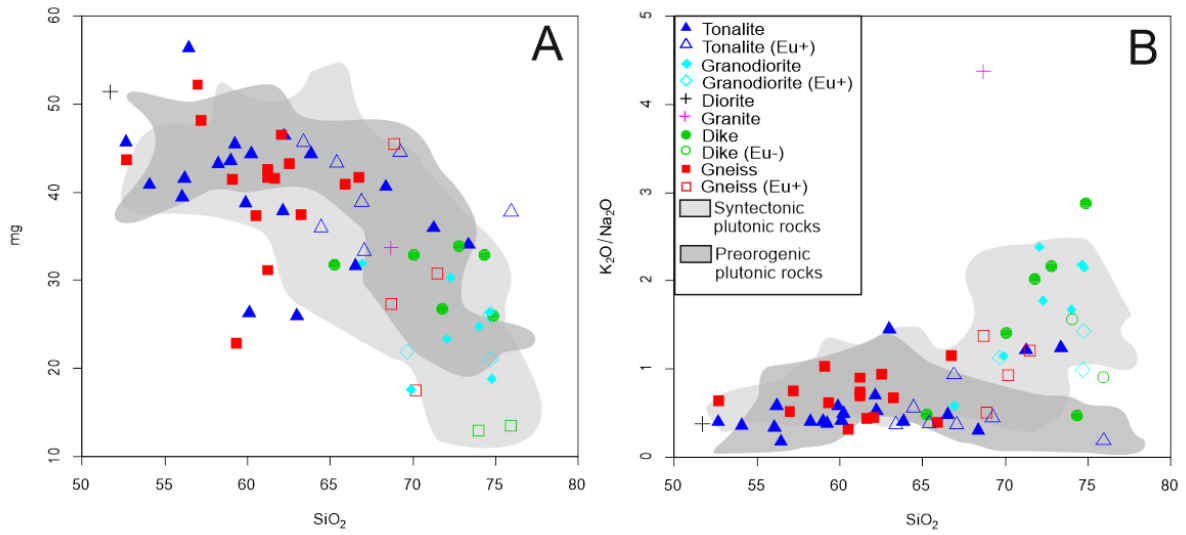

Figure 22. A) #mg versus SiO_2 of the studied samples and comparison data. B) K_2O/Na_2O versus SiO_2 of the studied samples and comparison data.

Adakitic features can be found in trace element chemistry and in REE relations as well. Usually, the amount of Y and HREE is relatively low, similar to concentration of high-field strength elements (HFSE) and Sr is usually relatively high (Moyen 2009). Majority of the samples in tonalites, gneisses, granodiorites and dikes are depleted in HREE (Figure 20). Moyen (2009) emphasizes the importance of the elevated Sr/Y versus. Y (Sr/Y at least 40) and La/Yb versus Yb values, presented firstly by Defant and Drummond (1990) and Martin (1999). Even though the Sr/Y and La/Yb values that indicate adakites have been set, it is common for actual adakites to have even more remarkable Sr/Y and La/Yb values. Adakites have been divided to high-silica adakites (HSA) and low-silica adakites (LSA) (Martin et al. 2005), where if the samples in this study represent adakites, they would be high-silica adakites.

Studied samples from the Pasalanmäki area have based on La/Yb versus Yb and Sr/Y versus Y diagrams, adakitic/TTG geochemical features (Figure 23). Samples with positive Eu-anomaly are pronounced in both diagrams, by having the clearest indications of adakitic geochemistry (Figure 22 A, B). From the comparison data, some of the preorogenic samples and syntectonic samples have adakitic features as well.

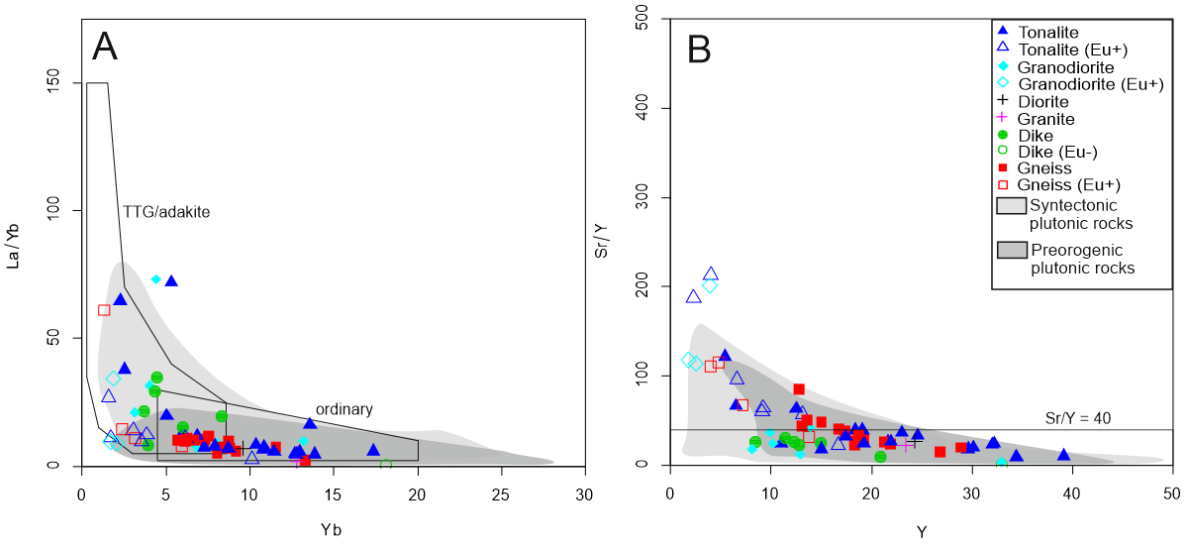

Figure 23. A) TTG/adakite classification diagram (Martin 1999) of the studied analyses. B) Sr/Y versus Y adakite discrimination diagrams (Moyen 2009) of the studied analyses.

The high Sr/Y and La/Yb values can be partially explained by magmatic processes, which create adakite like features to rocks that aren't actually adakites (Moyen 2009). When amphiboles are fractionating from the parental magma, the high K_D for HREE alters the composition of residual magma (Moyen 2009). Fractionation of plagioclase usually occurs simultaneously with amphibole, and this alters the La/Yb and Sr/Y values of the residual magma. In the end the Sr/Y values over 100, as seen in figure 23, can't be explained only by magma fractionating in a source that wouldn't be originally adakitic in composition (Moyen 2009). In this study the samples with Sr/Y over 100 are with exception of one, samples that could represent plagioclase cumulates (samples with positive Eu-anomaly). Another mineral that can similarly alter the chemistry of evolved magma to adakite type is garnet. Garnet, having high K_D for HREE (Table 2) can fractionate HREE from LREE, similarly seen in some of the studied samples in figure 20. This seen feature in some of the samples can be generated from rock forming environments were garnet is being stable in residual were the HSA (high-silica adakites)-like rocks originate from (Moyen 2009). Altogether, rocks that have elevated Sr (Figure 21) and Eu (Figure 20), low Yb and Y (Figure 21), fractionated REE-patterns (Figure 20) and high La/Yb versus Yb and High Sr/Y versus Y (Figure 23) can be generated from magmas, were garnet and amphibole were present as stabile minerals and plagioclase was fractionating phase, creating plagioclase cumulates (Martin et al. 2005).

5.2 Fractional crystallization of tonalites and gneisses in Pasalanmäki

Tonalites and plutonic gneisses are considered to be the oldest bedrock in the study area, based on field relationships. Granodiorites have geochemical similarities with tonalites and plutonic gneisses as well as dike group samples. Granodiorites, plutonic gneisses and tonalites could originate from the same magmatic source. Some of the dikes are based on field observations a part of later post-deformation magmatic event.

Variety of Eu-anomalies in the older magmatism in the study area (Figure 20) could be explained with fractional crystallization (Martin 1999). Seen negative correlation with the amount of Sr in relation to SiO_2 in the figure 19 C could be explained by plagioclase fractionating from parental magma (Castillo 1999). Another mineral which has a potential to create positive Eu-anomalies through fractional crystallization is K-feldspar (Streck and Grunder 1997). But where plagioclase has most likely crystallized from intermediate and felsic magmas, K-feldspar can be only crystallised from magma that is felsic in composition. Another way for studying the possible fractional crystallization of plagioclase is comparing the amount of Sr with Eu/Eu* anomaly's development.

In the figure 20 some samples in tonalite, gneiss and especially in granodiorite group have relatively more depleted in MREE (middle REEs) than HREE. This is considered to be a sign of amphibolite fractionation as well (Moyen 2009; Davidson et al. 2013). Clinopyroxene and amphibolites are common fractionating minerals in adakitic rocks and overall the fractionation and removal of amphibolites (hornblende in particular) and garnet creates La/Yb and Sr/Y relations similar to adakitic rocks (Moyen 2009).

In these models, it was estimated that the mafic samples that had lowest SiO_2 in them, was the parental magma. This estimation is based on the HSA (high-silica adakite) modelling that are modelled from mafic sources (Moyen 2009). It is commonly considered that the adakite source is basaltic and Sr is concentrated in the source (Martin 1999). Based on the studied samples, it was estimated that the parental magma for the fractionation and crystallization were the tonalite samples with lowest amounts of SiO_2 in them and relatively, highest Sr content (SiO_2 > 60 wt %.; Sr ~ 800 ppm; Figure 19 C). The actual parental magma could have had a different chemical composition as estimated in this study. There is also possibility for several different magma sources or constant development of the parental magma in these rocks as well. Most likely more

than the three minerals presented in this study were fractionating form the parental magma simultaneously.

5.2.1 Plagioclase fractionation and development of Eu/Eu* compared to Sr

Based on figure 24 fractionation of plagioclase could explain the seen development of the Eu/Eu* anomaly in relation to Sr content in the tonalites, gneisses and granodiorites of this study. For studying the possibility of fractional crystallization of plagioclase, a model for development of Sr content in relation to Eu-anomaly normalized in chondrite (Boynton 1984; Taylor and McLennan 1985; Equation 1) of the studied rocks was made. Model was made using Rayleigh fractionation formula (Rollinson (1993); Equation 2). Vector diagram (Figure 24) and the model, calculated for andesine melts and rhyolitic melts, was made using appropriate K_D values (Table 1,2).

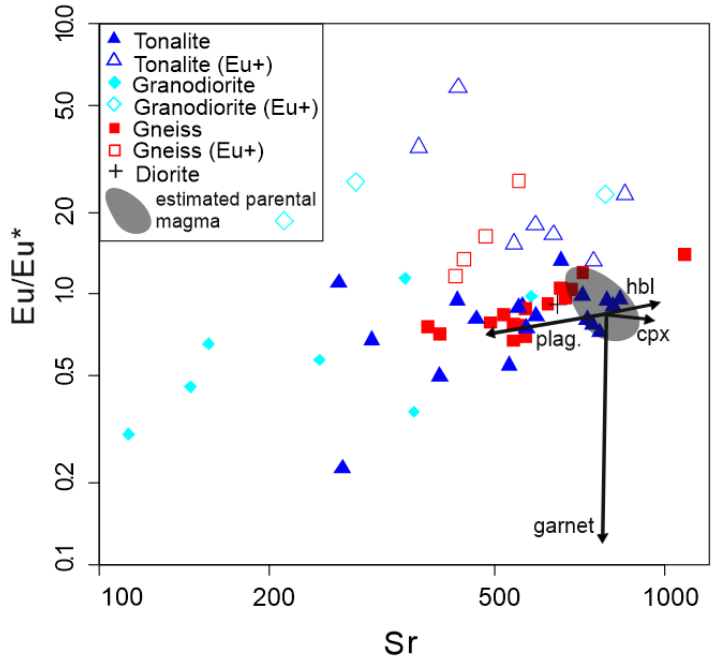

Figure 24. A vector diagram for fractionation of plagioclase (plag.), garnet, hornblende (hbl) and clinopyroxene (cpx) in andesine melts in Sr versus Eu/Eu*-anomaly.

Eu/Eu* = (Eu)cn/[(Sm)cn x (Gd)cn]^0.5 Equation 1

RayLiquid = C0 * (F ^ (D - 1)) Equation 2

Table 1. Elements, their concentration and K_D for plagioclase in andesine and rhyolitic melts.

Element	ppm in parental magma	**K_D** for plagioclase in andesine magma	**K_D** plagiclase in rhyolitic magma
Sr	800	2.625 (Dunn and Sen. 1994; GERM database)	31.00 (Brophy et al. 2011)
Eu	1.7	0.630 (Dunn and Sen. 1994; GERM database)	0.200 (Brophy et al. 2011)
Sm	6	0.046 (Dunn and Sen. 1994; GERM database)	0.100 (Brophy et al. 2011)
Gd	6	0.040 (Dunn and Sen. 1994; GERM database)	0.060 (Brophy et al. 2011)

Table 2. K_D values for hornblende, clinoproxene and garnet in andesine magma. nd*= no reliable data.

Element	ppm in parental magma	K_D for hornblende in andesine magma	K_D for clinopyroxene in andesine magma	K_D for garnet in andesine melts
Sr	800	0.28 (Brenan et al. 1995)	0.28 (Klein et al. 2000)	nd*
Eu	1.7	1.08 (Klein et al. 1997)	0.99 (Klein et al .2000)	1.540 (Klein et al. 2000)
Sm	6	1.37(Klein et al. 1997)	0.75 (Klein et al. 2000)	0.810 (Klein et al. 2000)
Gd	6	1.49(Klein et al. 1997)	0.91 (Klein et al. 2000)	4.590 (Klein et al. 2000)

Based on the calculated model of Eu/Eu* and its relation to the amount of Sr, fractionation of plagioclase could partially explain seen varieties in Eu-anomaly (Figure 25). The samples that have negative Eu-anomalies follow the calculated model of plagioclase fractionation, whereas the samples that have positive Eu-anomalies don't follow the calculated model. Based on the calculated model, the parental magma was andesine in composition, for this model to be relevant. In this model the plagioclase fractionation would have continued until 30% of the parental magma had been solidified (F= 70). After this point the development of the Sr when compared to Eu/Eu* becomes intermitted. During the fractional crystallization the Eu/Eu* in remaining melt would have decreased slightly and rocks that were plagioclase cumulates would have had positive Eu/Eu*.

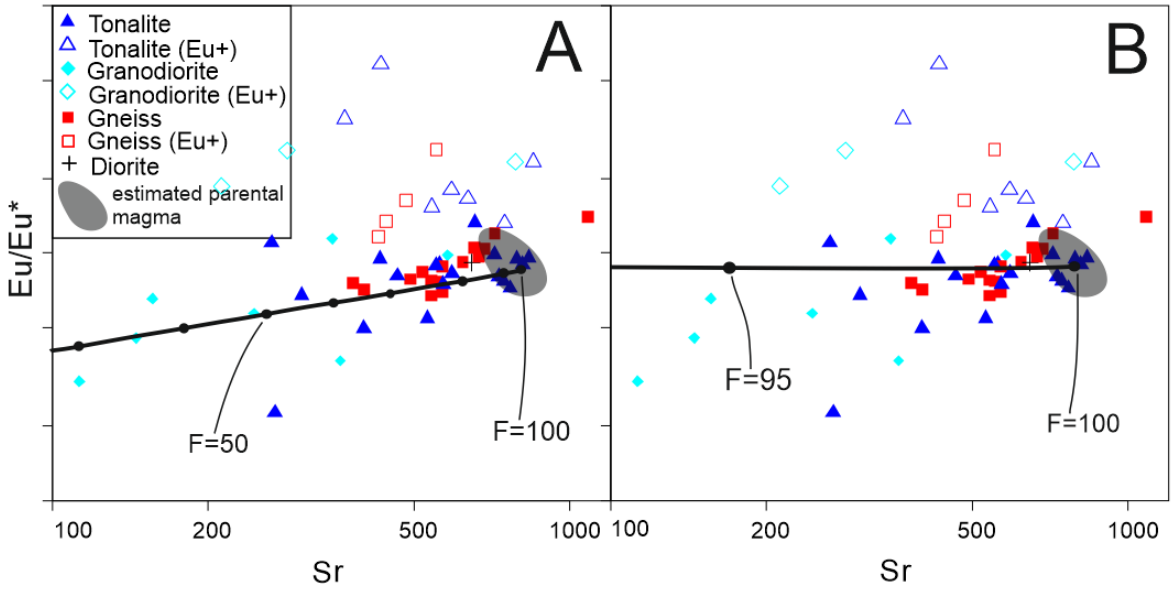

Figure 25. Calculated models for the development of Eu-anomaly and its relation to Sr content of the samples. a) Model calculated for intermediate. b) Model calculated for rhyolitic magma. F = proportion of liquid remaining.

The concentration of Sr is not enriched in the rocks with positive Eu-anomaly. This should be an observed trend as Sr has a K_D of 2.625 for plagioclase (Table 1). Another mineral that can have Sr in it is K-feldspar, as it has K_D of 5.9 for Sr (Streck and Grunder 1997). According to figure 21, all analyses with a positive Eu-anomaly have also a positive Sr-anomaly, whereas the samples with negative Eu-anomalies have negative Sr-anomaly or no Sr-anomaly at all. This implies that in relation to concentrations of Nd and Pr the plagioclase cumulates have been enriched in Sr. Accessory minerals could have affected the seen Sr concentrations in comparison to Eu/Eu* development that is seen in figure 25. Apatite has K_D of 24.000 for Sr in accessory phases (Brophy et al. 2011). If apatite has fractionated from the parental magma as well, it could leave a residual magma from which the seen plagioclase cumulates that have not been enriched in Sr would originate from. If apatite would have fractionated from the melt in large concentrations, it would have created positive Eu-anomaly in the residual melt as it has K_D of 42.0 for Sm and K_D of 45.0 for Gd and only K_D of 8.0 for Eu (Brophy et al. 2011).

Overall the seen Eu-anomalies and their relation to the amount of Sr cannot be explained using only calculated fractionation model. Where the samples that have positive Eu-anomalies should appear on the right side of the other samples in the figures, having more Sr in them, they seem to have as fluctuating amounts of Sr as the Eu-negative samples. A theory for explaining this could be that some of the studied samples have been crystallised from different magmatic pulse

or the parental magma partially crystallised before the crystallization that was studied using the calculated models took place.

5.2.2 Potassium feldspar fractionation in the gneisses and tonalites

When potassium feldspar is crystallizing for felsic melts, in granodiorites it can have HREE in its composition as well (Streck and Grunder 1997). This can create seen REE-patterns in granodiorites (figure 20 C), which have a slight enrichment of Er and Tm, when compared to Dy and Hb. K-feldspar crystals can have Sr in them, affecting the development of Sr in the residual magma (Streck and Grunder 1997) as seen in figure 25, similarly to plagioclase. For studying the K-feldspar fraction, the amount of Sr in the analyses was compared to the amount of Ba in the analyses and based on K_D values (Table 3) vectors for residual magma development were calculated. According to figure 26, some of the samples could be K-feldspar cumulates, but this is not generally a trend in the studied analyses. This is also a process that can take place only in felsic magmas as potassium feldspar doesn't crystallise in intermediate magmas.

Table 3. Estimated ppm for Sr and Ba and their K_D for potassium feldspar, amphibole, clinopyroxene, ortopyroxene and plagioclase in rhyolitic magmas.

Element	estimated ppm in parental magma	K_D for K-feldspar	K_D for amphibole	K_D for clinopyroxene	K_D for ortopyroxene	K_D for plagioclase
Sr	800	5.9 (Streck and Grunder 1997)	6.595 (Brophy et al. 2011)	0.23 (Iveson et al. 2018)	0.008 (Brophy et al. 2011)	31 (Brophy et al. 2011)
Ba	600	14.45 (Streck and Grunder 1997)	0.2 (Brophy et al. 2011)	0.01 (Iveson et al. 2018)	0.0007 (Brophy et al. 2011)	0.2 (Brophy et al. 2011)

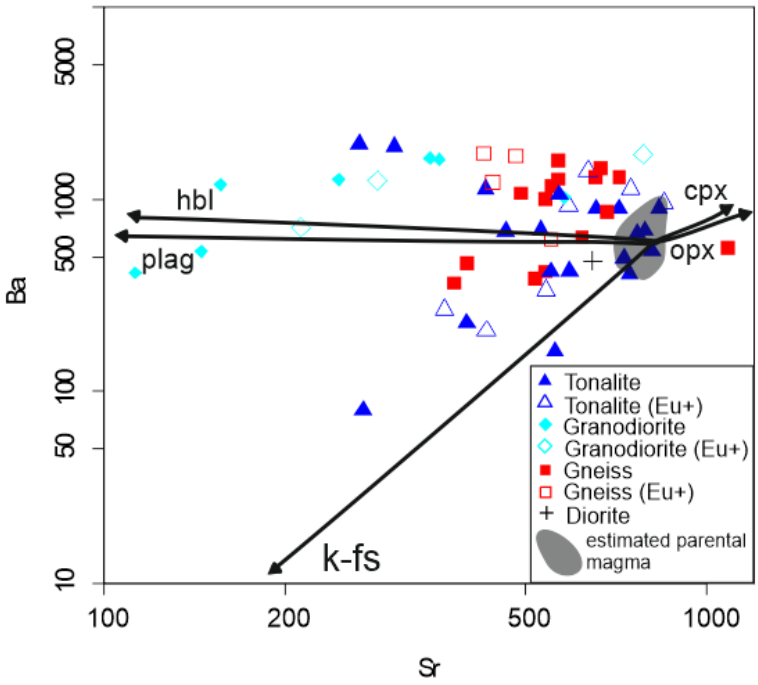

Figure 26. Vectors for K-feldspar (k-fs), orthopyroxene (opx), plagioclase (plag), clinopyrixene (cpx) and hornblene (hbl) fraction in rhyolitic melts. Vectors are calculated with 30 % of magma crystallizing.

5.2.3 The missing MREE in granodiorites and amphibole fractionation

Removal of amphiboles and pyroxenes from the developing melt can be studied using Dy/Yb relation to SiO_2, negative correlation of SiO_2 in relation to Dy/Yb can be seen as evidence of amphibole fraction (Davidson et al. 2013, Moyen 2009, and Davidson et al. 2007). Removal by fractionation of both, plagioclase and amphiboles, can be seen in increasing La/Yb values as seen in plagioclase cumulates in this study (Figure 23). In figure 27 is the Dy/Yb versus SiO_2 relation diagram of the samples, where vectors seen in this figure are calculated with 20 % of parental magma solidifying, and K_D for Dy and Yb for amphiboles are in tables 4 and 5. Based on the trend in these vector diagrams, all of the studied minerals could have fractionated from the andesine melt (Figure 27 A). A type of pyroxene and/or plagioclase could have fractionated in rhyolitic melt as well, but there is not indications of the hornblende fractionation in melts that are rhyolitic in composition (Figure 27 B).

Table 4. Estimated ppm of Dy and Yb and their K_D for amphibolite, clinopyroxene, ortopyroxene and plagioclase in rhyolitic magmas.

Element	Estimated ppm in parental magma	KD for amphibolite	KD for clinopyroxene	KD for ortopyroxene	KD for plagioclase
Dy	5	12.165 (Brophy et al. 2011)	1.00 (Huang et al. 2006)	0.345 (Brophy et al. 2011)	0.045 (Brophy et al. 2011)
Yb	3	29.465 (Brophy et al. 2011)	0.960 (Huang et al. 2006)	3.150 (Brophy et al. 2011)	0.025 (Brophy et al. 2011)

Table 5. Estimated ppm of Dy and Yb and their K_D for amphibolite, clinopyroxene, ortopyroxene and plagioclase in andesine magmas.

Element	Estimated ppm in parental magma	KD for amphibolite	KD for clinopyroxene	KD for ortopyroxene	KD for plagioclase
Dy	5	1.77 (Klein et al. 1997)	1.200 (Klein et al. 2000)	0.260 (Dunn and Sen 1994)	0.025 (Dunn and Sen 1994)
Yb	3	1.15 (Klein et al. 1997)	0.900 (Klein et al. 2000)	0.590 (Dunn and Sen 1994)	0.010 Dunn and Sen 1994)

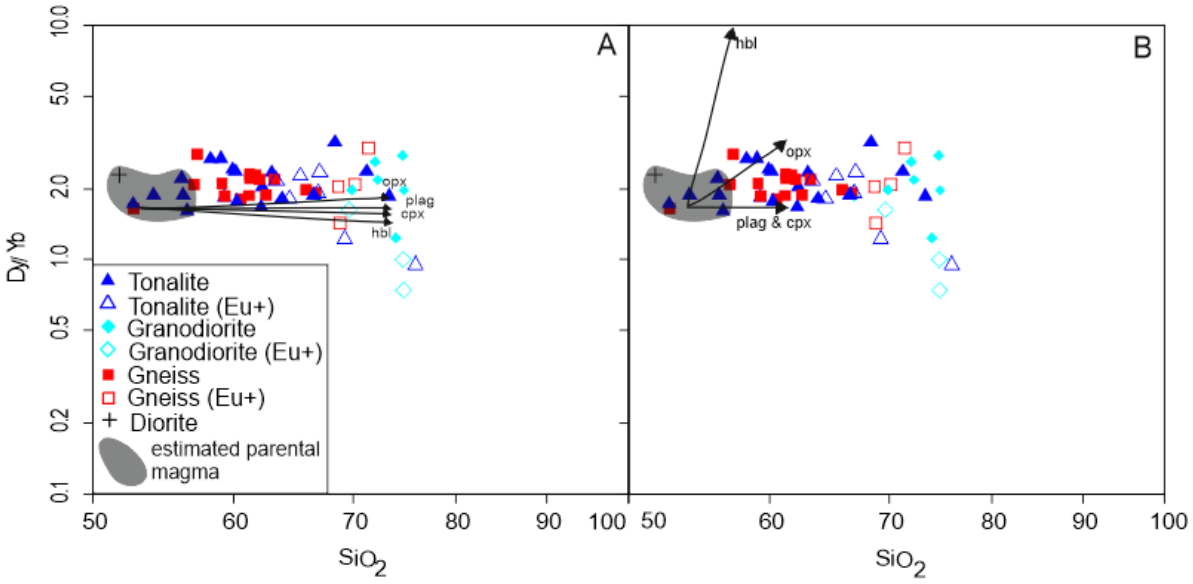

Figure 27. a) Vectors for orthopyroxene (opx), plagioclase (plag), clinopyrixene (cpx) and hornblene (hbl) fraction in andesine melts. b) Vectors for orthopyroxene, plagioclase, and clinopyroxene and hornblende fraction in rhyolitic melts. Vectors are calculated with 20 % magma crystallizing.

5.3 Magmatic evolution of the Pasalanmäki plutonic rocks

From field observations and age analyses, it was estimated that the felsic dikes represent the youngest unit of plutonic bedrock in Pasalanmäki (Tuppurainen et al. 2022). As some of the dikes had sings of deformation and some lacked this feature, it seems that magmatism in Pasalanmäki area was one continuous phenomenon partly postdating the deformation or dikes in the area were formed in multiple eras. Geochemical characteristics set dikes in Pasalanmäki aside from gneiss and tonalite groups. Granodiorites have geochemically similarities with tonalities and gneisses as well as dikes, even though similar REE-patterns and positive Eu-anomalies can be observed in tonalite, gneiss and granodiorite groups.

Six out of eight dikes had similar REE-patterns as other studied samples without positive Eu-anomaly, and two dike samples had very strong negative Eu-anomaly and enrichment of HREE when compared to LREE (Figure 20 D). These two samples are varying in mineralogy as well, as the two samples have garnet in them, and other dike samples don't. In Pasalanmäki, next to studied gneisses, tonalites and granodiorites, there are also paragneisses that have garnet bearing compositions. Partial melting of these paragneisses, that have been partly migmatised, could be a possible source for the dike magmatism. Peraluminous nature of the samples, felsic composition and presence of garnet in two analyses could imply dikes would have more sedimentary magmatism origin. One of the dike samples had inherited zircons from Archean era which could imply that the dike magmatism was affected by the surrounding paragneisses which have Archean detrital zircons in them (Tuppurainen et al. 2022).

The two dike analyses that were relatively enriched in HREE rather than LREE, have REE-patterns similar to granites that have M-type tetrad effect. The M-type refers to certain shape of the REE-pattern, where LREE and HREE have relatively similar quantities and Eu-anomaly is strongly negative (Irber 1999). The M-type tetrad effect can be found in granitic rocks that originate from highly evolved magmas that have been crystallised with aqueous fluid system and Eu has fractionated to the existing aqueous fluid. In the study made by Irber (1999) it was estimated that similar REE-patterns (similar HREE and LREE and relatively very strong negative Eu-anomaly) were created from highly evolved S-type granitic melts.

Discovering based on geochemistry, whether the dike group is actually I- or S-type granites remains partially unclear. According to Chappell and White (1974) S-type granites that have

approximately 5 wt. % of K_2O would have less than 3.2 wt. % of Na_2O in them. As some of the dike analyses have similar concentrations of both elements, there are at least four dike analyses that have more Na_2O in them than 3,2 wt. %. The higher than 3,2 wt. % concentration of Na_2O is considered to be typical for I-type granites (Chappell and White 1974). All dike samples are peralumionus, if this is not considered to be a sign of sedimentary origin of the dikes, peraluminous granites can be low-temperature I-type granites or they could originate from older metaluminous igneous source (Chappell and White 2001).

6. Conclusions

1. Based on the geochemical characteristics of the analyses and similarities with reference data, the plutonic gneisses and tonalites in Pasalanmäki likely represent arc magmatism from Paleoproterozoic era in close spatial relation to Archean-Proterozoic boundary.

2. Based on the available geochemical data, whether the studied bedrock in Pasalanmäki is part of the preorogenic magmatism from 1.93-1.91 Ga ago, or from synectonic Svecofennian magmatism 1.88-1.87 Ga ago, cannot be clearly distinguished.

3. Geochemical similarities in major and trace elements as in REE-patterns, indicates that tonalites and plutonic gneisses in the Pasalanmäki area have presumably same parental magma.

4. The analyses in Pasalanmäki tonalites, gneisses and granodiorites that have positive Eu-anomalies and increased La/Yb versus Yb and increased Sr/Y versus Y, are plagioclase cumulates.

5. Plagioclase cumulates in tonalites, gneisses and granodorites have adakitic features as high La/Yb versus Yb and Sr/Y versus Y values, where other samples of the Pasalanmäki area generally don’t have adakitic features.

6. Granodiorites have petrographycally similarities with more felsic, relatively K enriched dikes. Granodirites REE-patterns are similar with tonalites and gneisses indicating that granodiorites all originated via same rock forming process, where plagioclase was fractionating. This would imply that granodiorites have same parental magma as tonalities and plutonic gneisses, where granodiorites represent a more felsic, K enriched endmember.

7. Based on geochemical differences when compared to plutonic gneisses and tonalites in Pasalanmäki, the dikes represent same parental magma as highly developed granitic magma or/and different post deformation magmatic event.

Acknowledgements

First, I would like to express my gratitude for my master's thesis supervisors Esa Heilimo from University of Turku and Perttu Mikkola from Geological Survey of Finland for excellence guidance and feedback on this thesis. Furthermore, I am grateful to Markus Tuppurainen and Venla Vehanen for collecting the rock samples used in this study. Additionally, I would like thank laboratory technician Arto Peltola from University of Turku, for creating excellent thin sections from the rock samples and to Sören Fröjdö from Åbo Akademi in Turku for excellent and interesting guidance on SEM.

References

Aigner-Torres, M., Blundy, J., Ulmer, P., Pettke, T., 2007. Laser ablation ICPMS study for trace element partitioning between plagioclase and basaltic melts: an experimental approach. Contributions to Mineralogy and Petrology vol. 153, 647-667.

Bedrock of Finland − DigiKP. Digital map database [Electronic resource]. Espoo: Geological Survey of Finland [referred 26.10.2022].

Boynton, W.V., 1984. Geochemistry of Rare Earth Elements: Meteorite Studies. Henderson, P., Ed., Rare Earth Element Geochemistry, Elsevier, New York, 63-114.

Brenan, J.M., Shaw, H.F., Ryerson, F.J., Phinney, D.L, 1995. Experimental determination of trace-element partitioning between pargasite and a synthetic hydrous andesine melt. Earth and planetary science letters I35, 1-11.

Brophy, J.G., Ota, T., Kunihro, T., Tsujimori, T., Nakamura, E., 2011. In situ ion-microprobe determination of trace element partition coefficients for hornblende, plagioclase, orthopyroxene, and apatite in equilibrium with natural rhyolitic glass, Little Glass Mountain rhyolite, California. American Mineralogist 96, 1838-1850.

Castillo, P., 2012. Adakite petrogenesis. Lithos 134–135, 304-316.

Castillo, P.R., Janney, P.E., Solidum, R.U., 1999. Petrology and geochemistry of Camiguin Island, southern Philippines: Insights to the source of adakites and other lavas in a complex arc setting: Contributions to Mineralogy and Petrology 134, 33-51.

Chappell, B.W., White, J.R., 2001. Two contrasting granite types: 25 years later. Australian Journal of Earth Sciences 48, 489-499.

Chappell, B.W., White, J.R., 1974. Two contrasting granite types. Pacific Geology 8, 173-174.

Davidson J., MacPherson C., Turner S., 2007 Amphibole control in the differentiation of arc magmas. Geochimica et Cosmochimica Acta, 71 (15), A204-A204

Davidson, J., Turner, S., Plank, T., 2013. Dy/Dy*: Variations arising from mantle sources and petrogenetic processes: Journal of Petrology, v. 54, 525-537.

Defant M.J., Drummond M.S., 1990. Derivation of some modern arc magmas by melting of young subducted. Lithosphere. Nature 367, 662-665.

Dunn, T., Sen, C., 1994. Mineral/Matrix partition coefficients for orthopyroxene, plagioclase, and olivine in basaltic to andesitic systems: A combined analytical and experimental study. Geochimica et Cosmochimica Acta 58, 717-733.

McDonough, W.F. Sun, S.-S., 1995. Composition of the Earth. Chemical Geology 120, 223-253.

Ekdahl, E., 1993. Early Proterozoic and Svecofennian formations and the Evolution of the Raahe-Ladoga Ore Zone on the Pielavesi area, Central Finland. Geological Survey of Finland Bulletin 373, 137 p.

Fagertstörm, P., 1990 Karttulan kunnan Koskenkylän ja Airakselan alueen kivilajeista. Master's thesis. Helsingin yliopisto, 103 p. (unpublished, in finnish)

Fettes, D., Desmons, J., 2007. Metamorphic Rocks A Classification and Glossary of Terms Cambridge University Press, 244 p.

Gill, J.B., 1981 Orogenic Andesite and Plate Tectonics. Springer-Verlag, Berlin, 390 p.

Gorbatschev, R., Bogdanova, S., 1993. Frontiers in the Baltic Shield. Elsevier. Precambrian Research 64, 3-21.

Heilimo, E., Ahven, M., Mikkola, P., 2018. Geochemical characteristics of the plutonic rock units present at the south eastern boundary of the Central Finland Granitoid Complex. Geological Survey of Finland. Bulletin 407, 106-129.

Hermansson, T., Stephens, M., Corfu, F., Page, M., Andersson J., 2008. Migratory tectonic switching, western Svecofennian orogen, central Sweden: Constraints from U/Pb zircon and titanite geochronology. Precambrian research 161, 250-278.

Huang, F., Lundstrom, C.C., McDonough, W.F., 2006. Effect of melt structure on trace-element partitioning between clinopyroxene and silisic, alkaline, aluminous melts. American Mineralogist 91(8-9), 1385-1400.

Irber, W., 1999. The lanthanide tetrad effect and its correlation with K/Rb, Eu/Eu*, Sr/Eu, Y/Ho, and Zr/Hf of evolving peraluminous granite suites. Geochimica et Cosmochimica Acta, Vol. 63, 489-508.

Iveson, A.A., Rowe, M.C., Webster, J.D., Neil, O.K., 2018. Amphibole-, clinopyroxene- and plagioclase-melt partitioning of trace and economic metals in halogen bearing rhyodacitic melts. Journal oh petrology 59, 1597-1604.

Klein, M., Stosch, H-G., Seck, H-A., 1997. Partitioning of high fields-strength and rare-earth elements between amphibole and quartz-diorite to tonalitic melts: An experimental study. Chemical Geology 138, 257-271.

Klein, M., Stosch, H-G., Seck, H-A., Shimizu, N., 2000.Experimental partitioning of high field strength and rare earth elements between clinopyroxene and garnet in andesitic to tonalitic systems. Geochemica et Cosmochimica Acta 64, 99-105.

Korsman, K., Hölttä, P., Hautala, T., Wasenius, P. 1984. Metamorphism as an indicator of evolution and structure of the crust in eastern Finland. Geological Survey of Finland, Bulletin 328, 40 p.

Kousa, J., Huhma, H., Hokka, J., Mikkola, P., 2018. Extension of Svecofennian 1.91 Ga magmatism to the south, results of the reanalysed age determination samples from Joroinen, central Finland. Geological Survey of Finland. Bulletin 407, 56-62.

Lahtinen, R., 2012. Main geological features of Fennoscandia. Geological Survey of Finland. Special Paper 53, 13-18.

Lahtinen, R., 1994. Crustal evolution of the Svecofennian and Karelian domains during 2.1-1.79 Ga, with special emphasis on the geochemistry and origin of 1.93-1.91 Ga gneissic tonalites and associated supracrustal rocks in the Rautalampi area, central Finland. Ceological Survey of Finland. Bulletin 378, 128 p.

Lahtinen, R., Huhma, H., Lahaye, Y., Kousa, J., Luukas, J., 2015. Archean–Proterozoic collision boundary in central Fennoscandia: Revisited. Precambrian Research 261, 127-165.

Lahtinen, R., Korja, A., Nironen, M., 2005. Paleoproterozoic tectonic evolution. Precambrian Geology of Finland- Key to the Evolution of the Fennoscandian Shield. Elsevier. Amsterdam, 481-532.

Le Maitre, R.W., 1989. A Classification of Igneous Rocks and Glossary of Terms. Blackwell, 193 p.

Lukkarinen, H., 2008. Geological map of Finland 1:100 000. Explanation to the maps of Pre-Quaternary rocks, Sheets 3331 Siilinjärvi and 3242 Kuopio. Geological survey of Finland, 228 p.

Luukas, J., Kousa, J., Nironen, M., Vuollo, J., 2017. Major stratigraphic units in the bedrock of Finland, and an approach to tectonostratigraphic division. Geological Survey of Finland. Special Paper 60. 9-40.

Macpherson, C., Dreher, S., Thirlwall, M. 2006. Adakites without slab melting: High pressure differentiation of island arc magma, Mindanao, the Philippines. Earth and Planetary Science Letters 243, 581-593.

Martin, H., 1999. The adakitic magmas: modern analogues of Archaean granitoids. Lithos 46, 411-429.

Martin, H., Smithies R.H., Rapp R.P., Moyen J.-F., Champion D.C., 2005 An overview of adakite, tonalite–trondhjemite–granodiorite (TTG) and sanukitoid: relationships and some implications for crustal evolution. Lithos 79, 1-24.

Mikkola, P., Aatos, S., Halkoaho, T., Heinonen, S., Hietava, J., Hietala, S., Kurhila, M., Jäsberg, J., Laine, E.-L., Luukas, J., Niskanen, M., Nousiainen, M., Nygård, H., Piispanen, A., Pirinen, H., Rantanen, H., Romu, I., 2022. Geological evolution and structure along the western boundary of the Outokumpu allochthon. Geological Survey of Finland. Open File Research Report 23/2022, 117 p.

Mikkola, P., Lukkarinen, H., Luukas, J., 2016. Suonenjoen kartta-alueen 3241 kallioperä ja kivilajiyksiköt. Geological survey of Finland. File report 29/2016, 52 p.

Mäki, T., Imana, O., Kousa, J., Luukas, J., 2015. The Vihanti-Pyhäsalmi VMS Belt. Mineral deposits of Finland. Elsevier, Amsderdam, 507-530.

Parkkinen, J., 1974. Raportti Leppävirran aluetutkimuksista 1968-1973. Outokumpu Oy:n malmietsinnän raportit, 296 p.

Pearce, J., Harris, N., Tindle, A., 1984. Trace Element Discrimination Diagrams for the Tectonic Interpretation of Granitic Rocks. Journal of petrology, 956-983.

Rollinson, H.R., 1993. Using geochemical data: Evaluation, presentation, interpretation. Longman Scientific and Technical, Wiley, New York, 352 p.

Streck, M.J., Grunder, A.L., 1997. Compositional gradients and gaps in high-silica rhyolites of the Rattlesnake tuff, Oregon. Journal of petrology 38, 133-163.

Tatsumi, Y., Hamilton, D.L., Nesbitt R.W., 1986. Chemical characteristics of fluid phase released from a subducted lithosphere and origin of arc magmas: Evidence from high-pressure experiments and natural rocks. Journal of Volcanology and Geothermal Research 29, 293-309.

Taylor S.R., McLennan S.M., 1985. The Continental Crust: Its Composition and Evolution Blackwell, Oxford, 312 p.

Tuppurainen, M., Mikkola, P., Kurhila, M., 2022. New U-Pb age data from Pasalanmäki in Leppävirta, central Finland – older Svecofennian magmatism or not? Report S-72, Litosphere 2022, 187-190.

Vuollo, H., Huhma, H., 2005. Paleoproterozoic mafic dikes in NE Finland. In: Lehtinen, M., Nurmi, P.A., Rämö, O.T. (Eds.), Precambrian Geology of Finland: Key to the evolution of the Fennoscandian Shield. Developments in Precambrian Geology 14, 195-236.

Attachments

Attachment A. Sample code, x- and y-coordinates in ETRS-TM35FIN, field rock name and rock type

Sample code	X-coordinate	Y-coordinate	Field rock name	Rock type
KK8$-2020-1.2	532361	6932270	Hornblende gneiss	Gneiss
KK8$-2020-102.2	532303	6932415	Amfibolite	Amfibolite
KK8$-2020-104.2	535648	6929814	Trondhjemite	Trondhjemite
KK8$-2020-202.2	532182	6931538	Biotite granodiorite	Granodiorite
KK8$-2020-203.3	531043	6932604	Hornblende tonalite	Tonalite
KK8$-2020-208.1	532501	6930231	Paragneiss	Paragneiss
KK8$-2020-209.3	532884	6931175	Biotite-hornblendetonalite	Tonalite
KK8$-2020-302.2	533580	6929730	Biotitetonalite	Tonalite
KK8$-2020-305.1	532914	6930795	Graniitti	Granite
KK8$-2020-305.2	532914	6930795	Hornblende-biotite tonalite	Tonalite
KK8$-2020-406.4	533119	6930715	Biotite-hornblende tonalite	Tonalite
KK8$-2020-409.2	532622	6931141	Hornblende tonalite	Tonalite
KK8$-2020-427.2	532438	6930354	Granodioritic gneiss	Gneiss
KK8$-2020-603.2	532558	6931899	Hornblende-biotite gneiss	Gneiss
KK8$-2020-605.2	532811	6932061	Biotite gneiss	Gneiss
KK8$-2020-611.3	532750	6931387	Hornblende-biotite tonalite	Tonalite
KK8$-2020-611.4	532750	6931387	Felsic dike	Felsic dike
KK8$-2020-626.3	534295	6929508	Granodiorite	Granodiorite
KK8$-2020-702.2	532598	6930919	Hornblende gneiss	Gneiss
KK8$-2020-704.1	532799	6930831	Hornblende-biotite tonalite	Tonalite
KK8$-2020-706.2	532847	6930937	Biotite-hornblende gneiss	Gneiss
KK8$-2020-801.2	531896	6931417	Biotite-hornblende tonalite	Tonalite
KK8$-2020-810.1	533260	6930263	Hornblende-biotite gneiss	Gneiss
KK8$-2020-909.2	535699	6929757	Granodiorite	Granodiorite
KK8$-2020-1004.2	535393	6929866	Hornblende-biotite tonalite	Tonalite
KK8$-2020-1010.1	534305	6930006	Biotite tonalite	Tonalite
KK8$-2020-1111.3	534233	6930875	Felsic dike	Felsic dike
KK8$-2020-1111.4	534233	6930875	Hornblende tonalite-gneiss	Gneiss
KK8$-2020-1204.2	535097	6930338	Hornblende-biotite gneiss	Gneiss
KK8$-2020-1419.1	532957	6931207	Biotite-hornblende tonalite	Tonalite
KK8$-2020-1633.2	534763	6929655	Biotite-hornblende tonalite	Tonalite

KK8$-2020-1659.2	533179	6931203	Granite	Granite
MOTU-2021-9.1	535420	6930175	Tonalite	
MOTU-2021-11.1	533939	6931697	Biotite-hornblende gneiss	Gneiss
MOTU-2021-17.1	533928	6931201	Tonalite	Tonalite
MOTU-2021-22.1	531965	6932914	Biotite-hornblende tonalite	Tonalite
MOTU-2021-24.1	532239	6931511	Biotite-hornblende tonalite	Tonalite
MOTU-2021-25.1	532233	6931378	Hornblende-biotite gneiss	Gneiss
MOTU-2021-28.1	533319	6931125	Hornblende-biotite gneiss	Gneiss
MOTU-2021-32.1	533434	6932182	Hornblende-biotite gneiss	Gneiss
MOTU-2021-34.1	534071	6929524	Hornblende-biotite tonalite	Tonalite
VSVE-2021-1.1	534162	6929590	Biotitetonalite	Tonalite
VSVE-2021-6.1	532197	6930928	Granodiorite	Granodiorite
VSVE-2021-6.2	532197	6930928	Hornblende-biotite gneiss	Gneiss
VSVE-2021-6.3	532197	6930928	Hornblende-biotite gneiss	Gneiss
VSVE-2021-7.1	534038	6929672	Hornblende-biotite tonalite	Tonalite
VSVE-2021-9.1	531735	6933327	Biotite-hornblende tonalite	Tonalite
VSVE-2021-9.3	531735	6933327	Granodiorite	Granodiorite
VSVE-2021-10.1	532035	6933036	Granodiorite	Granodiorite
VSVE-2021-10.2	532035	6933036	Hornblende-biotite gneiss	Gneiss
VSVE-2021-11.1	531962	6933009	Granodiorite	Granodiorite
VSVE-2021-11.2	531962	6933009	Hornblende-biotite gneiss	Gneiss
VSVE-2021-11.3	531962	6933009	Felsic dike	Felsic dike
VSVE-2021-12.1	532582	6931852	Granodiorite	Granodiorite
VSVE-2021-14.1	533388	6931087	Hornblende-biotite tonalite	Tonalite
VSVE-2021-15.1	532738	6931436	Hornblende-biotite tonalite	Tonalite
VSVE-2021-16.1	532032	6931794	Hornblende-biotite tonalite	Tonalite
VSVE-2021-17.2	532822	6930421	Biotite tonalite	Tonalite

Attachment B. SEM-report of some studied minerals

AinoSavakko_NoOx

User name: PHENOM-WORLD-PC\Phenom-World
Contains 12 images with a total of 22 analyses

01. 1 Min 1
3 analyses: 3x spot

02. 2 Min 2
1 analysis: 1x spot

03. 3 Min 3
2 analyses: 2x spot

04. 4 Min 4
1 analysis: 1x spot

05. 5 Min 5
2 analyses: 2x spot

06. 6 Min 5 vaalea sulk a
1 analysis: 1x spot

07. 7 Min 5 vaalea sulk b
1 analysis: 1x spot

08. 8 Min 6 a
2 analyses: 2x spot

09. 9 Min 6 b
4 analyses: 4x spot

10. 10 Hie 1 Image 10 zirkon
1 analysis: 1x spot

11. 11 Min 1 vaalea A
1 analysis: 1x spot

12. 12 Min 1 vaalea B
3 analyses: 3x spot

1 Min 1

1. spot

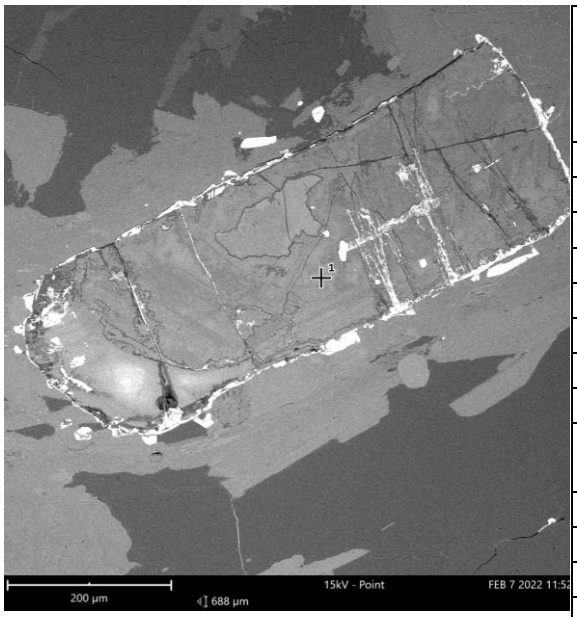

Element Number	Element Symbol	Element Name	Atomic Conc.	Weight Conc.
8	O	Oxygen	66.42	45.46
14	Si	Silicon	17.97	21.59
13	Al	Aluminium	6.49	7.49
58	Ce	Cerium	0.90	5.37
90	Th	Thorium	0.38	3.81
11	Na	Sodium	3.28	3.23
26	Fe	Iron	1.30	3.10
60	Nd	Neodymium	0.44	2.73
59	Pr	Praseodymium	0.33	1.98
20	Ca	Calcium	0.76	1.31
57	La	Lanthanum	0.21	1.23
12	Mg	Magnesium	0.74	0.77
62	Sm	Samarium	0.11	0.71
19	K	Potassium	0.42	0.70
22	Ti	Titanium	0.17	0.35
25	Mn	Manganese	0.07	0.16

FOV: 688 µm, Mode: 15kV - Point, Detector: BSD Full, Time: FEB 7 2022 11:52

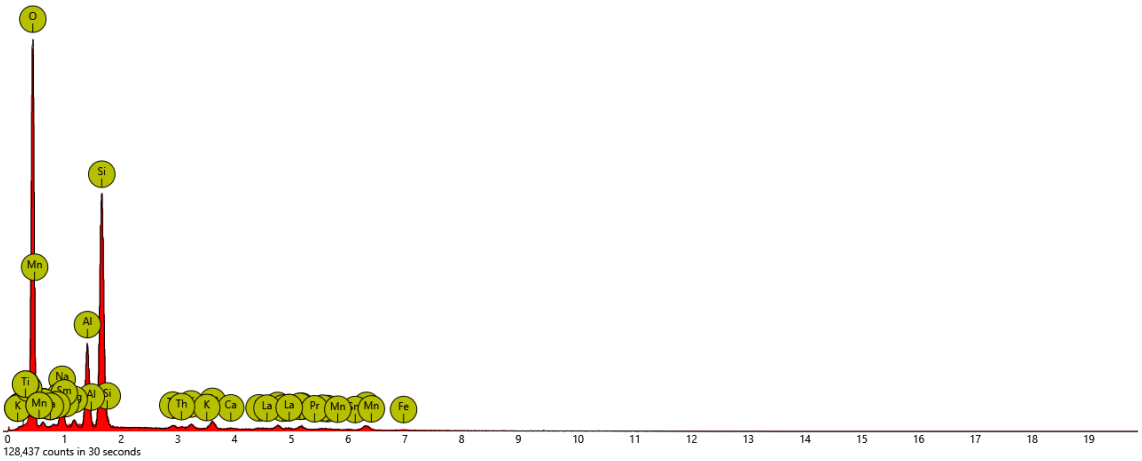

Disabled elements: Ag, At, B, Bi, Br, C, Cs, Fr, Ga, I, N, Po, Ra, Re, Rn, Sb, Se, Sr, Tb, Tc, Te, W

2. spot

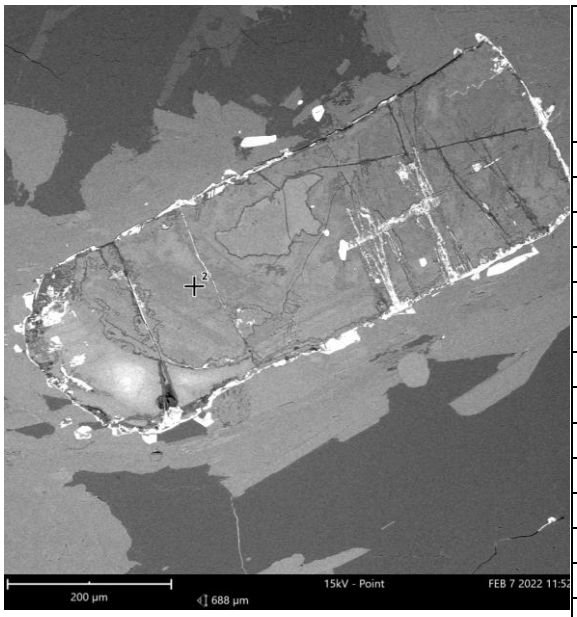

Element Number	Element Symbol	Element Name	Atomic Conc.	Weight Conc.
8	O	Oxygen	69.73	53.20
14	Si	Silicon	16.66	22.31
13	Al	Aluminium	6.48	8.34
26	Fe	Iron	1.39	3.71
11	Na	Sodium	3.04	3.33
90	Th	Thorium	0.29	3.20
58	Ce	Cerium	0.35	2.37
20	Ca	Calcium	0.73	1.39
12	Mg	Magnesium	0.82	0.95
19	K	Potassium	0.39	0.73
60	Nd	Neodymium	0.04	0.31
22	Ti	Titanium	0.07	0.16
25	Mn	Manganese	0.00	0.00
57	La	Lanthanum	0.00	0.00
59	Pr	Praseodymium	0.00	0.00
62	Sm	Samarium	0.00	0.00

FOV: 688 µm, Mode: 15kV - Point, Detector: BSD Full, Time: FEB 7 2022 11:52

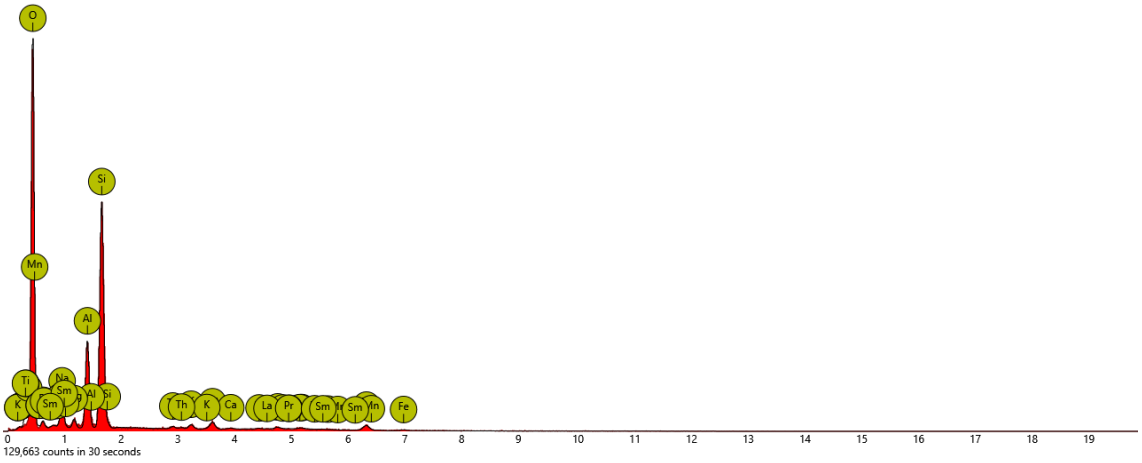

Disabled elements: Ag, At, B, Bi, Br, C, Cs, Er, Fr, Ga, I, N, Po, Ra, Re, Rn, Sb, Se, Sr, Tb, Tc, Te, W

3. spot

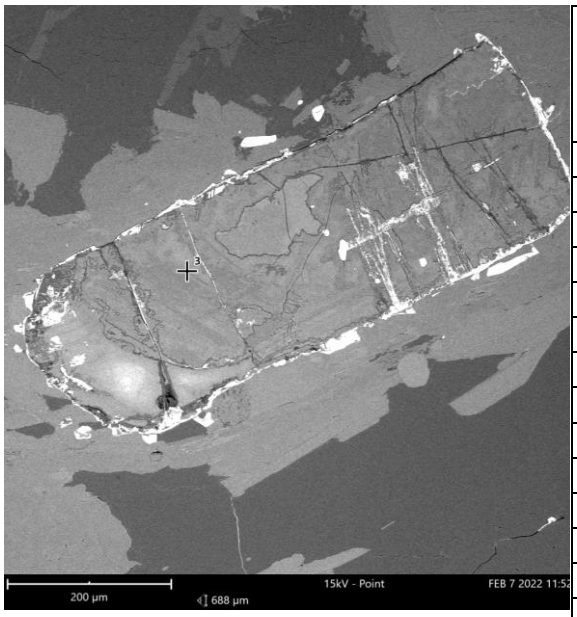

Element Number	Element Symbol	Element Name	Atomic Conc.	Weight Conc.
8	O	Oxygen	67.03	47.93
14	Si	Silicon	17.40	21.85
13	Al	Aluminium	6.70	8.08
58	Ce	Cerium	0.72	4.51
11	Na	Sodium	4.07	4.18
90	Th	Thorium	0.31	3.17
26	Fe	Iron	1.14	2.84
60	Nd	Neodymium	0.35	2.28
20	Ca	Calcium	0.71	1.27
57	La	Lanthanum	0.18	1.13
19	K	Potassium	0.45	0.78
12	Mg	Magnesium	0.61	0.66
62	Sm	Samarium	0.08	0.52
59	Pr	Praseodymium	0.06	0.36
22	Ti	Titanium	0.16	0.35
25	Mn	Manganese	0.04	0.10

FOV: 688 µm, Mode: 15kV - Point, Detector: BSD Full, Time: FEB 7 2022 11:52

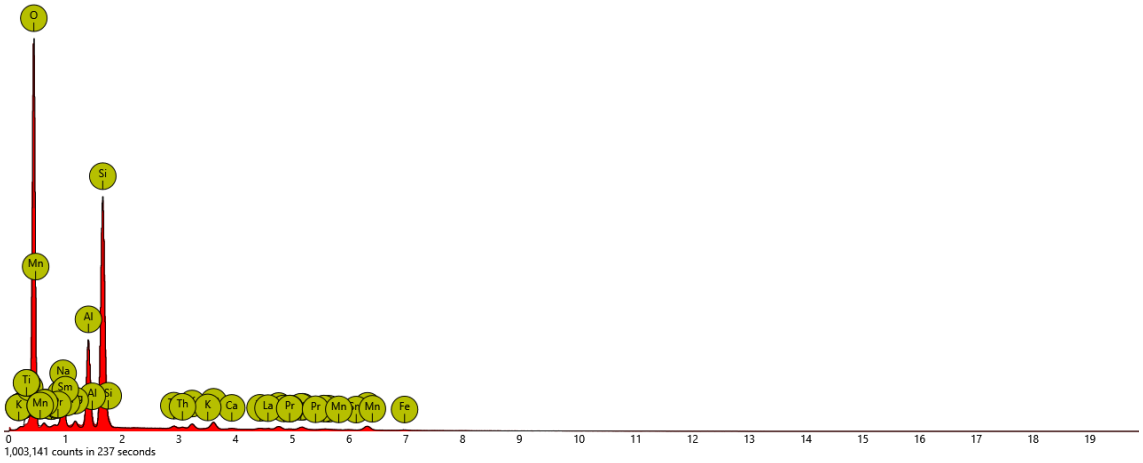

Disabled elements: Ag, At, B, Bi, Br, C, Cs, Fr, Ga, I, N, Po, Ra, Re, Rn, Sb, Se, Sr, Tb, Tc, Te, W

2 Min 2

1. spot

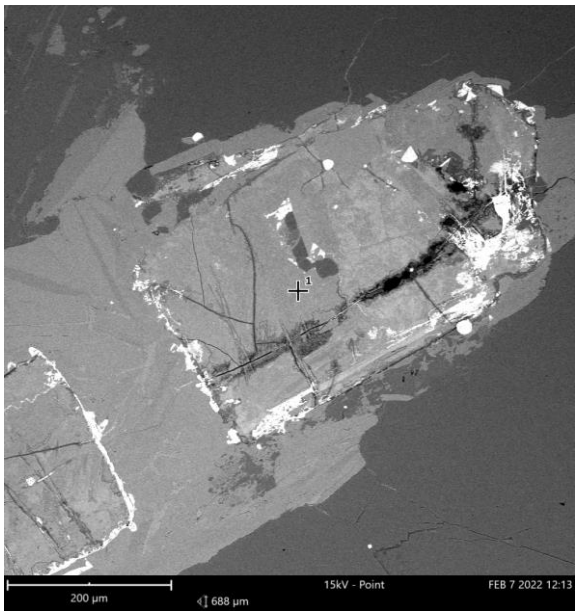

Element Number	Element Symbol	Element Name	Atomic Conc.	Weight Conc.
8	O	Oxygen	67.64	48.72
14	Si	Silicon	17.41	22.01
13	Al	Aluminium	6.36	7.73
58	Ce	Cerium	0.67	4.23
26	Fe	Iron	1.66	4.17
11	Na	Sodium	3.34	3.46
90	Th	Thorium	0.29	3.05
60	Nd	Neodymium	0.33	2.11
20	Ca	Calcium	0.80	1.44
57	La	Lanthanum	0.14	0.86
12	Mg	Magnesium	0.77	0.85
19	K	Potassium	0.38	0.67
62	Sm	Samarium	0.05	0.34
22	Ti	Titanium	0.13	0.27
25	Mn	Manganese	0.04	0.09

FOV: 688 µm, Mode: 15kV - Point, Detector: BSD Full, Time: FEB 7 2022 12:13

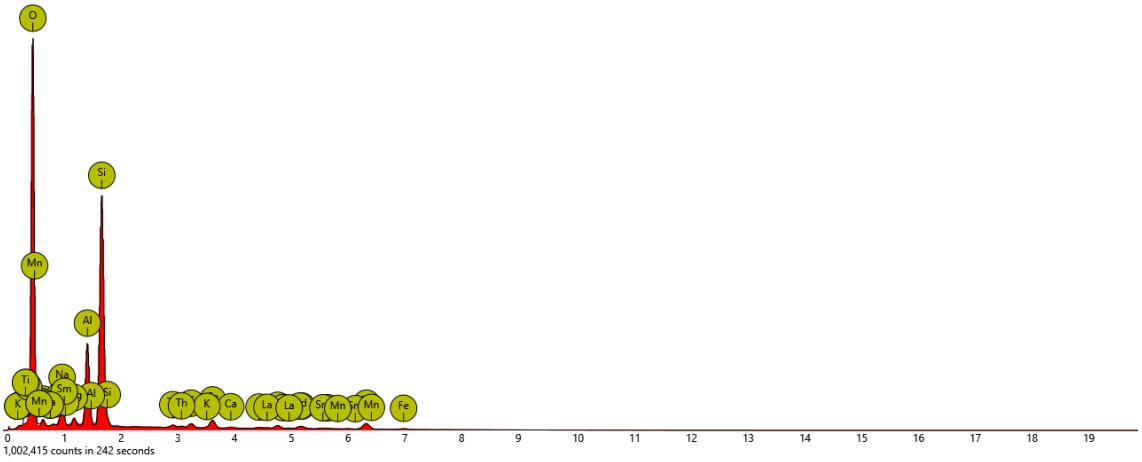

Disabled elements: Ag, At, B, Bi, Br, C, Cs, Fr, Ga, I, N, Po, Ra, Re, Rn, Sb, Se, Sr, Tb, Tc, Te, W

3 Min 3

1. spot

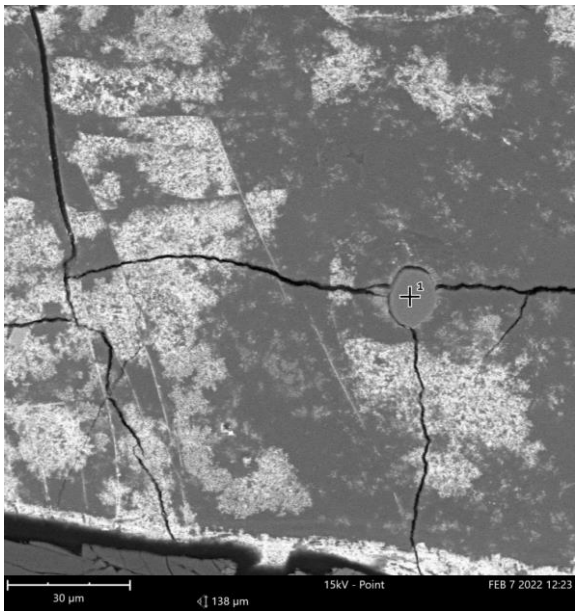

Element Number	Element Symbol	Element Name	Atomic Conc.	Weight Conc.
8	O	Oxygen	67.94	48.94
20	Ca	Calcium	13.95	25.16
15	P	Phosphorus	9.46	13.20
14	Si	Silicon	4.01	5.07
26	Fe	Iron	0.89	2.23
13	Al	Aluminium	1.77	2.15
90	Th	Thorium	0.10	1.08
12	Mg	Magnesium	0.98	1.07
11	Na	Sodium	0.70	0.72
19	K	Potassium	0.16	0.27
25	Mn	Manganese	0.04	0.10
62	Sm	Samarium	0.00	0.00
22	Ti	Titanium	0.00	0.00

FOV: 138 µm, Mode: 15kV - Point, Detector: BSD Full, Time: FEB 7 2022 12:23

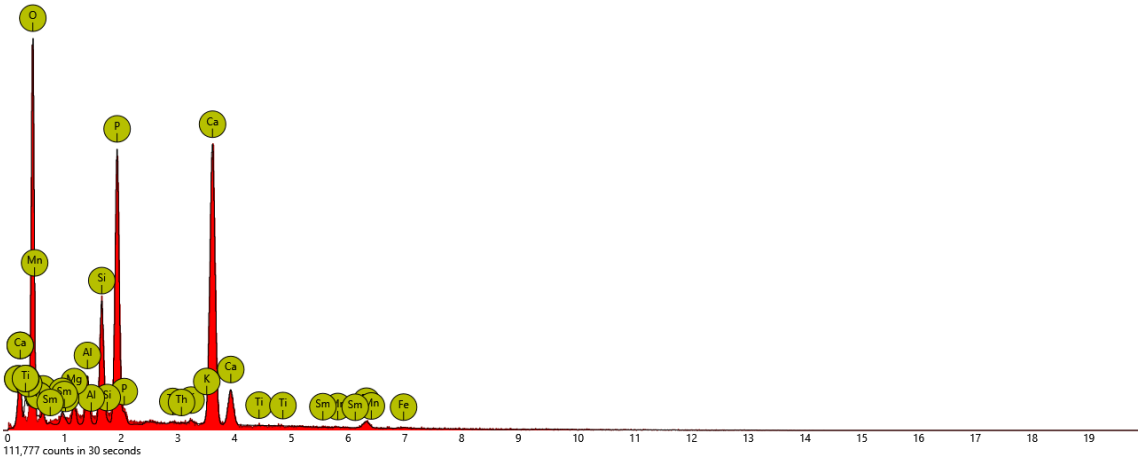

Disabled elements: Ag, At, B, Bi, Br, C, Cs, Fr, Ga, I, N, Po, Ra, Re, Rn, Sb, Se, Sr, Tb, Tc, Te, W

2. spot

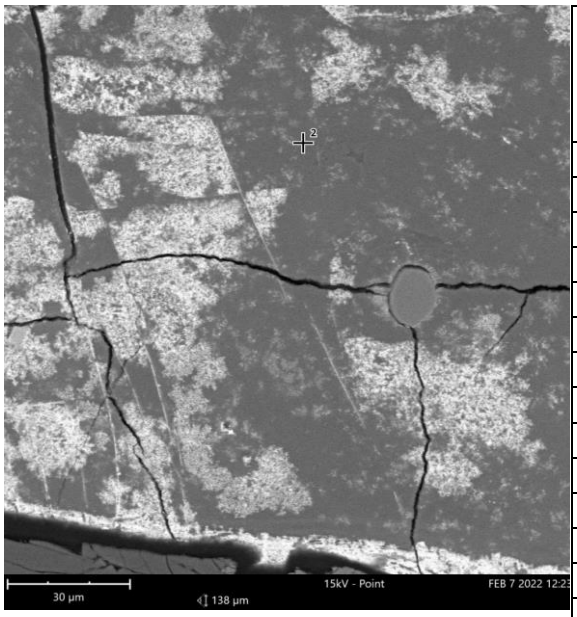

Element Number	Element Symbol	Element Name	Atomic Conc.	Weight Conc.
8	O	Oxygen	67.34	49.69
14	Si	Silicon	13.96	18.08
26	Fe	Iron	3.84	9.88
13	Al	Aluminium	7.83	9.74
12	Mg	Magnesium	4.59	5.14
90	Th	Thorium	0.21	2.20
20	Ca	Calcium	0.56	1.03
58	Ce	Cerium	0.15	0.99
11	Na	Sodium	0.79	0.84
57	La	Lanthanum	0.10	0.67
25	Mn	Manganese	0.21	0.54
60	Nd	Neodymium	0.08	0.53
19	K	Potassium	0.23	0.42
22	Ti	Titanium	0.12	0.26
59	Pr	Praseodymium	0.00	0.00
62	Sm	Samarium	0.00	0.00

FOV: 138 µm, Mode: 15kV - Point, Detector: BSD Full, Time: FEB 7 2022 12:23

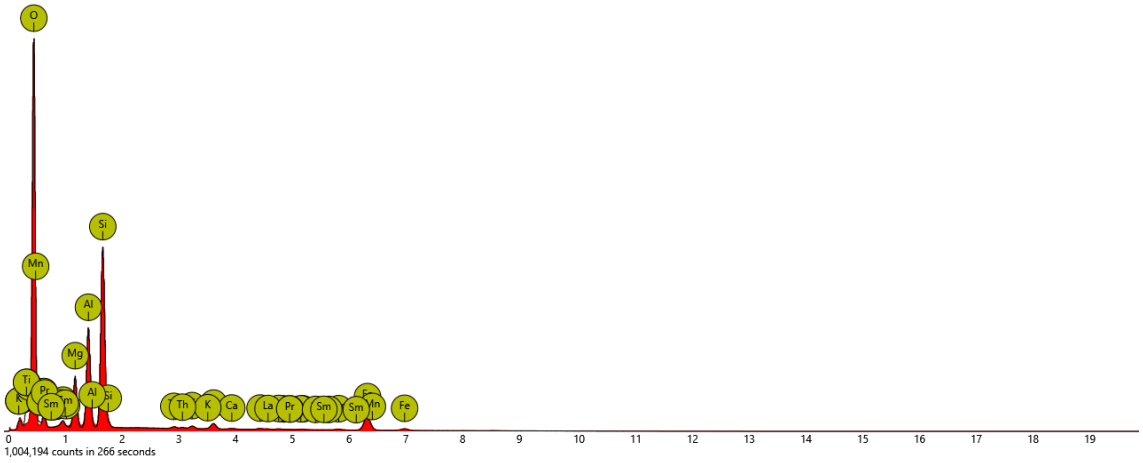

Disabled elements: Ag, At, B, Bi, Br, C, Cs, Fr, Ga, I, N, Po, Ra, Re, Rn, Sb, Se, Sr, Tb, Tc, Te, W

4 Min 4

1. spot

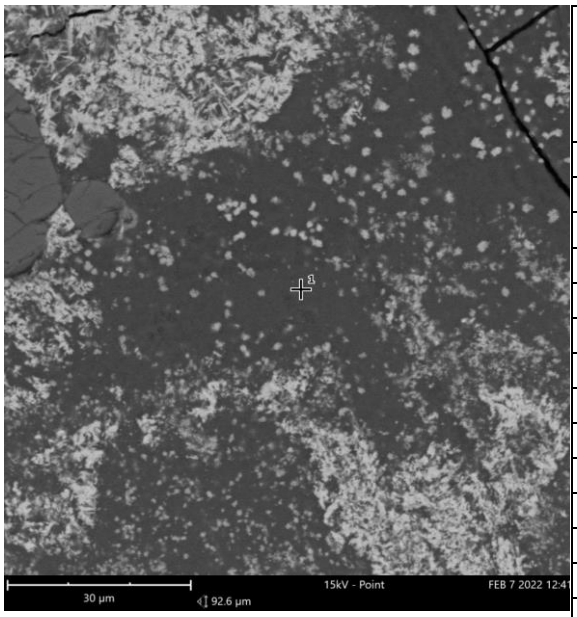

Element Number	Element Symbol	Element Name	Atomic Conc.	Weight Conc.
8	O	Oxygen	67.40	49.94
14	Si	Silicon	13.85	18.02
26	Fe	Iron	4.19	10.84
13	Al	Aluminium	6.08	7.59
12	Mg	Magnesium	6.42	7.23
90	Th	Thorium	0.14	1.48
58	Ce	Cerium	0.21	1.36
20	Ca	Calcium	0.36	0.67
11	Na	Sodium	0.62	0.66
19	K	Potassium	0.33	0.59
60	Nd	Neodymium	0.08	0.53
57	La	Lanthanum	0.07	0.48
25	Mn	Manganese	0.13	0.32
15	P	Phosphorus	0.09	0.13
59	Pr	Praseodymium	0.02	0.12
22	Ti	Titanium	0.01	0.02
62	Sm	Samarium	0.00	0.00

FOV: 92.6 µm, Mode: 15kV - Point, Detector: BSD Full, Time: FEB 7 2022 12:41

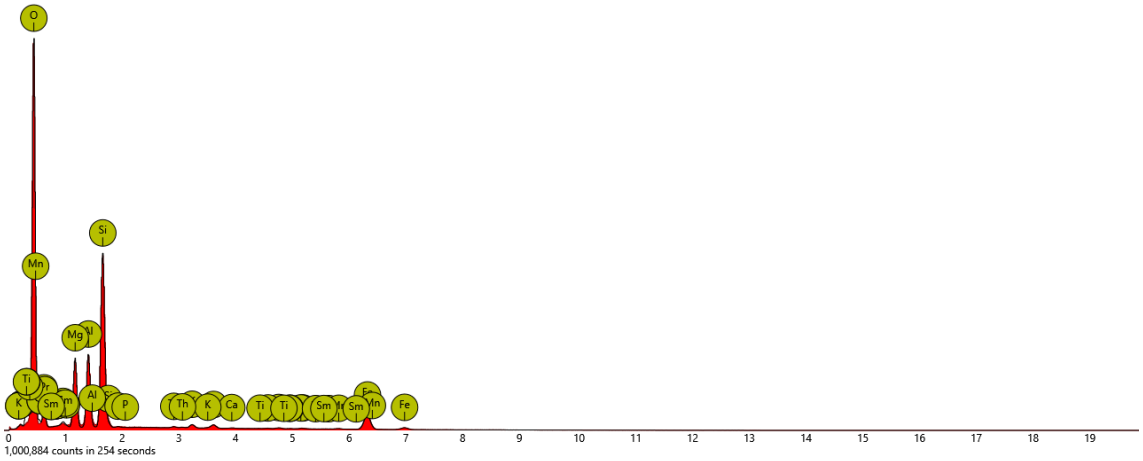

Disabled elements: Ag, At, B, Bi, Br, C, Cs, Fr, Ga, I, N, Po, Ra, Re, Rn, Sb, Se, Sr, Tb, Tc, Te, W

5 Min 5

1. spot

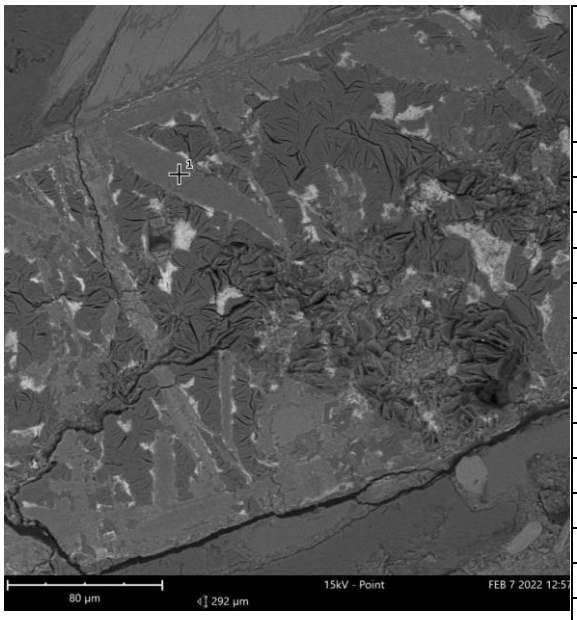

Element Number	Element Symbol	Element Name	Atomic Conc.	Weight Conc.
8	O	Oxygen	66.44	50.01
14	Si	Silicon	13.89	18.35
26	Fe	Iron	4.12	10.83
12	Mg	Magnesium	7.49	8.56
13	Al	Aluminium	6.19	7.86
90	Th	Thorium	0.17	1.86
11	Na	Sodium	0.95	1.02
20	Ca	Calcium	0.41	0.77
19	K	Potassium	0.20	0.36
25	Mn	Manganese	0.13	0.33
22	Ti	Titanium	0.03	0.06
58	Ce	Cerium	0.00	0.00
57	La	Lanthanum	0.00	0.00
59	Pr	Praseodymium	0.00	0.00
60	Nd	Neodymium	0.00	0.00
62	Sm	Samarium	0.00	0.00

FOV: 292 µm, Mode: 15kV - Point, Detector: BSD Full, Time: FEB 7 2022 12:57

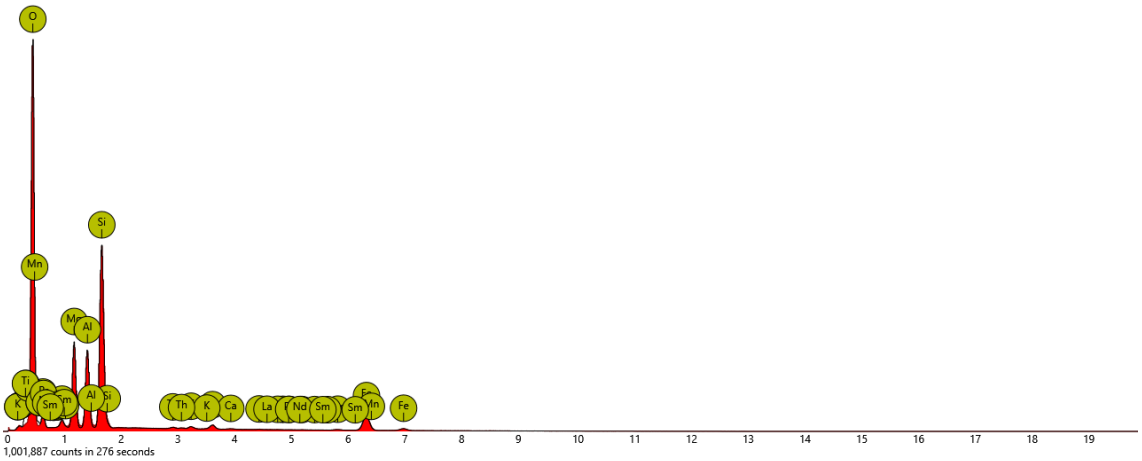

Disabled elements: Ag, At, B, Bi, Br, C, Cs, Fr, Ga, I, N, Po, Ra, Re, Rn, Sb, Se, Sr, Tb, Tc, Te, W

2. spot

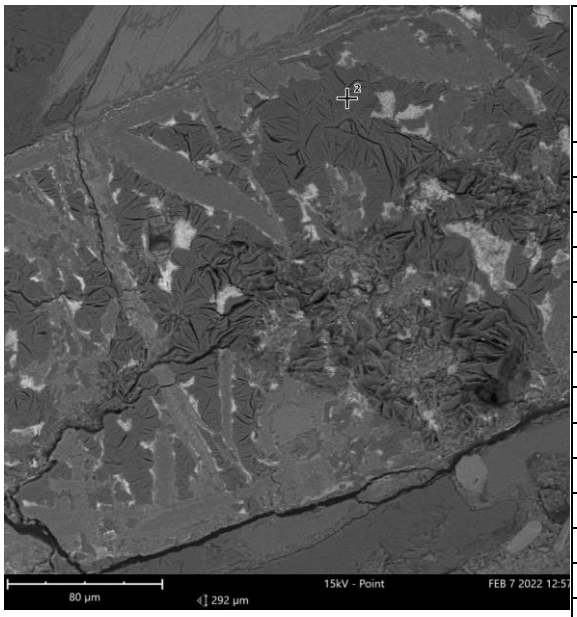

Element Number	Element Symbol	Element Name	Atomic Conc.	Weight Conc.
8	O	Oxygen	66.64	52.10
14	Si	Silicon	13.52	18.55
12	Mg	Magnesium	9.60	11.40
13	Al	Aluminium	6.23	8.22
26	Fe	Iron	2.52	6.87
11	Na	Sodium	0.84	0.94
90	Th	Thorium	0.06	0.64
20	Ca	Calcium	0.27	0.54
19	K	Potassium	0.19	0.37
25	Mn	Manganese	0.10	0.27
57	La	Lanthanum	0.01	0.06
22	Ti	Titanium	0.02	0.05
58	Ce	Cerium	0.00	0.00
59	Pr	Praseodymium	0.00	0.00
60	Nd	Neodymium	0.00	0.00
62	Sm	Samarium	0.00	0.00

FOV: 292 µm, Mode: 15kV - Point, Detector: BSD Full, Time: FEB 7 2022 12:57

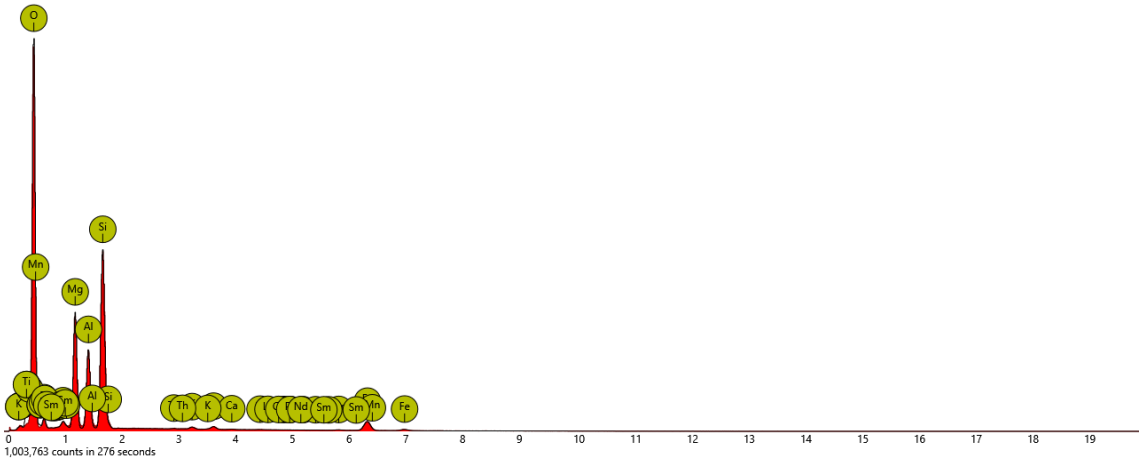

Disabled elements: Ag, At, B, Bi, Br, C, Cs, Fr, Ga, I, N, Po, Ra, Re, Rn, Sb, Se, Sr, Tb, Tc, Te, W

6 Min 5 vaalea sulk a

1. spot

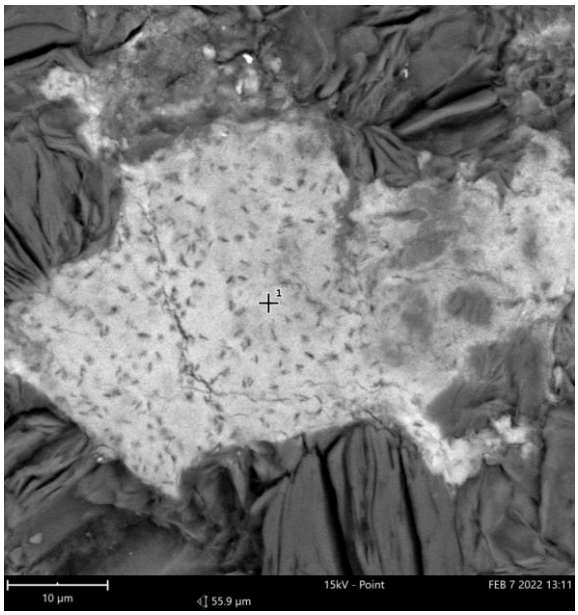

Element Number	Element Symbol	Element Name	Atomic Conc.	Weight Conc.
90	Th	Thorium	6.28	41.07
8	O	Oxygen	64.09	28.92
14	Si	Silicon	16.70	13.23
40	Zr	Zirconium	1.87	4.81
26	Fe	Iron	3.04	4.79
13	Al	Aluminium	4.61	3.51
12	Mg	Magnesium	2.35	1.61
39	Y	Yttrium	0.49	1.23
19	K	Potassium	0.28	0.31
20	Ca	Calcium	0.23	0.26
58	Ce	Cerium	0.06	0.25
57	La	Lanthanum	0.00	0.00

FOV: 55.9 µm, Mode: 15kV - Point, Detector: BSD Full, Time: FEB 7 2022 13:11

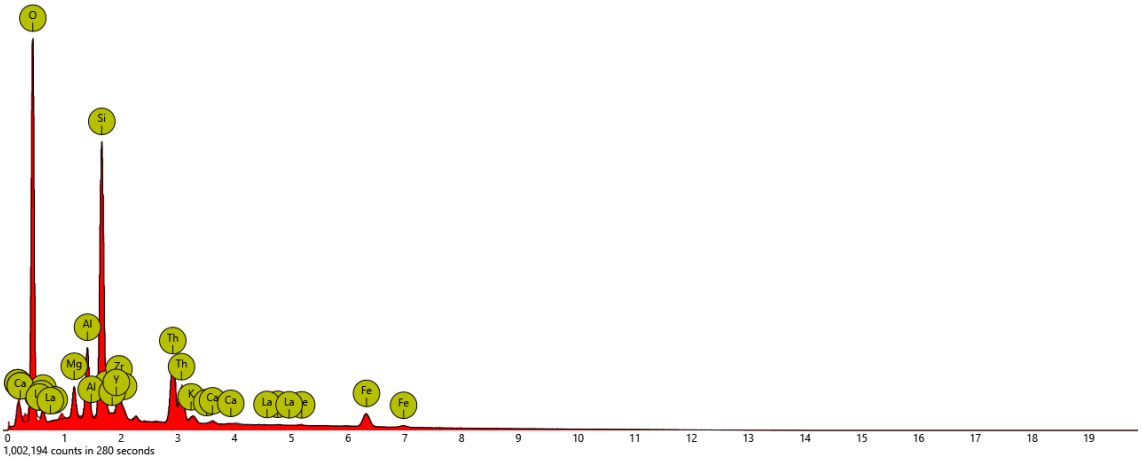

Disabled elements: Ag, At, B, Bi, Br, C, Cs, Fr, Ga, I, In, N, Po, Ra, Re, Rn, Sb, Se, Sr, Tb, Tc, Te, W

7 Min 5 vaalea sulk b

1. spot

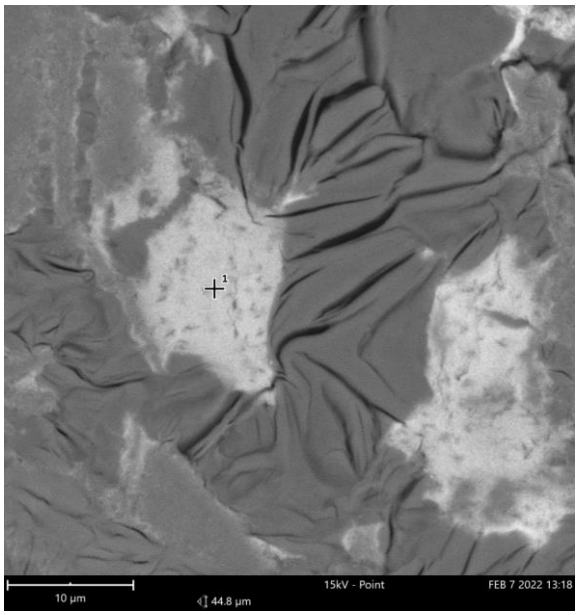

Element Number	Element Symbol	Element Name	Atomic Conc.	Weight Conc.
90	Th	Thorium	6.57	42.30
8	O	Oxygen	64.93	28.84
14	Si	Silicon	14.43	11.25
40	Zr	Zirconium	2.38	6.03
26	Fe	Iron	2.46	3.82
13	Al	Aluminium	4.35	3.26
12	Mg	Magnesium	2.84	1.92
60	Nd	Neodymium	0.24	0.95
11	Na	Sodium	1.34	0.85
58	Ce	Cerium	0.07	0.28
20	Ca	Calcium	0.19	0.21
19	K	Potassium	0.17	0.18
62	Sm	Samarium	0.03	0.12
57	La	Lanthanum	0.00	0.00

FOV: 44.8 µm, Mode: 15kV - Point, Detector: BSD Full, Time: FEB 7 2022 13:18

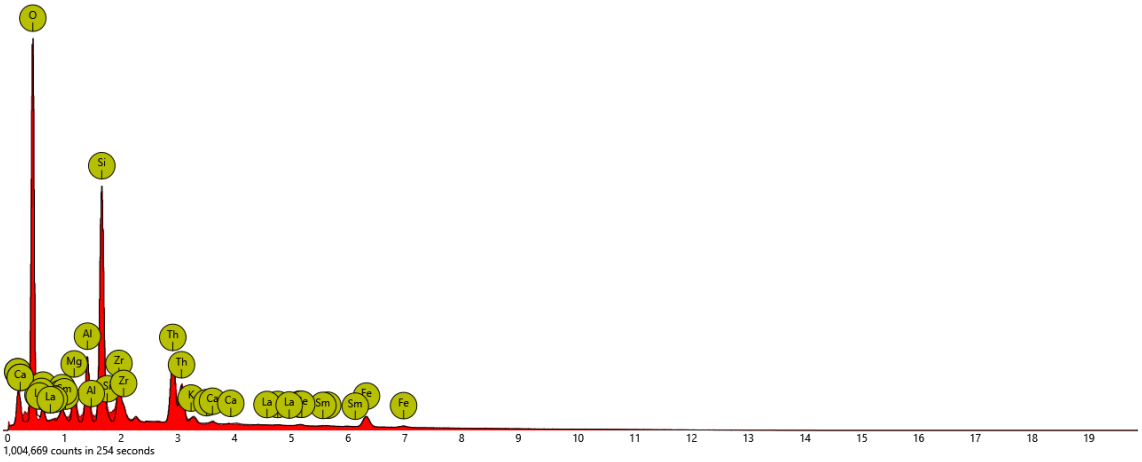

Disabled elements: Ag, At, B, Bi, Br, C, Cs, Fr, Ga, I, In, N, Po, Ra, Re, Rn, Sb, Se, Sr, Tb, Tc, Te, W

8 Min 6 a

1. spot

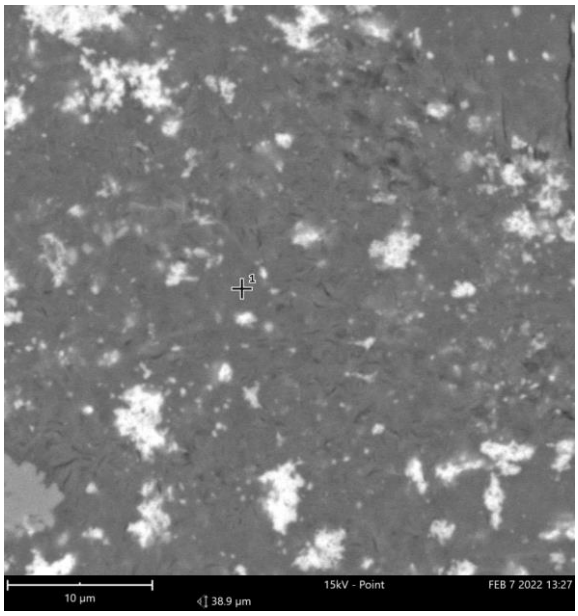

Element Number	Element Symbol	Element Name	Atomic Conc.	Weight Conc.
8	O	Oxygen	67.86	52.27
14	Si	Silicon	13.15	17.78
12	Mg	Magnesium	8.04	9.41
13	Al	Aluminium	6.25	8.12
26	Fe	Iron	3.01	8.09
90	Th	Thorium	0.16	1.84
11	Na	Sodium	0.70	0.78
20	Ca	Calcium	0.33	0.64
19	K	Potassium	0.26	0.50
25	Mn	Manganese	0.17	0.44
22	Ti	Titanium	0.06	0.15

FOV: 38.9 µm, Mode: 15kV - Point, Detector: BSD Full, Time: FEB 7 2022 13:27

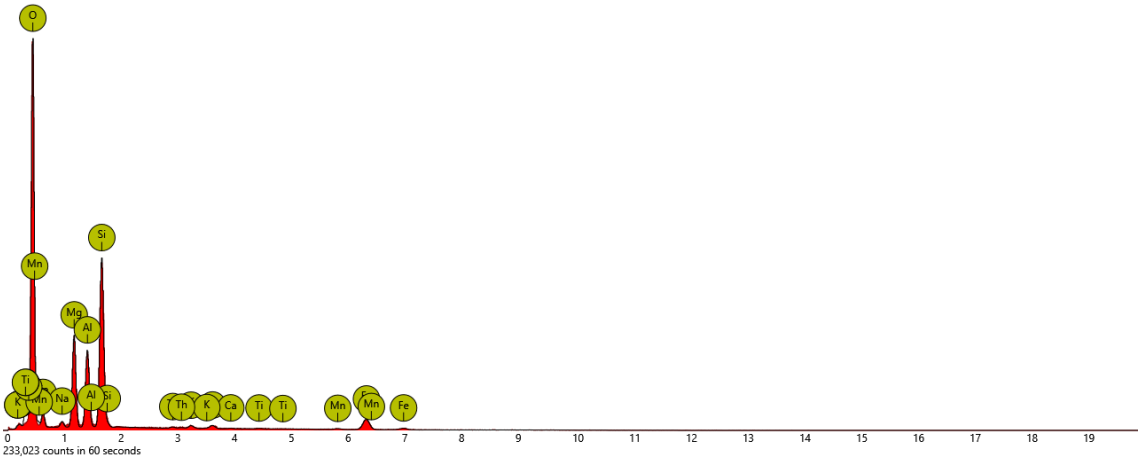

Disabled elements: Ag, At, B, Bi, Br, C, Cs, Fr, Ga, I, N, Po, Ra, Re, Rn, Sb, Se, Sr, Tb, Tc, Te, W

2. spot

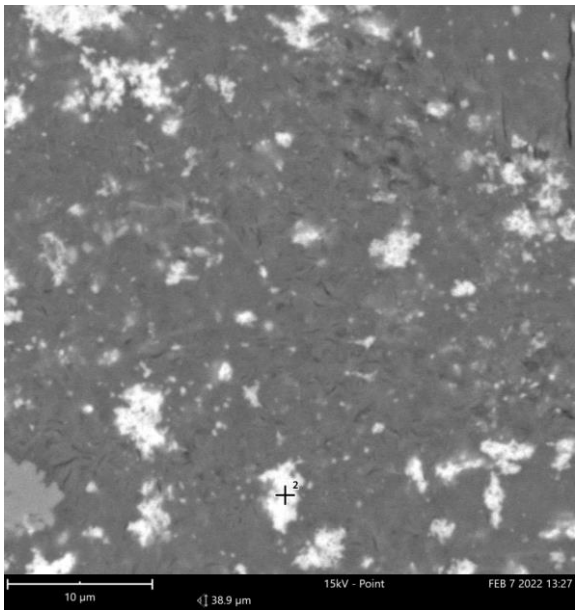

Element Number	Element Symbol	Element Name	Atomic Conc.	Weight Conc.
90	Th	Thorium	5.80	38.18
8	O	Oxygen	65.09	29.55
14	Si	Silicon	14.46	11.53
40	Zr	Zirconium	2.58	6.69
26	Fe	Iron	2.08	3.30
13	Al	Aluminium	3.89	2.98
12	Mg	Magnesium	2.92	2.01
39	Y	Yttrium	0.61	1.54
60	Nd	Neodymium	0.35	1.45
11	Na	Sodium	1.05	0.68
58	Ce	Cerium	0.16	0.65
20	Ca	Calcium	0.39	0.44
19	K	Potassium	0.32	0.35
57	La	Lanthanum	0.08	0.33
22	Ti	Titanium	0.12	0.17
25	Mn	Manganese	0.08	0.13

FOV: 38.9 µm, Mode: 15kV - Point, Detector: BSD Full, Time: FEB 7 2022 13:27

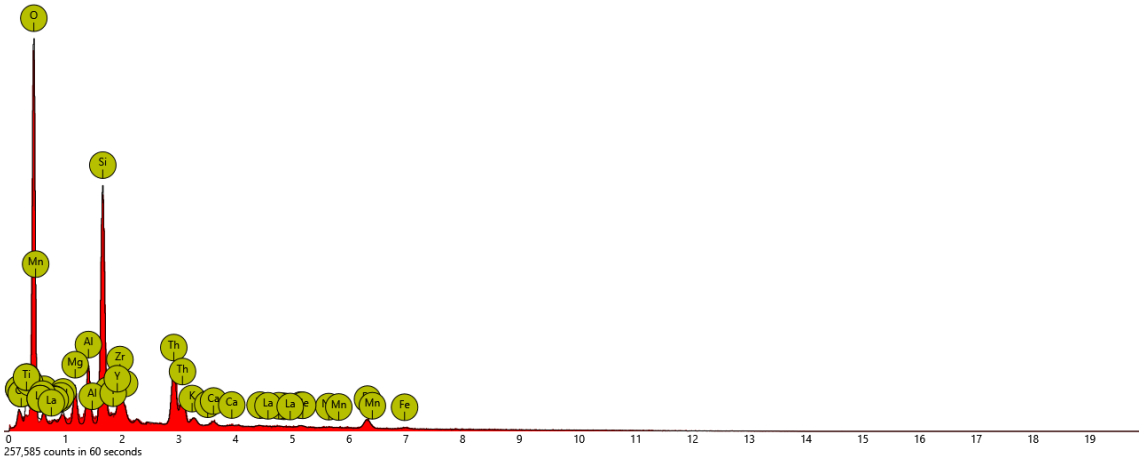

Disabled elements: Ag, At, B, Bi, Br, C, Cs, Fr, Ga, I, N, Po, Ra, Re, Rn, Sb, Se, Sr, Tb, Tc, Te, W

9 Min 6 b

1. spot

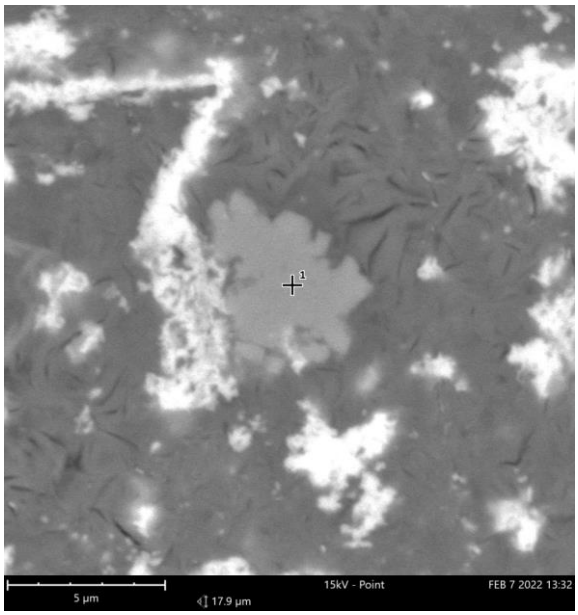

Element Number	Element Symbol	Element Name	Atomic Conc.	Weight Conc.
8	O	Oxygen	76.47	56.28
22	Ti	Titanium	13.54	29.81
14	Si	Silicon	5.10	6.59
26	Fe	Iron	0.98	2.52
13	Al	Aluminium	1.78	2.21
12	Mg	Magnesium	1.37	1.54
11	Na	Sodium	0.44	0.46
19	K	Potassium	0.15	0.27
20	Ca	Calcium	0.13	0.24
25	Mn	Manganese	0.03	0.07

FOV: 17.9 µm, Mode: 15kV - Point, Detector: BSD Full, Time: FEB 7 2022 13:32

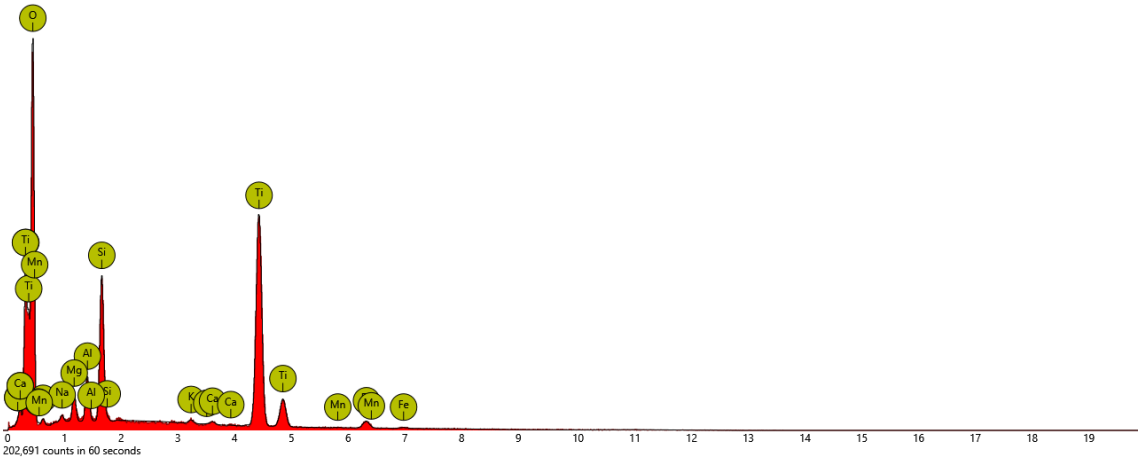

Disabled elements: Ag, At, B, Bi, Br, C, Cs, Fr, Ga, I, N, Po, Ra, Re, Rn, Sb, Se, Sr, Tb, Tc, Te, W

2. spot

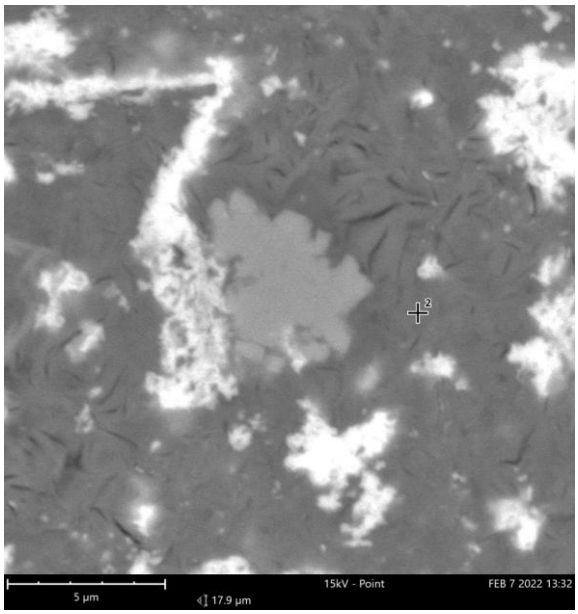

Element Number	Element Symbol	Element Name	Atomic Conc.	Weight Conc.
8	O	Oxygen	66.94	51.37
14	Si	Silicon	13.67	18.42
12	Mg	Magnesium	8.24	9.61
26	Fe	Iron	3.16	8.46
13	Al	Aluminium	6.40	8.28
90	Th	Thorium	0.14	1.53
11	Na	Sodium	0.71	0.78
20	Ca	Calcium	0.28	0.54
19	K	Potassium	0.23	0.44
25	Mn	Manganese	0.13	0.33
22	Ti	Titanium	0.11	0.24
57	La	Lanthanum	0.00	0.00
58	Ce	Cerium	0.00	0.00

FOV: 17.9 µm, Mode: 15kV - Point, Detector: BSD Full, Time: FEB 7 2022 13:32

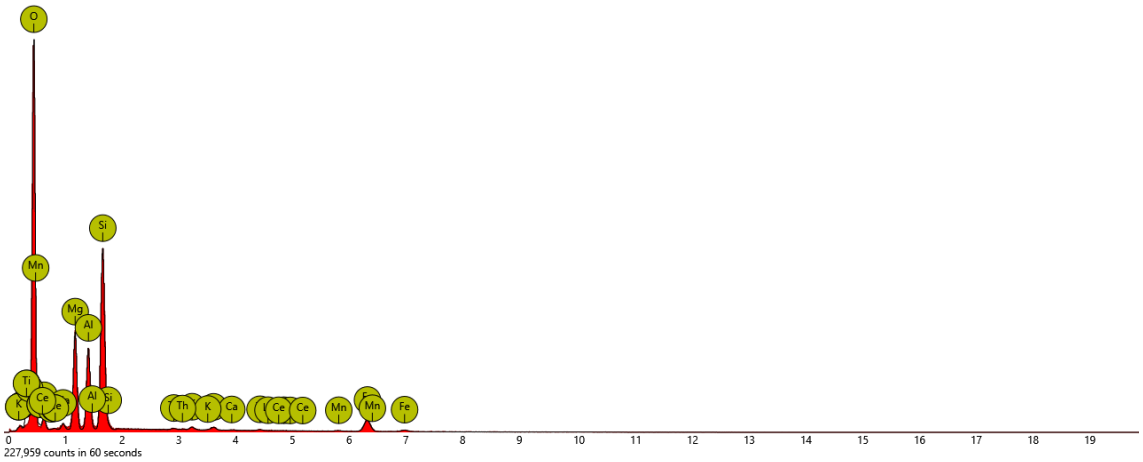

Disabled elements: Ag, At, B, Bi, Br, C, Cs, Fr, Ga, I, N, Po, Ra, Re, Rn, Sb, Se, Sr, Tb, Tc, Te, W

3. spot

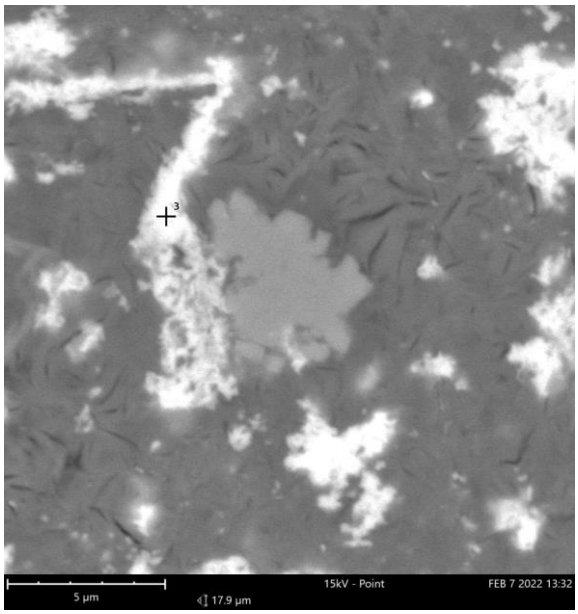

Element Number	Element Symbol	Element Name	Atomic Conc.	Weight Conc.
90	Th	Thorium	4.96	35.97
8	O	Oxygen	68.26	34.10
14	Si	Silicon	13.77	12.08
40	Zr	Zirconium	2.04	5.80
26	Fe	Iron	2.17	3.78
13	Al	Aluminium	3.87	3.26
12	Mg	Magnesium	3.20	2.43
39	Y	Yttrium	0.40	1.11
20	Ca	Calcium	0.42	0.53
19	K	Potassium	0.30	0.36
11	Na	Sodium	0.44	0.31
22	Ti	Titanium	0.18	0.26
25	Mn	Manganese	0.00	0.00
60	Nd	Neodymium	0.00	0.00
58	Ce	Cerium	0.00	0.00
57	La	Lanthanum	0.00	0.00

FOV: 17.9 µm, Mode: 15kV - Point, Detector: BSD Full, Time: FEB 7 2022 13:32

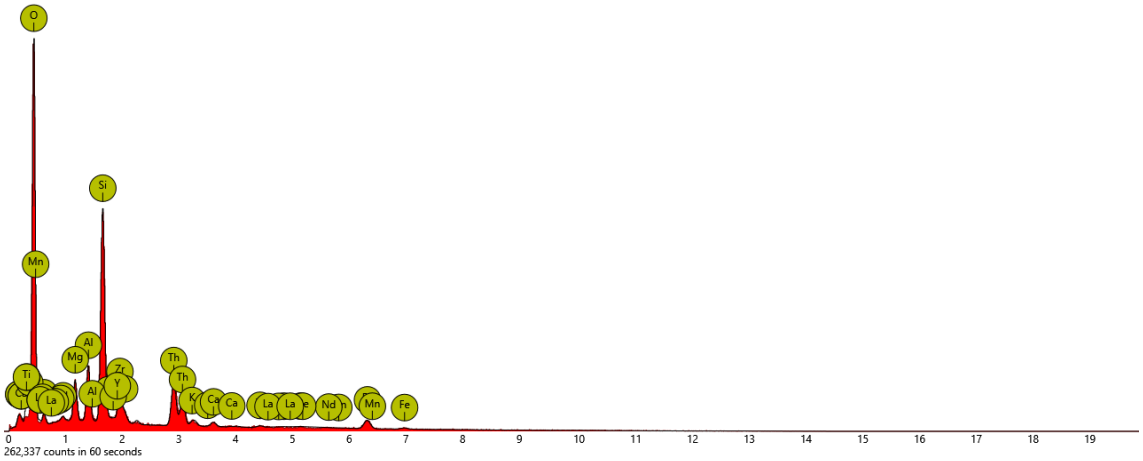

Disabled elements: Ag, At, B, Bi, Br, C, Cs, Fr, Ga, I, N, Pa, Po, Ra, Re, Rn, Sb, Se, Sr, Tb, Tc, Te, W

4. spot

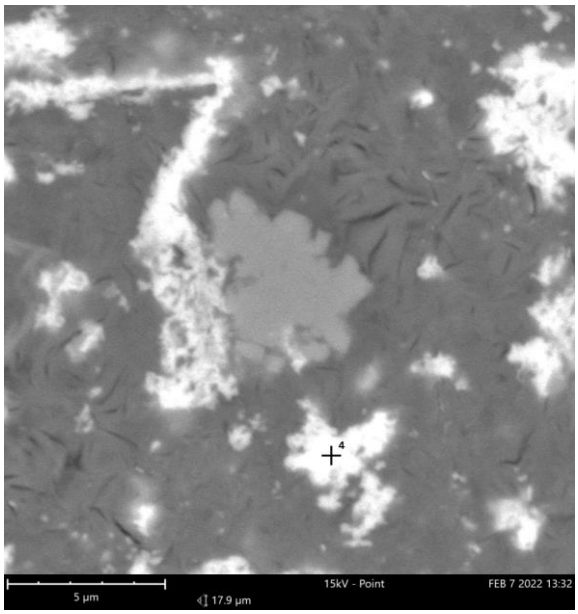

Element Number	Element Symbol	Element Name	Atomic Conc.	Weight Conc.
90	Th	Thorium	6.45	41.17
8	O	Oxygen	64.33	28.33
14	Si	Silicon	15.02	11.61
40	Zr	Zirconium	2.67	6.71
26	Fe	Iron	1.96	3.01
13	Al	Aluminium	3.98	2.95
12	Mg	Magnesium	3.15	2.11
60	Nd	Neodymium	0.24	0.94
58	Ce	Cerium	0.20	0.79
11	Na	Sodium	0.94	0.59
62	Sm	Samarium	0.12	0.48
20	Ca	Calcium	0.37	0.41
19	K	Potassium	0.29	0.32
57	La	Lanthanum	0.08	0.29
22	Ti	Titanium	0.20	0.26
25	Mn	Manganese	0.02	0.03

FOV: 17.9 µm, Mode: 15kV - Point, Detector: BSD Full, Time: FEB 7 2022 13:32

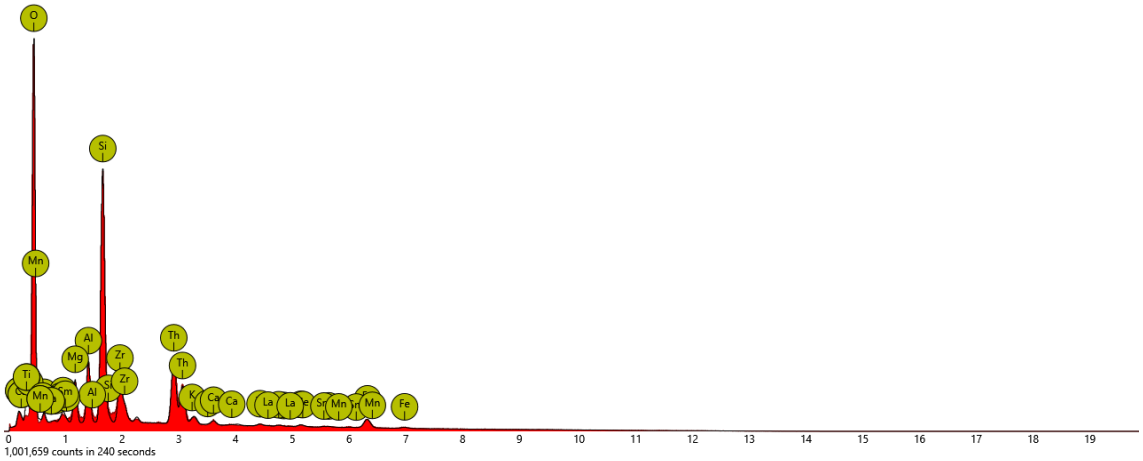

Disabled elements: Ag, At, B, Bi, Br, C, Cs, Fr, Ga, I, N, Po, Ra, Re, Rn, Sb, Se, Sr, Tb, Tc, Te, W

10 Hie 1 Image 10 zirkon

1. spot

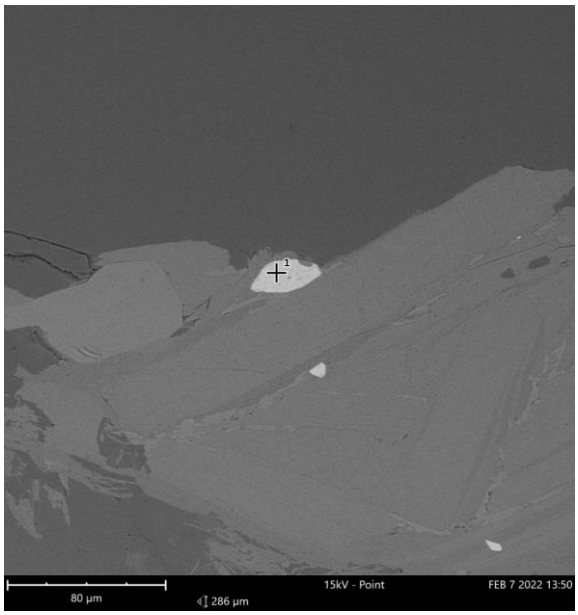

Element Number	Element Symbol	Element Name	Atomic Conc.	Weight Conc.
8	O	Oxygen	72.72	44.98
40	Zr	Zirconium	10.40	36.67
14	Si	Silicon	15.50	16.83
13	Al	Aluminium	1.30	1.35

FOV: 286 µm, Mode: 15kV - Point, Detector: BSD Full, Time: FEB 7 2022 13:50

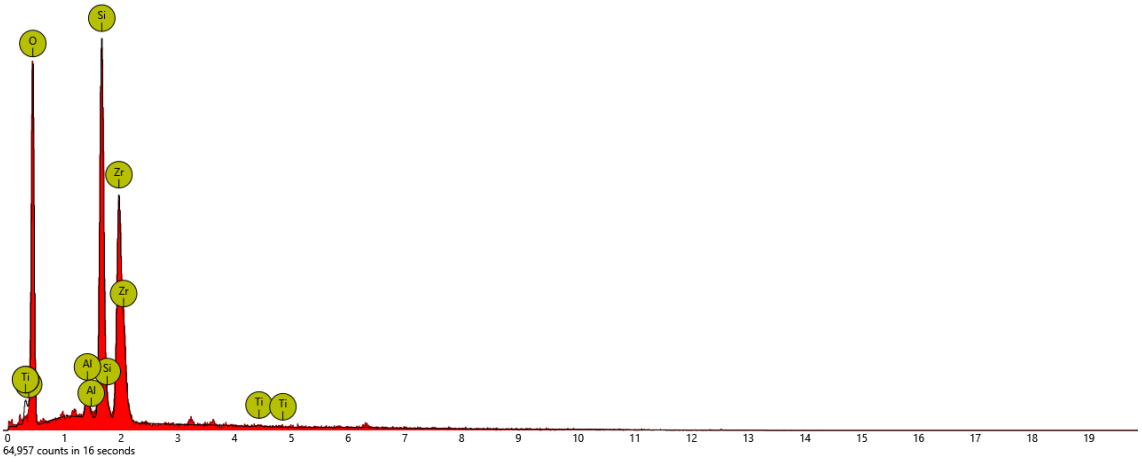

Disabled elements: Ag, At, B, Bi, Br, C, Cs, Fr, Ga, I, In, N, Po, Ra, Re, Rn, Sb, Se, Sr, Tb, Tc, Te, W

11 Min 1 vaalea A

1. spot

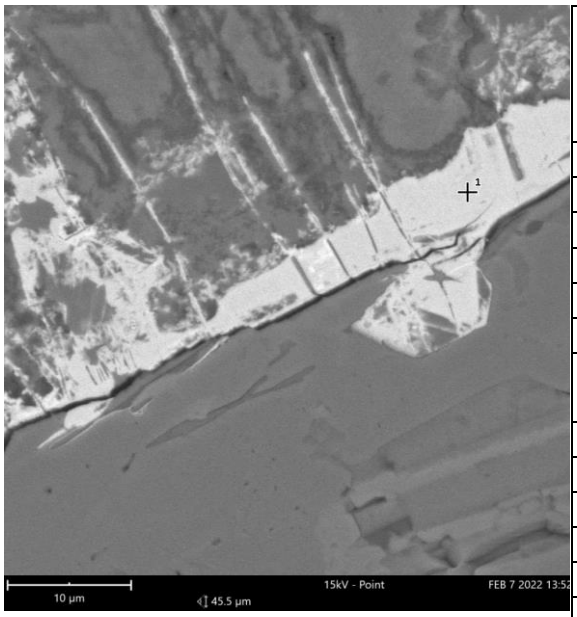

Element Number	Element Symbol	Element Name	Atomic Conc.	Weight Conc.
8	O	Oxygen	64.49	30.68
58	Ce	Cerium	6.40	26.65
14	Si	Silicon	14.41	12.04
60	Nd	Neodymium	2.19	9.41
57	La	Lanthanum	1.84	7.59
13	Al	Aluminium	4.08	3.27
59	Pr	Praseodymium	0.67	2.82
26	Fe	Iron	1.35	2.24
20	Ca	Calcium	1.43	1.71
11	Na	Sodium	1.81	1.24
90	Th	Thorium	0.15	1.03
12	Mg	Magnesium	0.76	0.55
62	Sm	Samarium	0.07	0.33
22	Ti	Titanium	0.17	0.24
19	K	Potassium	0.19	0.22
25	Mn	Manganese	0.00	0.00

FOV: 45.5 µm, Mode: 15kV - Point, Detector: BSD Full, Time: FEB 7 2022 13:52

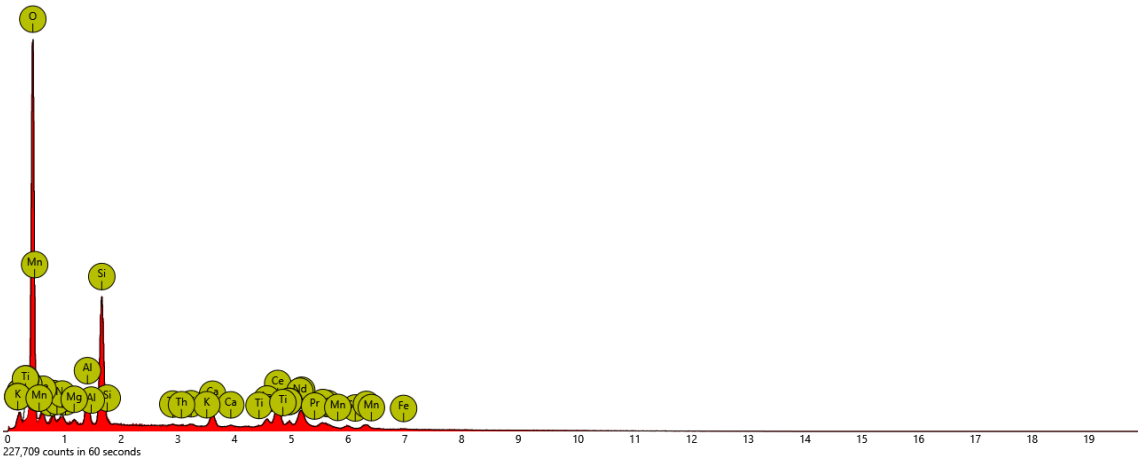

Disabled elements: Ag, At, B, Bi, Br, C, Cs, Fr, Ga, I, N, Po, Ra, Re, Rn, Sb, Se, Sr, Tb, Tc, Te, W

12 Min 1 vaalea B

1. spot

Element Number	Element Symbol	Element Name	Atomic Conc.	Weight Conc.
58	Ce	Cerium	7.93	31.15
8	O	Oxygen	62.12	27.88
14	Si	Silicon	15.24	12.00
60	Nd	Neodymium	2.38	9.63
57	La	Lanthanum	2.25	8.79
13	Al	Aluminium	4.13	3.12
26	Fe	Iron	1.43	2.24
20	Ca	Calcium	1.71	1.93
90	Th	Thorium	0.17	1.12
11	Na	Sodium	1.27	0.82
12	Mg	Magnesium	0.71	0.48
22	Ti	Titanium	0.26	0.35
19	K	Potassium	0.28	0.31
25	Mn	Manganese	0.11	0.18

FOV: 122 µm, Mode: 15kV - Point, Detector: BSD Full, Time: FEB 7 2022 13:55

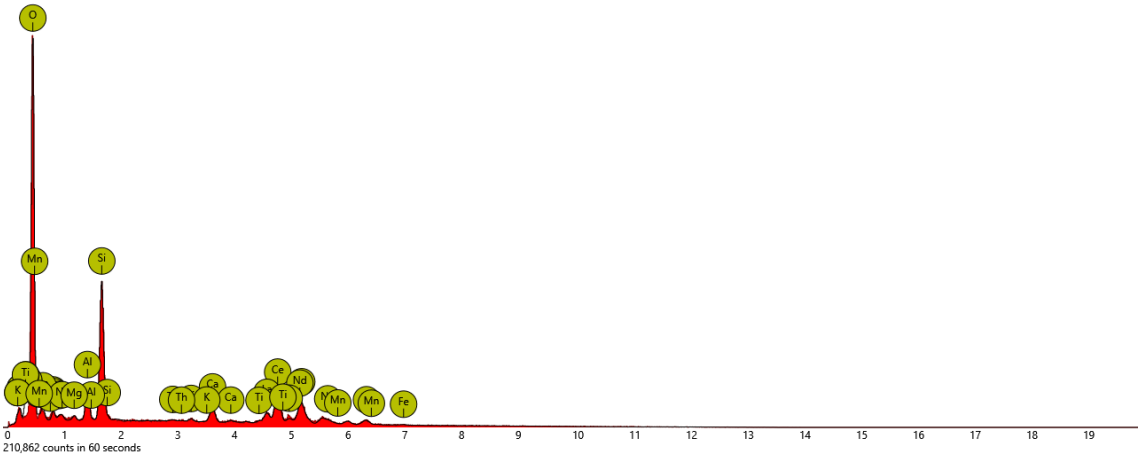

Disabled elements: Ag, At, B, Bi, Br, C, Cs, Fr, Ga, I, N, Po, Ra, Re, Rn, Sb, Se, Sr, Tb, Tc, Te, W

2. spot

Element Number	Element Symbol	Element Name	Atomic Conc.	Weight Conc.
8	O	Oxygen	73.63	46.04
40	Zr	Zirconium	10.17	36.24
14	Si	Silicon	14.56	15.98
13	Al	Aluminium	1.65	1.74

FOV: 122 µm, Mode: 15kV - Point, Detector: BSD Full, Time: FEB 7 2022 13:55

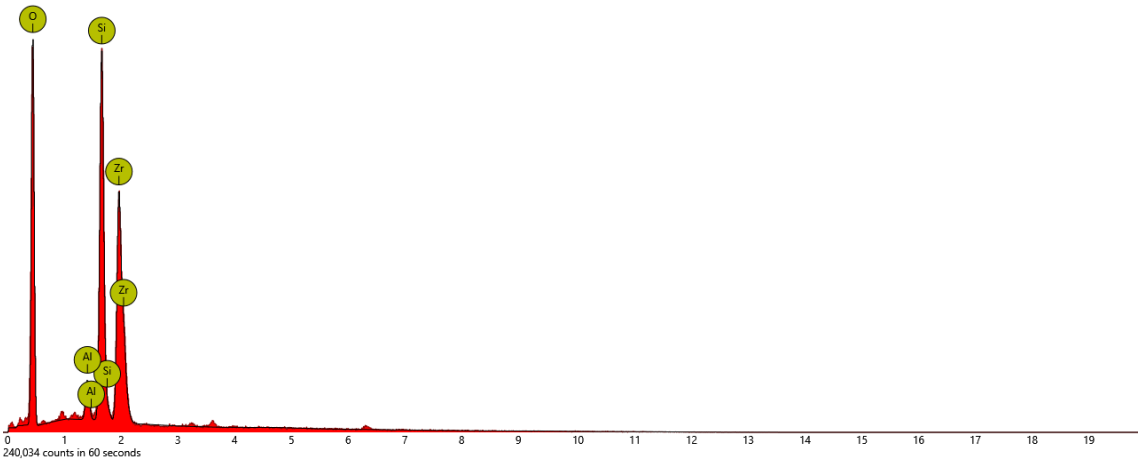

Disabled elements: Ag, At, B, Bi, Br, C, Cs, Fr, Ga, I, N, Po, Ra, Re, Rn, Sb, Se, Sr, Tb, Tc, Te, W

3. spot

Element Number	Element Symbol	Element Name	Atomic Conc.	Weight Conc.
8	O	Oxygen	67.09	47.90
14	Si	Silicon	18.55	23.24
13	Al	Aluminium	6.63	7.98
58	Ce	Cerium	0.77	4.80
90	Th	Thorium	0.40	4.12
11	Na	Sodium	3.34	3.42
60	Nd	Neodymium	0.38	2.48
26	Fe	Iron	0.84	2.10
20	Ca	Calcium	0.79	1.41
57	La	Lanthanum	0.14	0.86
19	K	Potassium	0.34	0.59
12	Mg	Magnesium	0.47	0.51
22	Ti	Titanium	0.20	0.42
25	Mn	Manganese	0.06	0.15
62	Sm	Samarium	0.00	0.00

FOV: 122 µm, Mode: 15kV - Point, Detector: BSD Full, Time: FEB 7 2022 13:55

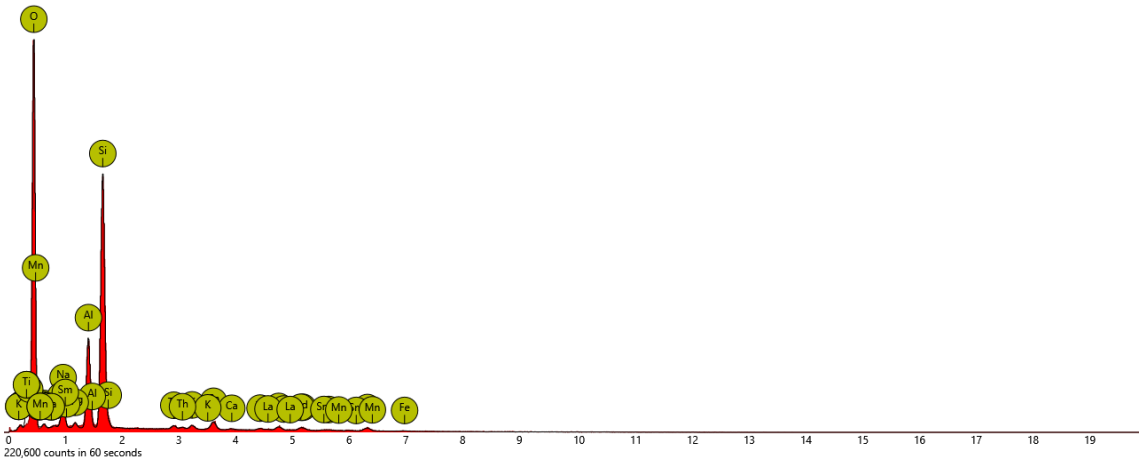

Disabled elements: Ag, At, B, Bi, Br, C, Cs, Fr, Ga, I, N, Po, Ra, Re, Rn, Sb, Se, Sr, Tb, Tc, Te, W

Attachment C. Petrography of the studied samples

Sample code	Rock type (petrography)	Group	Main minerals (over 10 %)	Common minerals (5-10 %)	Accessory minerals (less than 5 %)
KK8$-2020-1.2	Biotite-Hornblende-Gneiss	Gneisses	hbl, bt, plg	qtz	mv, tt, allanite, opaque minerals, chl
KK8$-2020-102.2	Tonalite	Tonalites	plg, qtz, bt	hbl, colorless clinoamphibole (tschermakite or pargasite)	tt, opaque minerals, zr
KK8$-2020-104.2	Tonalitic Dike, leucocratic	Dikes	plg, qtz	bt, mv	zr, opaque minerals
KK8$-2020-202.2	Granodiorite	Granodiorites	qtz, plg, kfs	bt	ms, allanite, opaque minerals
KK8$-2020-203.3	Hornblende Tonalite	Tonalites	plg, qtz, hbl	bt	allanite, tt, zr, ap, mv
KK8$-2020-208.1	Hornblende-Biotite-Gneiss	Gneisses	plg, qtz, bt, hbl	tt	allanite, monazite, zr
KK8$-2020-209.3	Tonalite	Tonalites	plg, qtz, bt, hbl		tt, allanite, opaque minerals, iron oxides, zr
KK8$-2020-302.2	Granodiorite	Granodiorites	qtz, plg, kfs, bt		chl, tt, zr, allanite
KK8$-2020-305.1	Tonalitic Dike	Dikes	plg, qtz, bt		Iron oxides, opaque minerals, tt, allanite, (epidote), mv, zr
KK8$-2020-305.2	Hornblende Tonalite	Tonalites	plg, hbl, bt, qtz	tt	zr, allanite, opaque minerals, ap
KK8$-2020-406.4	Tonalite	Tonalites	plg, qtz, bt	hbl	tt, ap

KK8$-2020-409.2	Hornblende Tonalite	Tonalites	hbl, plg, qtz		tt, bt, chl, mv
KK8$-2020-427.2	Hornblende-Gneiss	Gneisses	plg, hbl, qtz	bt	tt, chl
KK8$-2020-603.2	Chlorite-Biotite-Gneiss	Gneisses	plg, bt, qtz, chl	hbl, zr, kfs	opaque minerals, ap, tt
KK8$-2020-605.2	Hornblende-Gneiss	Gneisses	hbl, plg, qtz		tt, zr, opaque minerals, allanite
KK8$-2020-611.3	Tonalite	Tonalites	plg, qtz, bt	hbl	tt, zr, ap, chl
KK8$-2020-611.4	Granitic Dike, leucocratic	Dikes	qtz, kfs, plg		bt, gt
KK8$-2020-626.3	Tonalite, leucocratic	Tonalites	plg, qtz	chl, mv	opaque minerals
KK8$-2020-702.2	Biotite-Gneiss	Gneisses	plg, qtz, bt	hbl, kfs	tt, opaque minerals, zr, allanite
KK8$-2020-702.6	Granodiorite		Qtz, kfs, plg	bt	opaque minerals, bt, allanite, iron oxide
KK8$-2020-704.1	Granodiorite	Granodiorites	qtz, plg, kfs, hbl	tt, bt	opaque minerals(ilmenite-magnetite), allanite, chl
KK8$-2020-706.2	Hornblende-Biotite-Gneiss	Gneisses	plg(andesine), qtz, bt, hbl		allanite, tt, zr, chl, opaque minerals
KK8$-2020-706.3	Biotite-K-feldspar-Hornblende-Gneiss	Gneisses	plg, qtz, hbl, kfs	bt	allanite, tt, chl, zr, mv, opaque minerals
KK8$-2020-718.5	Granitic Dike, leucocratic	Dikes	qtz, plg, kfs		mv, opaque minerals, chl

KK8$-2020-719.2	Biotite Hornblende Tonalite	Tonalites	plg, hbl, qtz, bt		tt, opaque minerals, zr, mv
KK8$-2020-801.2	Tonalite	Tonalites	plg, qtz	bt	zr, tt
KK8$-2020-801.4	Tonalite	Tonalites	plg, qtz, bt, hbl		zr, opaque minerals, tt, chl
KK8$-2020-801.5	Granodioritic Dike	Dikes	plg, qtz, kfs	bt	zr, opaque minerals, tt, chl, allanite
KK8$-2020-810.1	Biotite-Hornblende-Gneiss	Gneisses	qtz, plg, hbl, bt	kfs	tt, allanite, opaque minerals, zr
KK8$-2020-909.2	Tonalite	Tonalites	plg, qtz, bt	gt	tt, zr
KK8$-2020-1004.2	Amfibolite-Gneiss	Tonalites	plg, qtz, bt, hbl-colorless clinoamfibole		zr, opaque minerals, allanite
KK8$-2020-1010.1	Biotite Hornblende Tonalite	Tonalites	hbl, plg, bt, qtz		allanite, iron hydroxide, opaque minerals, tt, zr,
KK8$-2020-1111.3	Granodioritic Dike, leucocratic	Dikes	qtz, plg, kfs		bt, allanite, opaque minerals, gt
KK8$-2020-1111.4	Hornblende-Biotite-Gneiss	Gneisses	plg, qtz, bt, hbl		tt, opaque minerals, zr, allanite
KK8$-2020-1204.2	Amfibolite-Gneiss	Gneisses	plg (An25), hbl-colorless clinoamphibole, qtz	bt	zr, gt, opaque minerals
KK8$-2020-1419.1	Tonalite	Tonalites	plg, bt, qtz	hbl, tt	zr
KK8$-2020-1633.2	Hornblende Tonalite	Tonalites	plg, hbl, bt, qtz, chl	tt	opaque minerals, zr, allanite
KK8$-2020-1659.2	Granitic Dike	Dikes	qtz, plg, kfs		allanite, bt

MOTU-2021-9.1	Diorite	Diorite	plg (An55-60), bt, cpx	qtz, hbl	chl, tt-ag
MOTU-2021-11.1	Hornblende-gneiss	Gneisses	plg, hbl, qtz, bt		zr, ap, chl, opaque minerals, tt, mv
MOTU-2021-17.1	Granodiorite, leucocratic	Granodiorites	qtz, plg, kfs	bt	zr, mv, chl,
MOTU-2021-22.1	Chlorite Tonalite	Tonalites	plg, qtz, hbl, chl		monazite, allanite, mv, ap
MOTU-2021-24.1	Tonalite	Tonalites	plg, qtz, bt, hbl		ap, tt, zr, chl
MOTU-2021-25.1	Biotite-K-feldspar-Gneiss	Gneisses	plg, qtz, bt, kfs	hbl	zr, tt, opaque minerals, allanite, mv
MOTU-2021-28.1	Biotite K-feldspar-Gneiss	Gneisses	plg, qtz, kfs	bt	chl, mv
MOTU-2021-32.1	Biotite-Gneiss	Gneisses	plg, bt, qtz	hbl	opaque minerals, zr, tt
MOTU-2021-34.1	Tonalite	Tonalites	plg, qtz, bt	hbl	allanite, zr, ap, tt, opaque minerals, chl
VSVE-2021-1.1	Granodiorite, leucocratic	Granodiorites	qtz, plg, kfs	bt	chl, allanite, opaque minerals, zr
VSVE-2021-1.4	Granodiorite		qtz, plg, kfs	tt, bt	allanite, chl, opaque minerals
VSVE-2021-6.1	Granodiorite	Granodiorites	plg, qtz, bt	hbl, kfs	mv, allanite, opaque minerals, zr, tt,
VSVE-2021-6.2	Biotite-Hornblende-Gneiss	Gneisses	plg, qtz, hbl, bt	kfs	allanite, tt, zr, chl
VSVE-2021-6.3	Hornblende-Biotite-Gneiss	Gneisses	plg, bt, hbl, qtz	tt	opaque minerals

VSVE-2021-7.1	Hornblende Tonalite	Tonalites	plg, hbl, qtz	tt, bt	allanite, zr, chl
VSVE-2021-9.1	Tonalite	Tonalites	plg, qtz, hbl-colorless clino amphibole, bt		zr
VSVE-2021-9.3	Granodiorite, leucocratic	Granodiorites	plg, qtz, kfs	bt	mv
VSVE-2021-10.1	Granite, leucocratic	Granite	plg, qtz, kfs	bt, gr, tt	opaque minerals, chl, allanite
VSVE-2021-10.2	Garnet-Hornblende-gneiss	Gneisses	plg, qtz, hbl, gt	tt, bt	zr
VSVE-2021-11.1	Granodiorite	Granodiorites	qtz, plg, kfs	bt	zr, chl, allanite,
VSVE-2021-11.2	Biotite-Gneiss	Gneisses	plg, qtz, bt	hbl	zr, allanite, chl, hbl
VSVE-2021-11.3	granodioritic Dike	Dikes	plg, qtz, kfs	bt	allanite
VSVE-2021-12.1	Tonalite	Tonalites	plg, qtz, bt, hbl	gr, tt	zr
VSVE-2021-14.1	Tonalite	Tonalites	plg, qtz, bt	hbl	tt, allanite, zr, opaque minerals
VSVE-2021-15.1	Tonalite	Tonalites	plg, qtz, bt, hbl	chl	tt
VSVE-2021-16.1	Tonalite	Tonalites	plg, qtz, bt, hbl	tt	opaque minerals, zr, allanite, monazite, mv, chl
VSVE-2021-17.2	Tonalite	Tonalites	plg, qtz, bt	chl	zr, allanite, opaque minerals, epidote

Attachment D. Geochemical analyses of the samples

SAMPLE	**KK8$-2020-1.2**	**KK8$-2020-102.2**	**KK8$-2020-104.2**	**KK8$-2020-202.2**	**KK8$-2020-203.3**	**KK8$-2020-208.1**	**KK8$-2020-209.3**
Group	**Gneiss**	**Tonalites**	**Dikes**	**Granodiorites**	**Tonalites**	**Gneiss**	**Tonalites(Eu+)**
Al_2O_3	16.58	14.87	14.03	13.48	16.79	17.14	15.88
BaO	0.06	0.23	0.09	0.15	0.09	0.06	0.12
CaO	6.58	3.34	1.64	0.82	5.50	4.55	4.05
Cr_2O_3	<0.01	<0.01	<0.01	<0.01	<0.01	<0.01	<0.01
Fe_2O_3	11.58	7.58	2.14	2.05	5.38	6.20	4.36
K2O	2.40	4.37	2.04	5.08	2.07	1.99	1.71
MgO	4.54	1.34	0.53	0.34	2.35	2.23	1.10
MnO	0.21	0.10	0.03	0.03	0.11	0.11	0.08
Na_2O	3.78	3.02	4.28	3.04	3.97	4.56	4.68
P_2O_5	0.18	0.42	0.06	0.05	0.20	0.28	0.14
SO_3	0.01	0.02	<0.01	<0.01	<0.01	0.03	0.07
SiO_2	52.67	63.00	74.28	74.00	62.22	61.65	67.05
SrO	0.06	0.05	0.03	0.02	0.08	0.07	0.08
TiO_2	1.28	1.08	0.26	0.22	0.54	0.70	0.46
Ba	366.00	1875.00	739.00	1195.00	691.00	420.00	917.00
Ce	25.40	138.50	112.00	67.90	43.10	47.70	26.10
Cr	10.00	10.00	10.00	<10.00	20.00	20.00	20.00
Cs	3.69	0.82	2.37	2.96	1.64	2.16	1.13
Dy	4.83	7.04	4.09	2.19	5.75	3.71	2.01
Er	2.79	3.47	1.93	1.37	3.09	1.87	1.05
Eu	1.22	2.28	1.20	0.50	1.20	1.00	1.49
Ga	18.60	20.6	16.40	15.20	16.60	17.90	15.90
Gd	5.22	9.25	5.82	2.14	6.72	4.30	2.40
Hf	1.70	11.40	6.80	5.50	2.40	4.20	4.20
Ho	0.95	1.27	0.70	0.43	1.06	0.67	0.35
La	10.70	72.60	53.40	24.00	19.30	25.20	15.60
Lu	0.44	0.41	0.26	0.28	0.40	0.24	0.13
Nb	10.70	21.10	14.00	9.50	7.30	9.80	2.80
Nd	17.00	62.80	43.60	16.30	27.90	22.70	12.90
Pr	3.83	16.95	12.80	5.17	6.41	5.69	3.16
Rb	100.00	98.60	76.40	152.00	52.60	80.80	39.70
Sm	4.64	11.55	7.87	2.55	6.8	4.81	2.67
Sn	4.00	1.00	2.00	1.00	3.00	3.00	2.00
Sr	381.00	303.00	206.00	156.00	531.00	539.00	590.00
Ta	0.80	0.80	1.10	1.00	0.70	0.50	0.10
Tb	0.77	1.28	0.82	0.38	1.01	0.63	0.34

Th	1.72	9.44	20.60	13.60	3.14	6.77	0.97
Tm	0.40	0.44	0.26	0.22	0.43	0.24	0.12
U	0.69	0.68	4.34	4.45	0.57	0.73	0.47
V	293.00	51.00	16.00	13.00	77.00	92.00	46.00
W	1.00	<1.00	1.00	<1.00	<1.00	<1.00	<1.00
Y	26.80	34.40	20.80	12.90	29.60	19.20	9.20
Yb	2.93	2.99	1.82	1.77	2.81	1.61	0.85
Zr	56.00	465.00	243.00	189.00	84.00	153.00	165.00
Eu*	0.25	0.22	0.18	0.21	0.18	0.22	0.59
Eu/Eu*	0.76	0.67	0.54	0.65	0.54	0.67	1.80
$(La/Yb)_n$	2.46	16.37	19.78	9.14	4.63	10.55	12.37

SAMPLE	**KK8$-2020-302.2**	**KK8$-2020-305.1**	**KK8$-2020-305.2**	**KK8$-2020-406.4**	**KK8$-2020-409.2**	**KK8$-2020-427.2**	**KK8$-2020-603.2**
Group	**Granodiorites**	**Dikes**	**Tonalites**	**Tonalites**	**Tonalites**	**Gneiss**	**Gneiss**
Al_2O_3	13.51	15.18	15.86	15.91	15.36	15.77	15.97
BaO	0.20	0.03	0.06	0.08	0.03	0.16	0.07
CaO	1.27	3.42	8.15	4.79	8.50	5.07	5.45
Cr_2O_3	<0.01	<0.01	0.01	0.01	<0.01	<0.01	0.03
Fe_2O_3	2.80	6.78	11.49	5.72	8.24	7.13	8.90
K_2O	6.05	1.93	1.41	1.68	0.69	2.65	2.31
MgO	0.43	1.60	4.88	2.30	5.38	2.67	4.17
MnO	0.03	0.09	0.22	0.09	0.19	0.13	0.19
Na_2O	2.54	3.96	3.56	4.16	3.95	3.84	3.09
P_2O_5	0.07	0.34	0.26	0.20	0.11	0.21	0.42
SO_3	<0.01	0.34	0.05	0.08	0.02	0.19	<0.01
SiO_2	72.05	65.25	52.65	63.84	56.46	61.23	57.19
SrO	0.05	0.04	0.08	0.10	0.08	0.08	0.05
TiO_2	0.37	0.68	1.04	0.62	0.62	0.81	1.00
Ba	1615.00	175.50	423.00	687.00	161.50	1310.00	462.00
Ce	202.00	22.40	50.30	44.00	58.00	43.10	41.60
Cr	<10.00	10.00	60.00	40.00	20.00	20.00	170.00
Cs	1.50	2.44	0.86	0.89	0.42	0.71	5.52
Dy	2.54	2.37	5.28	2.37	3.86	3.53	3.81
Er	1.04	1.19	3.16	1.34	2.17	1.88	1.67
Eu	0.94	0.61	1.70	1.04	1.48	1.56	1.22
Ga	13.20	18.40	18.90	16.80	16.20	16.20	18.30
Gd	5.73	2.80	5.96	3.05	4.61	4.23	5.02
Hf	9.40	3.90	1.70	3.20	1.40	3.60	3.00
Ho	0.39	0.44	1.02	0.43	0.75	0.64	0.65
La	106.50	10.90	21.80	23.80	26.20	22.90	19.50
Lu	0.17	0.13	0.45	0.17	0.32	0.21	0.21
Nb	4.90	11.60	11.20	7.60	7.80	7.80	8.80
Nd	76.80	11.00	30.00	19.90	29.00	23.00	23.70

Pr	23.30	2.73	7.11	5.36	7.67	5.68	5.54
Rb	120.50	107.00	33.20	41.10	11.40	48.10	132.00
Sm	10.70	2.70	6.57	3.67	5.44	4.86	5.50
Sn	1.00	3.00	2.00	1.00	4.00	1.00	4.00
Sr	360.00	325.00	592.00	790.00	560.00	653.00	400.00
Ta	0.10	0.50	0.50	0.20	0.40	0.20	0.40
Tb	0.62	0.42	0.93	0.42	0.65	0.59	0.70
Th	25.90	3.85	4.91	1.92	3.15	0.85	3.69
Tm	0.14	0.14	0.44	0.17	0.32	0.24	0.20
U	0.99	0.90	0.52	0.23	0.81	0.32	1.13
V	17.00	63.00	300.00	98.00	231.00	123.00	175.00
W	<1.00	<1.00	1.00	<1.00	<1.00	<1.00	1.00
Y	9.90	12.20	30.10	12.50	21.60	17.30	18.30
Yb	0.97	0.86	3.05	1.30	2.39	1.59	1.35
Zr	363.00	135.00	57.00	120.00	41.00	142.00	110.00
Eu*	0.12	0.22	0.27	0.31	0.29	0.34	0.23
Eu/Eu*	0.37	0.68	0.83	0.95	0.90	1.05	0.71
$(La/Yb)_n$	74.02	8.54	4.82	12.34	7.39	9.71	9.73

SAMPLE	**KK8$-2020-605.2**	**KK8$-2020-611.3**	**KK8$-2020-611.4**	**KK8$-2020-626.3**	**KK8$-2020-702.2**	**KK8$-2020-702.6**	**KK8$-2020-704.1**
Groups	**Gneiss**	**Tonalites**	**Dikes(Eu-)**	**Tonalites**	**Gneiss(Eu+)**	**Granodiorites**	**Granodiorites**
Al_2O_3	12.40	17.40	14.02	13.94	14.68	14.64	15.12
BaO	0.06	0.11	0.03	0.23	0.20	0.19	0.13
CaO	8.44	6.02	0.43	1.00	1.82	1.84	3.66
Cr_2O_3	0.05	0.01	<0.01	<0.01	<0.01	<0.01	<0.01
Fe_2O_3	11.06	8.85	1.07	1.73	3.74	3.72	5.41
K_2O	1.04	2.22	5.90	4.50	3.98	4.38	2.27
MgO	6.10	3.18	0.08	0.45	0.40	0.40	1.28
MnO	0.34	0.17	0.27	0.02	0.05	0.06	0.10
Na_2O	2.02	3.84	3.76	3.63	4.30	3.83	3.93
P_2O_5	0.28	0.41	0.03	0.06	0.07	0.07	0.22
SO_3	0.02	0.05	<0.01	0.13	<0.01	<0.01	0.10
SiO_2	56.98	56.19	73.98	73.37	70.17	69.90	66.92
SrO	0.07	0.10	0.01	0.04	0.06	0.05	0.08
TiO_2	0.82	1.04	0.04	0.19	0.35	0.33	0.64
Ba	388.00	895.00	201.00	1945.00	1730.00	1640.00	1020.00
Ce	43.40	55.50	20.40	59.30	27.20	33.80	41.10
Cr	330.00	50.00	<10	10.00	10.00	10.00	20.00
Cs	1.65	2.35	1.47	0.66	0.35	0.82	1.21
Dy	4.22	4.30	11.15	2.07	2.75	2.99	2.70
Er	2.07	2.32	5.80	1.03	1.50	1.59	1.53
Eu	1.69	1.74	0.14	1.14	1.26	1.27	1.10
Ga	14.10	21.00	22.20	10.90	15.40	17.10	17.70

Gd	6.08	5.20	6.39	2.78	3.29	3.19	3.24
Hf	3.00	3.60	3.70	3.30	4.70	5.10	4.80
Ho	0.78	0.79	1.96	0.37	0.53	0.56	0.54
La	17.600	28.90	5.90	32.70	15.20	16.00	20.50
Lu	0.28	0.32	0.95	0.17	0.18	0.19	0.22
Nb	7.00	11.00	24.80	5.40	3.10	4.40	12.50
Nd	27.90	29.40	8.70	22.20	15.50	16.70	19.10
Pr	6.21	7.27	2.30	6.67	3.63	4.00	4.97
Rb	39.70	78.50	245.00	106.50	38.50	66.00	70.10
Sm	6.26	5.95	3.90	3.62	3.30	3.60	3.62
Sn	2.00	1.00	2.00	1.00	1.00	1.00	1.00
Sr	519.00	833.00	53.60	265.00	427.00	347.00	581.00
Ta	0.30	0.40	6.10	0.40	0.10	0.10	0.80
Tb	0.81	0.74	1.72	0.39	0.47	0.45	0.42
Th	2.28	3.14	8.73	11.85	0.49	0.85	3.53
Tm	0.30	0.30	0.91	0.15	0.19	0.22	0.20
U	0.61	0.70	3.64	3.05	0.44	0.65	0.98
V	261.00	128.00	<5.00	21.00	5.00	5.00	48.00
W	1.00	<1.00	<1.00	<1.00	<1.00	<1.00	1.00
Y	21.90	23.00	66.10	11.00	13.80	14.80	13.90
Yb	2.02	2.28	7.37	1.11	1.31	1.51	1.45
Zr	111.00	144.00	54.00	124.00	188.00	203.00	188.00
Eu*	0.27	0.31	0.03	0.36	0.38	0.37	0.32
Eu/Eu*	0.83	0.96	0.09	1.09	1.17	1.15	0.98
$(La/Yb)_n$	5.87	8.54	0.54	19.86	7.82	7.14	9.53

SAMPLE	**KK8$-2020-706.2**	**KK8$-2020-706.3**	**KK8$-2020-718.5**	**KK8$-2020-719.2**	**KK8$-2020-801.2**	**KK8$-2020-801.4**	**KK8$-2020-801.5**
Group	**Gneiss**	**Gneiss**	**Dikes**	**Tonalites**	**Tonalites(Eu+)**	**Tonalites**	**Dikes**
Al_2O_3	14.54	15.17	13.89	17.6	13.25	16.42	14.31
BaO	0.18	0.14	0.15	0.06	0.03	0.11	0.13
CaO	3.64	4.71	1.40	5.95	3.20	5.28	2.02
Cr_2O_3	0.01	0.01	<0.01	<0.01	<0.01	<0.01	<0.01
Fe_2O_3	5.38	7.04	2.92	7.28	1.60	7.64	3.59
K_2O	3.30	2.88	5.63	1.74	0.72	2.31	4.47
MgO	1.94	2.71	0.54	2.80	0.49	2.44	0.89
MnO	0.14	0.17	0.03	0.12	0.02	0.16	0.06
Na_2O	2.88	3.07	2.78	4.37	3.95	4.03	3.17
P_2O_5	0.13	0.18	0.09	0.47	<0.01	0.38	0.14
SO_3	0.01	0.01	0.02	0.11	<0.01	0.12	0.04
SiO_2	66.73	62.53	71.75	58.22	75.93	59.9	70.04
SrO	0.07	0.07	0.05	0.10	0.05	0.09	0.05
TiO_2	0.57	0.74	0.20	0.79	0.19	0.88	0.45
Ba	1585.00	1175.00	1240.00	411.00	206.00	891.00	1145.00

Ce	44.10	43.40	66.30	56.80	10.10	37.20	107.00
Cr	60.00	90.00	20.00	20.00	20.00	40.00	20.00
Cs	0.92	1.07	1.66	3.06	1.14	2.54	4.16
Dy	2.64	3.63	2.03	4.06	0.36	3.89	2.98
Er	1.41	2.01	1.19	2.02	0.22	1.96	1.26
Eu	1.00	1.13	0.60	1.48	0.90	1.54	1.12
Ga	16.80	18.20	15.30	20.70	13.80	19.40	16.60
Gd	3.29	4.23	2.89	5.58	0.43	4.68	4.67
Hf	4.60	4.30	11.00	1.60	8.50	3.10	5.50
Ho	0.48	0.68	0.35	0.71	0.03	0.71	0.49
La	22.50	20.00	30.10	27.00	6.30	17.70	50.90
Lu	0.19	0.28	0.18	0.20	0.04	0.24	0.12
Nb	7.60	10.80	4.70	10.90	2.70	9.90	11.90
Nd	19.60	22.30	24.10	30.30	3.30	22.50	42.50
Pr	5.11	5.60	6.97	7.12	0.98	4.90	11.90
Rb	71.30	74.70	133.50	66.30	30.20	64.20	124.00
Sm	3.65	4.77	4.20	6.16	0.52	4.86	6.77
Sn	1.00	2.00	1.00	2.00	<1.00	1.00	2.00
Sr	568.00	553.00	352.00	745.00	431.00	715.00	377.00
Ta	0.20	0.40	0.40	0.50	0.10	0.80	0.50
Tb	0.42	0.59	0.33	0.68	0.02	0.57	0.51
Th	2.38	1.68	14.45	2.54	0.89	2.12	16.20
Tm	0.20	0.31	0.14	0.23	0.01	0.22	0.13
U	0.50	0.51	2.76	1.25	0.85	0.84	1.57
V	79.00	117.00	23.00	112.00	24.00	99.00	29.00
W	<1.00	<1.00	1.00	1.00	<1.00	1.00	1.00
Y	13.10	19.10	11.30	19.10	2.30	18.40	14.90
Yb	1.37	1.93	1.31	1.51	0.38	1.60	0.97
Zr	176.00	172.00	397.00	60.00	350.00	117.00	219.00
Eu*	0.29	0.25	0.17	0.25	1.90	0.32	0.19
Eu/Eu*	0.88	0.77	0.53	0.77	5.82	0.99	0.61
$(La/Yb)_n$	11.07	6.99	15.49	12.06	11.18	7.46	35.38

SAMPLE	**KK8$-2020-810.1**	**KK8$-2020-909.2**	**KK8$-2020-1004.2**	**KK8$-2020-1010.1**	**KK8$-2020-1111.3**	**KK8$-2020-1111.4**	**KK8$-2020-1204.2**
Group	**Gneiss**	**Tonalites(Eu+)**	**Tonalites**	**Tonalites**	**Dikes(Eu-)**	**Gneiss**	**Gneiss**
Al_2O_3	16.06	15.24	17.67	18.02	13.3	15.98	18.59
BaO	0.16	0.04	0.11	0.07	0.02	0.09	0.08
CaO	4.54	4.00	5.50	7.17	0.65	3.81	5.82
Cr_2O_3	<0.01	0.01	0.01	<0.01	<0.01	<0.01	<0.01
Fe_2O_3	7.58	4.20	7.41	9.08	1.02	4.58	6.02
K_2O	2.92	1.32	1.54	1.56	4.01	1.84	1.29
MgO	1.73	1.70	2.89	3.16	0.08	1.60	1.81
MnO	0.11	0.07	0.07	0.20	0.03	0.07	0.13

Na_2O	3.96	2.97	3.86	4.39	4.40	4.75	4.14
P_2O_5	0.39	0.05	0.35	0.33	0.02	0.19	0.30
SO_3	0.07	0.08	0.04	0.01	<0.01	0.01	0.09
SiO_2	61.22	69.24	58.98	54.07	75.92	65.89	60.53
SrO	0.08	0.05	0.09	0.10	0.01	0.08	0.13
TiO_2	0.96	0.46	1.18	0.90	0.04	0.63	0.60
Ba	1275.00	265.00	890.00	541.00	73.80	636.00	558.00
Ce	63.40	16.10	89.80	47.50	13.50	30.30	43.40
Cr	10.00	50.00	60.00	20.00	10.00	20.00	30.00
Cs	1.55	2.01	0.46	1.63	2.65	2.10	1.31
Dy	5.91	2.73	1.35	4.74	6.40	3.52	2.65
Er	3.12	2.11	0.54	2.73	3.87	2.16	1.50
Eu	1.67	1.48	1.46	1.70	0.10	1.27	1.64
Ga	18.60	16.50	22.90	21.00	19.50	17.30	19.40
Gd	7.01	1.47	2.67	5.55	3.92	4.23	3.41
Hf	4.60	4.00	7.20	2.70	3.10	6.50	3.00
Ho	1.15	0.62	0.19	0.91	1.25	0.70	0.50
La	28.80	9.40	48.60	21.60	3.90	13.30	22.10
Lu	0.37	0.31	0.04	0.36	0.60	0.27	0.25
Nb	11.00	4.40	11.50	9.50	40.00	10.30	7.90
Nd	35.80	6.00	33.00	28.50	5.00	17.00	20.30
Pr	8.33	1.68	9.54	6.59	1.21	4.04	5.24
Rb	77.10	48.10	46.10	44.10	264.00	64.60	29.20
Sm	7.73	1.14	4.24	5.97	2.52	4.19	3.74
Sn	2.00	<1.00	<1.00	5.00	4.00	2.00	1.00
Sr	567.00	367.00	655.00	811.00	21.10	621.00	1085.00
Ta	0.40	0.30	0.20	0.40	5.10	0.50	0.50
Tb	0.93	0.29	0.23	0.77	0.87	0.65	0.46
Th	1.56	0.37	3.99	0.58	13.45	1.00	2.11
Tm	0.44	0.32	0.04	0.37	0.60	0.28	0.21
U	0.55	0.50	0.62	0.37	5.97	0.93	0.64
V	56.00	70.00	114.00	162.00	<5.00	49.00	122.00
W	<1.00	<1.00	<1.00	<1.00	<1.00	<1.00	<1.00
Y	28.90	16.70	5.40	24.60	32.90	18.70	12.80
Yb	2.54	2.23	0.50	2.52	3.97	1.77	1.46
Zr	172.00	159.00	333.00	107.00	48.00	245.00	112.00
Eu*	0.23	1.14	0.43	0.29	0.03	0.30	0.46
Eu/Eu*	0.69	3.49	1.33	0.90	0.09	0.92	1.40
$(La/Yb)_n$	7.64	2.84	65.53	5.78	0.66	5.07	10.21

SAMPLE	KK8$-2020-1419.1	KK8$-2020-1633.2	KK8$-2020-1659.2	MOTU-2021-9.1	MOTU-2021-11.1	MOTU-2021-17.1	MOTU-2021-22.1
Group	**Tonalites(Eu+)**	**Tonalites**	**Dikes**	**Diorite**	**Gneiss**	**Granodiorites**	**Tonalites**
Al_2O_3	16.09	18.02	13.04	17.18	15.68	12.90	14.82
BaO	0.15	0.09	0.07	0.06	0.10	0.05	0.14
CaO	4.27	5.69	0.66	7.92	5.56	0.58	2.07
Cr_2O_3	<0.01	<0.01	<0.01	0.02	0.01	<0.01	<0.01
Fe_2O_3	5.64	8.31	1.24	10.62	6.42	1.54	2.19
K_2O	2.13	1.52	6.67	1.27	1.74	5.84	4.11
MgO	1.60	2.73	0.22	5.67	2.82	0.18	0.62
MnO	0.10	0.16	0.02	0.16	0.13	0.03	0.03
Na_2O	3.80	4.55	2.31	3.38	3.88	2.72	3.40
P_2O_5	0.34	0.42	0.02	0.37	0.18	0.03	0.09
SO_3	0.02	0.05	<0.01	0.05	<0.01	<0.01	0.02
SiO_2	64.46	56.06	74.84	51.70	62.04	74.77	71.25
SrO	0.10	0.10	0.03	0.08	0.08	0.02	0.05
TiO_2	0.98	1.14	0.10	1.38	0.61	0.13	0.23
Ba	1130.00	667.00	508.00	476.00	864.00	413.00	1135.00
Ce	44.00	59.20	53.50	49.60	35.80	85.70	59.80
Cr	10.00	30.00	10.00	180.00	70.00	10.00	20.00
Cs	2.49	1.85	1.38	0.88	2.12	12.05	1.32
Dy	2.48	6.34	1.65	4.86	2.76	5.73	1.33
Er	1.47	3.36	0.82	2.71	1.54	3.23	0.67
Eu	1.48	1.80	0.68	1.81	1.12	0.65	0.81
Ga	15.60	20.80	11.90	20.60	17.90	17.50	15.70
Gd	3.20	7.61	2.61	6.04	3.26	6.40	2.16
Hf	3.90	3.80	1.90	2.70	2.70	4.40	4.30
Ho	0.50	1.21	0.29	0.91	0.50	1.06	0.25
La	22.30	24.40	26.10	22.10	18.80	42.90	31.70
Lu	0.24	0.44	0.12	0.34	0.22	0.46	0.10
Nb	12.60	14.80	4.60	15.40	6.90	14.70	8.80
Nd	20.30	33.70	21.30	28.00	16.90	33.50	19.90
Pr	5.23	7.99	5.87	6.57	4.21	9.87	6.06
Rb	51.70	48.20	139.00	46.20	45.30	226.00	98.40
Sm	3.64	7.61	3.78	6.05	3.32	6.75	3.15
Sn	1.00	23.00	1.00	1.00	2.00	6.00	<1.00
Sr	749.00	766.00	222.00	647.00	684.00	112.50	430.00
Ta	0.90	0.80	0.40	0.70	0.50	1.90	0.30
Tb	0.43	1.09	0.34	0.89	0.49	1.02	0.29
Th	3.77	1.38	17.25	0.22	2.24	24.40	11.70
Tm	0.21	0.45	0.12	0.35	0.20	0.42	0.09
U	1.34	0.82	1.86	0.17	0.88	4.93	1.37
V	71.00	169.00	7.00	236.00	133.00	7.00	25.00
W	1.00	1.00	<1.00	<1.00	<1.00	1.00	<1.00

Y	13.10	32.20	8.40	24.30	13.60	32.90	6.50
Yb	1.36	2.85	0.80	2.11	1.25	2.90	0.56
Zr	148.00	144.00	56.00	106.00	99.00	128.00	154.00
Eu*	0.43	0.24	0.22	0.29	0.34	0.09	0.31
Eu/Eu*	1.33	0.72	0.66	0.92	1.04	0.30	0.95
$(La/Yb)_n$	11.05	5.77	21.99	7.06	10.14	9.97	38.16

SAMPLE	**MOTU-2021-24.1**	**MOTU-2021-25.1**	**MOTU-2021-28.1**	**MOTU-2021-32.1**	**MOTU-2021-34.1**	**VSVE-2021-1.1**	**VSVE-2021-1.4**
Group	**Tonalites (Eu+)**	**Gneiss (Eu+)**	**Gneiss (Eu+)**	**Gneiss**	**Tonalites (Eu+)**	**Granodiorites (Eu+)**	**Granodiorites (Eu+)**
Al_2O_3	15.74	14.87	14.96	16.21	15.58	12.82	13.20
BaO	0.11	0.19	0.15	0.16	0.18	0.16	0.09
CaO	4.73	1.93	2.04	4.02	3.50	1.28	1.36
Cr_2O_3	0.01	<0.01	<0.01	<0.01	<0.01	<0.01	<0.01
Fe_2O_3	5.20	4.07	1.96	6.63	4.21	2.46	1.96
K_2O	1.53	4.77	4.35	2.36	3.39	4.37	3.66
MgO	2.01	0.77	0.44	2.00	1.35	0.33	0.35
MnO	0.08	0.06	0.03	0.12	0.10	0.03	0.02
Na_2O	4.07	3.47	3.62	3.54	3.65	3.06	3.70
P_2O_5	0.13	0.09	0.04	0.28	0.16	0.01	0.01
SO_3	<0.01	0.01	<0.01	0.05	<0.01	0.03	0.01
SiO_2	65.39	68.69	71.46	63.22	66.9	74.74	74.7
SrO	0.09	0.06	0.06	0.09	0.09	0.04	0.03
TiO_2	0.55	0.43	0.21	0.76	0.49	0.17	0.15
Ba	955.00	1680.00	1225.00	1295.00	1405.00	1250.00	713.00
Ce	22.20	22.90	52.10	44.10	25.40	11.40	12.60
Cr	40.00	20.00	10.00	20.00	10.00	10.00	10.00
Cs	2.19	2.02	1.50	1.19	1.75	1.02	1.02
Dy	0.80	1.43	0.87	3.05	1.29	0.34	0.37
Er	0.42	0.81	0.39	1.67	0.68	0.29	0.26
Eu	0.96	1.04	0.88	1.56	1.11	0.68	0.56
Ga	17.60	15.60	14.10	17.50	14.20	11.40	11.80
Gd	1.15	1.91	1.58	3.71	1.88	0.66	0.76
Hf	3.40	5.30	2.50	3.60	3.00	8.00	6.30
Ho	0.16	0.28	0.14	0.57	0.25	0.08	0.07
La	14.10	11.50	26.60	20.90	14.00	6.20	5.30
Lu	0.08	0.13	0.06	0.22	0.13	0.12	0.10
Nb	4.80	5.60	4.30	7.80	7.20	2.30	2.20
Nd	7.70	9.50	16.40	21.70	10.80	5.30	5.80
Pr	2.19	2.37	5.06	5.26	2.88	1.35	1.24
Rb	58.80	110.00	112.50	46.10	75.50	76.50	61.10
Sm	1.36	1.99	2.51	4.26	2.22	0.97	1.11
Sn	1.00	3.00	1.00	<1.00	3.00	1.00	1.00
Sr	851.00	482.00	442.00	716.00	635.00	284.00	212.00

Ta	0.30	0.20	0.20	0.20	0.40	0.10	0.10
Tb	0.15	0.25	0.18	0.52	0.23	0.07	0.07
Th	1.99	5.89	15.10	1.16	0.87	2.72	3.47
Tm	0.06	0.11	0.05	0.21	0.10	0.06	0.05
U	0.50	1.19	0.46	0.50	0.48	1.13	0.80
V	116.00	39.00	11.00	74.00	60.00	6.00	<5.00
W	<1.00	1.00	<1.00	<1.00	<1.00	<1.00	9.00
Y	4.00	7.20	4.00	15.00	6.60	2.50	1.80
Yb	0.35	0.70	0.29	1.38	0.67	0.46	0.37
Zr	123.00	198.00	86.00	136.00	116.00	296.00	235.00
Eu*	0.77	0.53	0.44	0.39	0.54	0.85	0.61
Eu/Eu*	2.35	1.63	1.35	1.19	1.66	2.59	1.86
$(La/Yb)_n$	27.16	11.08	61.84	10.21	14.09	9.09	9.66

SAMPLE	**VSVE-2021-6.1**	**VSVE-2021-6.2**	**VSVE-2021-6.3**	**VSVE-2021-7.1**	**VSVE-2021-9.1**	**VSVE-2021-9.3**	**VSVE-2021-10.1**
Group	**Granodiorites(Eu+)**	**Gneiss**	**Gneiss**	**Tonalites**	**Tonalites(Eu+)**	**Granodiorites**	**Granite**
Al_2O_3	15.52	16.10	15.42	15.53	15.77	13.30	15.20
BaO	0.21	0.18	0.13	0.04	0.05	0.07	0.61
CaO	2.30	4.73	4.88	6.01	4.65	0.57	1.14
Cr_2O_3	<0.01	0.01	0.01	0.01	0.01	<0.01	<0.01
Fe_2O_3	3.25	6.74	8.19	8.32	6.58	1.55	2.07
K_2O	3.96	3.24	3.39	1.56	1.29	5.84	8.31
MgO	0.46	2.43	2.93	3.50	2.79	0.28	0.53
MnO	0.06	0.12	0.15	0.19	0.11	0.02	0.09
Na_2O	3.52	3.61	3.31	4.09	3.52	2.68	1.90
P_2O_5	0.06	0.25	0.48	0.18	0.16	0.04	0.33
SO_3	0.05	0.02	0.07	0.01	0.03	<0.01	<0.01
SiO_2	69.65	61.21	59.07	59.25	63.38	74.63	68.68
SrO	0.10	0.09	0.07	0.06	0.07	0.02	0.07
TiO_2	0.20	0.73	1.12	0.77	0.60	0.14	0.03
Ba	1710.00	1450.00	1005.00	226.00	334.00	536.00	5150.00
Ce	38.40	57.00	59.10	79.90	21.10	45.80	29.10
Cr	<10	30.00	30.00	60.00	60.00	<10	<10
Cs	1.15	1.35	1.82	1.19	1.98	1.12	1.23
Dy	0.67	3.12	4.05	7.04	1.70	1.92	3.53
Er	0.34	1.72	2.15	3.97	0.92	0.67	2.63
Eu	1.09	1.33	1.43	1.40	1.04	0.48	0.71
Ga	15.70	18.00	18.30	19.90	18.30	13.80	12.70
Gd	1.22	4.14	5.28	8.18	2.06	3.06	3.13
Hf	3.40	2.90	3.00	2.70	3.20	3.40	0.90
Ho	0.14	0.64	0.80	1.40	0.33	0.30	0.87
La	21.10	29.40	28.00	34.10	11.40	21.80	8.30
Lu	0.06	0.24	0.27	0.53	0.14	0.11	0.41

Nb	1.40	8.90	11.70	14.20	5.70	8.20	4.70
Nd	13.30	25.00	30.90	45.40	10.30	17.30	9.50
Pr	3.85	6.65	7.51	11.25	2.61	5.07	2.31
Rb	61.50	82.60	85.00	51.20	39.80	120.50	139.00
Sm	1.67	4.27	5.99	9.08	2.09	3.43	2.40
Sn	<1.00	1.00	1.00	2.00	<1.00	<1.00	<1.00
Sr	784.00	666.00	539.00	400.00	541.00	145.00	518.00
Ta	0.10	0.40	0.60	0.70	0.30	0.40	0.40
Tb	0.12	0.53	0.70	1.15	0.30	0.38	0.54
Th	4.33	3.54	1.63	1.36	0.95	14.65	3.65
Tm	0.04	0.24	0.28	0.52	0.11	0.09	0.40
U	0.42	0.84	0.53	0.63	0.52	1.76	0.72
V	<5.00	98.00	113.00	128.00	114.00	6.00	<5.00
W	<1.00	<1.00	<1.00	<1.00	<1.00	<1.00	<1.00
Y	3.90	16.70	21.30	39.10	9.10	8.10	23.40
Yb	0.41	1.66	1.92	3.82	0.78	0.69	2.82
Zr	153.00	136.00	138.00	119.00	141.00	118.00	31.00
Eu*	0.76	0.32	0.25	0.16	0.50	0.15	0.26
Eu/Eu*	2.33	0.97	0.78	0.49	1.53	0.45	0.79
$(La/Yb)_n$	34.69	11.94	9.83	6.02	9.85	21.30	1.98

SAMPLE	**VSVE-2021-10.2**	**VSVE-2021-11.1**	**VSVE-2021-11.2**	**VSVE-2021-11.3**	**VSVE-2021-12.1**	**VSVE-2021-14.1**	**VSVE-2021-15.1**
Group	**Gneiss**	**Granodiorites**	**Gneiss(Eu+)**	**Dikes**	**Tonalites**	**Tonalites**	**Tonalites**
Al_2O_3	16.10	14.02	14.85	14.17	16.57	15.74	16.46
BaO	0.14	0.14	0.08	0.12	0.07	0.09	0.14
CaO	7.59	1.32	3.92	1.29	4.66	3.41	4.67
Cr_2O_3	0.01	<0.01	0.01	<0.01	<0.01	<0.01	<0.01
Fe_2O_3	8.58	2.37	4.51	1.31	8.72	5.22	6.37
K_2O	1.88	5.18	1.65	6.09	1.85	2.07	2.78
MgO	1.28	0.52	1.90	0.34	1.57	1.22	1.96
MnO	0.22	0.04	0.07	0.02	0.24	0.09	0.13
Na_2O	3.06	2.92	3.27	2.81	4.50	4.32	3.99
P_2O_5	0.25	0.06	0.08	0.04	0.33	0.17	0.22
SO_3	<0.01	<0.01	0.02	0.02	0.01	0.01	0.04
SiO_2	59.31	72.28	68.85	72.76	60.10	66.53	62.15
SrO	0.07	0.03	0.07	0.04	0.10	0.06	0.08
TiO_2	0.94	0.25	0.56	0.10	1.08	0.64	0.66
Ba	1075.00	1265.00	618.00	957.00	494.00	682.00	1055.00
Ce	45.30	85.80	20.10	89.10	49.60	43.50	53.50
Cr	30.00	<10.00	40.00	<10.00	<10.00	<10.00	10.00
Cs	0.48	2.09	2.36	0.94	2.52	2.39	1.82
Dy	3.40	1.95	0.76	2.73	6.64	3.62	3.97

Er	1.80	1.02	0.52	1.24	3.47	2.10	2.30
Eu	1.12	0.64	0.90	0.78	1.99	1.08	1.25
Ga	17.50	17.50	17.80	13.90	19.30	18.90	19.10
Gd	4.21	2.90	1.06	4.56	7.71	4.23	4.92
Hf	3.10	4.60	3.80	1.90	2.30	4.40	3.60
Ho	0.65	0.37	0.15	0.48	1.27	0.76	0.81
La	20.50	42.10	11.40	42.30	20.30	20.40	23.80
Lu	0.24	0.13	0.08	0.14	0.38	0.23	0.33
Nb	10.40	11.30	7.10	4.20	14.70	11.00	9.30
Nd	23.60	27.50	6.90	34.20	32.30	19.20	27.90
Pr	5.90	8.33	2.02	9.52	7.14	4.90	6.84
Rb	25.70	140.50	58.10	98.70	49.40	93.20	64.10
Sm	4.53	4.05	1.03	5.76	7.44	3.95	5.32
Sn	3.00	<1.00	<1.00	<1.00	1.00	1.00	3.00
Sr	492.00	245.00	552.00	292.00	729.00	464.00	569.00
Ta	0.60	0.70	0.40	0.40	0.90	0.50	0.40
Tb	0.59	0.38	0.13	0.53	1.08	0.62	0.69
Th	1.58	16.05	1.56	26.40	1.58	3.10	0.65
Tm	0.24	0.12	0.07	0.14	0.43	0.27	0.32
U	0.29	1.82	0.62	2.65	0.77	0.53	0.28
V	162.00	16.00	85.00	6.00	<5.00	36.00	89.00
W	1.00	<1.00	<1.00	<1.00	<1.00	<1.00	<1.00
Y	18.30	10.20	4.80	12.70	32.00	19.20	21.90
Yb	1.82	0.89	0.53	0.95	2.79	1.92	2.37
Zr	133.00	199.00	169.00	67.00	97.00	189.00	146.00
Eu*	0.26	0.19	0.86	0.15	0.26	0.26	0.24
Eu/Eu*	0.78	0.57	2.63	0.47	0.80	0.81	0.75
$(La/Yb)_n$	7.59	31.89	14.50	30.02	4.91	7.16	6.77

SAMPLE	**VSVE-2021-16.1**	**VSVE-2021-17.2**
Group	**Tonalites**	**Tonalites**
Al_2O_3	16.07	14.97
BaO	0.06	0.02
CaO	5.36	3.24
Cr_2O_3	0.02	<0.01
Fe_2O_3	7.63	4.23
K_2O	1.89	1.27
MgO	3.07	1.46
MnO	0.18	0.08

Na_2O	3.84	4.21
P_2O_5	0.24	0.10
SO_3	0.02	0.06
SiO_2	60.22	68.37
SrO	0.07	0.03
TiO_2	0.91	0.40
Ba	420.00	79.20
Ce	41.60	260.00
Cr	110.00	20.00
Cs	2.75	3.56
Dy	3.08	3.71
Er	1.76	1.40
Eu	1.22	0.74
Ga	20.00	22.70
Gd	4.09	7.63
Hf	3.70	8.10
Ho	0.65	0.61
La	20.10	126.50
Lu	0.25	0.14
Nb	13.20	15.00
Nd	21.10	94.00
Pr	5.12	27.90
Rb	76.30	89.10
Sm	4.27	13.10
Sn	1.00	5.00
Sr	551.00	269.00
Ta	0.80	0.80
Tb	0.53	0.79
Th	1.93	47.00
Tm	0.25	0.17
U	0.86	2.39
V	134.00	34.00
W	<1.00	<1.00
Y	17.40	15.00
Yb	1.74	1.17
Zr	168.00	318.00
Eu*	0.29	0.07
Eu/Eu*	0.89	0.22
$(La/Yb)_n$	7.79	72.89